



**HAL**  
open science

# Enhanced Hough transforms for image processing

Chunling Tu

► **To cite this version:**

Chunling Tu. Enhanced Hough transforms for image processing. Signal and Image Processing. Université Paris-Est, 2014. English. NNT : 2014PEST1103 . tel-01140138

**HAL Id: tel-01140138**

**<https://theses.hal.science/tel-01140138>**

Submitted on 7 Apr 2015

**HAL** is a multi-disciplinary open access archive for the deposit and dissemination of scientific research documents, whether they are published or not. The documents may come from teaching and research institutions in France or abroad, or from public or private research centers.

L'archive ouverte pluridisciplinaire **HAL**, est destinée au dépôt et à la diffusion de documents scientifiques de niveau recherche, publiés ou non, émanant des établissements d'enseignement et de recherche français ou étrangers, des laboratoires publics ou privés.



UNIVERSITÉ PARIS-EST

ÉCOLE DOCTORALE : MSTIC

**Thèse de doctorat**

**Informatique, Traitement d'images**

**Chunling TU**

Améliorations de la Transformée de Hough en traitement d'images

*Thèse dirigée par  
Karim Djouani et Barend Jacobus Van Wyk*

Soutenue le 23 Septembre 2014

**Jury :**

Prof: Anton VAN WYK, Witwatersrand University, South Africa  
Prof. Johan E. CARLSON, Luleå University of Technology, Sweden  
Prof: Patrick HENAFF, Ecole des Mines de Nancy, France  
Prof. Yskandar HAMAM, Tshwane University of Technology, South Africa  
Prof. Barend J. VAN WYK, Tshwane University of Technology, South Africa  
Prof. Karim DJOUANI, Université Paris Est Créteil, France

Les travaux effectués dans le cadre de la présente thèse concernent l'analyse et les améliorations apportées à la transformée de Hough Standard (SHT), utilisée en traitement d'image comme simple outil de détection de segments de lignes droites.

La transformée de Hough a reçu, depuis sa proposition en 1962, une attention particulière de la part de la communauté. La HT est considérée comme une méthode robuste, dont le principe repose sur la transformation du problème initial de détection de segments de lignes droites en un problème de sélection des sommets dans l'espace des paramètres, appelé aussi espace HT ou espace de Hough.

Les points candidats dans l'espace image sont mis en correspondance avec les points dans l'espace de Hough, en utilisant le principe avancé par la transformée de Hough est qu'il existe un nombre infini de lignes qui passent par un point, dont la seule différence est l'orientation (l'angle). La transformée de Hough permet de déterminer lesquelles de ces lignes passent au plus près du domaine d'intérêt.

Les cellules dans l'espace de Hough échantillonné obtiennent des votes des points candidats. Les maxima locaux correspondant aux sommets sont construits lorsque les cellules considérées obtiennent plus de votes que les cellules voisines. Les sommets détectés alors dans l'espace des paramètres sont transformés dans l'espace image pour validation.

Malheureusement, les opérations de transformation directe, de l'espace image vers l'espace des paramètres, et inverse engendrent des opérations d'approximation, sources de plusieurs problèmes de la transformée de Hough, qui affectent les aspects de robustesse, précision et résolution. On se propose de résoudre ces problèmes dans le cadre des travaux engagés dans le cadre de la thèse.

Les contributions, détaillées ci-dessous, ont pu être proposées.

A) Pour adresser le problème de limitation en termes de résolution de la SHT, les points concernant la sélection d'une bonne résolution, l'extension de la résolution de la SHT et l'utilisation des techniques de super-résolution pour la HT ont été couverts et de nouvelles propositions ont été faites et qui sont d'une utilité certaine pour les applications de traitement d'image.

Ainsi, une relation entre la performance de la HT et la résolution est proposée, ce qui permet de garantir le bon choix. Par ailleurs, une technique de super-résolution est proposée en s'appuyant sur le principe de la HT. Finalement, une autosimilarité dans les échantillons HT a été découverte et a été utilisée pour obtenir une résolution supérieure de la HT avec une grande fidélité.

B) Pour adresser le problème de la précision de la SHT, les erreurs de la HT ont été analysées, lorsque l'on fait subir des transformations géométriques à l'image source. Les erreurs ainsi détectées ont été utilisées pour compenser le manque de précision de la SHT, aboutissant ainsi à une HT plus précise.

Afin de permettre l'évaluation de performance des approches proposées dans le cadre de la thèse, une transformée de Hough idéale est proposée comme référence.

# **Enhanced Hough Transforms for Image Processing**

by

**Chunling Tu**

Submitted in partial fulfillment of the requirements for the degree

**DOCTOR TECHNOLOGIAE**

in the

F'SATI/Electrical Engineering Department

FACULTY OF ENGINEERING AND BUILT ENVIRONMENT

**TSHWANE UNIVERSITY OF TECHNOLOGY**

Supervisor: Prof Barend van Wyk

Prof Karim Djouani

Co-Supervisor: Prof Yskandar Hamam

September 2014

## DECLARATION BY CANDIDATE

“I hereby declare that the thesis submitted for the degree D Tech at Tshwane University of Technology is my own original work and has not previously been submitted to any other institution of higher education. I further declare that all sources cited or quoted are indicated and acknowledged by means of a comprehensive list of references”.

C. Tu



2014-12-18

*“Perspectives determine methods.”*

# ACKNOWLEDGEMENTS

My sincere thanks to my supervisors, Prof Ben van Wyk, Prof Karim Djouani and Prof Yskandar Hamam who guided me with their friendly supervision, their helpful comments and encouragement. Without their continued support I would not have been able to complete this project.

I would like to thank FSATI (French South African Institute of Technology), Tshwane University of Technology(TUT) and University Paris-Est(UPE) for all the opportunities and facilities provided during my study. Special thanks all the lecturers and secretaries of FSATI, TUT and UPE for all their assistance from the beginning of my study and research.

I am thankful to Tshwane University of Technology, FSATI, the French Embassy in South Africa and the NRF for their financial support.

# ABSTRACT

The thesis addresses the improvements of the Standard Hough Transform (SHT) for image processing applications. As a common tool for straight line segment detection, the Hough Transform (HT) has received extensive attention since its proposal in 1962. The HT is robust since it converts the straight line detection problem to a peak seeking problem in the parameter space (also called HT space or Hough space). Feature points in the image space are mapped to the parameter space, according to the normal formulation of the possible straight lines crossing them. The cells in the digitalised parameter space obtain votes from the feature points. The local maxima that is, peaks are built when these cells obtain more votes than the ones around them. The peaks detected in the parameter space are then mapped back to the image space for validation. Unfortunately, when mapping feature points in the image space to the parameter space in conjunction with the voting process, rounding operations are employed, which leads to several problems for the HT. The robustness, accuracy and resolution are all affected.

This thesis aims to solve these problems, and the following contributions were made towards this goal:

**A:** Because of the resolution limitation of SHT, the topics of how to select a “good” resolution, how to extend the resolutions of SHT and how to employ the super-resolution technique in HT are covered. In the research of these topics, several outputs are obtained, which are helpful to image processing applications. These include:

- The map of HT performance versus resolution is drawn, according to which “good” choices of resolution can be found.
- The HT resolution are extended by geometrical analysis of the HT butterflies.
- Super resolution HT is proposed with consideration to the features of the HT.
- Self-similarity of the HT butterflies is discovered and employed to obtain high resolution HT with high reliability.

**B:** For the accuracy defect of SHT, the error system of HT is studied when the image is shifted in the image space. The detection errors are employed to compensate for the defect, and an accurate HT is proposed.

In order to evaluate existing HT varieties, an ideal HT is proposed as a standard.

Keywords: Hough Transform (HT), HT butterfly, Straight line detection, Segment detection.

# LIST OF PUBLICATIONS

1. C. Tu, BJ. van Wyk, Y. Hamam, K. Djouani, S. Du. Vehicle Position Monitoring Using Hough Transform. International Conference on Electrical Engineering and Computer Science. 2013.
2. C. Tu, Y. Hamam, BJ. van Wyk, K. Djouani, S. Du. Ideal HT: An Useful Tool for Hough Transforms Assessment. SAIEE, Africa Research Journal. Vol. 104, No. 3, pp. 107-114, 2013.
3. C. Tu, K. Djouani, BJ. van Wyk, Y. Hamam and S. Du, Good Resolutions for Hough Transform, Proceedings of the 10th World Congress on Intelligent Control and Automation, Beijing, China, pp. 4917-4920, July 6-8, 2012.
4. C. Tu, S. Du, B.J. van Wyk, K. Djouani, and Y. Hamam. High Resolution Hough Transform Based on Butterfly Self-Similarity. Electronic Letters, vol 47, No.26. pp: 1360 - 1361, 2011
5. C. Tu, BJ van Wyk, K Djuwane, A Hamam, S. Du, Using Super Resolution Algorithm to improve Hough Transform Resolution. 8th INTERNATIONAL CONFERENCE ON IMAGE ANALYSIS AND RECOGNITION (ICIAR 2011), June 22-24, 2011, Burnaby, BC, Canada.
6. C. Tu, BJ. van Wyk, K. Djouani, Y. Hamam, S. Du. Super Resolution Reconstruction based on Iterated Back-Projection for Hough Transform. Submitted to Pattern Recognition.
7. C. Tu, K. Djouani, BJ. van Wyk, Y. Hamam, S. Du. Generating High Resolution Hough Transform Butterflies. Submitted to Pattern Recognition.

# CONTENTS

	<b>PAGE</b>
<b>DECLARATION BY CANDIDATE</b>	<b>i</b>
<b>ACKNOWLEDGEMENTS</b>	<b>iii</b>
<b>ABSTRACT</b>	<b>iv</b>
<b>LIST OF FIGURES</b>	<b>x</b>
<b>LIST OF TABLES</b>	<b>xii</b>
<b>ABBREVIATIONS</b>	<b>xiii</b>
<b>SYMBOLS</b>	<b>xiv</b>
<b>I HOUGH TRANSFORM: LOVE IT OR LEAVE IT?</b>	<b>3</b>
<b>1 Progress of HT Theoretical Research and Applications</b>	<b>4</b>
1.1 The History of HT . . . . .	4
1.2 Progress of HT Theoretical Research . . . . .	6
1.2.1 Progress on Improving the Resolution and Accuracy . . . . .	6
1.2.2 Progress on Decreasing the Computation Load and Storage Requirements . . . . .	8
1.3 Applications of HT . . . . .	9
<b>2 Critical Review and Problem Definition</b>	<b>11</b>
2.1 Expectations of HT . . . . .	12
2.2 HT Problems . . . . .	13
2.2.1 The Precision Problem of Low Resolution HT . . . . .	13
2.2.2 High Resolution HT Problems . . . . .	14
2.3 Error Sources of HT . . . . .	19
2.3.1 Discretisation Error in the Image Space . . . . .	19
2.3.2 Discretisation Error in the Parameter Space . . . . .	21

2.3.3	Sensitivity to Input Image Shifts . . . . .	21
2.4	HT Butterflies are More Meaningful than the Peak . . . . .	23
<b>3</b>	<b>Contributions Towards Solving the HT Problems</b>	<b>26</b>
3.1	Criteria of HT Resolution Selection . . . . .	26
3.2	Self-similarity of the HT Butterfly . . . . .	26
3.3	Super Resolution Method . . . . .	27
3.4	Extend Resolution in HT Butterflies through Geometry Analysis . . . . .	27
3.5	Error Compensation for Straight Line Detection . . . . .	28
3.6	Ideal HT: One Useful Tool to Evaluate the HT Butterflies . . . . .	28
<b>II</b>	<b>EFFORTS FOR ENHANCING THE HT</b>	<b>30</b>
<b>4</b>	<b>Good Resolutions for HT</b>	<b>33</b>
4.1	What are “Good” Resolutions of HT? . . . . .	34
4.2	Inflexion of Error-Resolution Curves . . . . .	36
4.3	The Factors Affecting the Inflexion . . . . .	36
4.3.1	The Effect of the Straight Segment Position ( $\theta_0$ and $\rho_0$ ) on the Inflexion . . . . .	37
4.3.2	The Effect of Straight Segment Length ( $l$ ) on the Inflexion . . . . .	38
4.3.3	The Effect of Straight Segment Width ( $w$ ) on the Inflexion . . . . .	39
4.4	A Global View of “Good” Resolutions . . . . .	39
<b>5</b>	<b>High Resolution HT Based on Butterfly Self-Similarity</b>	<b>46</b>
5.1	Self-similarity . . . . .	46
5.2	Method for High Resolution HT . . . . .	49
5.3	Results . . . . .	51
<b>6</b>	<b>Generating High Resolution HT Butterflies</b>	<b>53</b>
6.1	Generating High Resolution HT Butterflies . . . . .	53
6.1.1	Extending the $\theta$ -resolution of Butterflies: $HT(\Delta\rho, \Delta\theta) \implies HT(\Delta\rho, \frac{\Delta\theta}{n})$ . . . . .	54
6.1.2	Extending the $\rho$ -resolution: $HT(\Delta\rho, \frac{\Delta\theta}{n}) \implies HT(\frac{\Delta\rho}{m}, \frac{\Delta\theta}{n})$ . . . . .	65
6.2	Summary and Discussion of the Proposed Method . . . . .	67
6.2.1	Steps to Implement the Proposed Method: . . . . .	67
6.2.2	Running Time and Memory Storage . . . . .	69
6.3	Experiments . . . . .	71
6.3.1	The Peak Becomes More Distinct . . . . .	71
6.3.2	Comparison of the “Ideal” HT Butterfly . . . . .	73
6.3.3	Straight Line Positioning Accuracy (the Accuracy of the Generated Peak) . . . . .	74
<b>7</b>	<b>Super Resolution HT</b>	<b>80</b>
7.1	Super Resolution HT (SRHT) . . . . .	80

7.1.1	Availability of Low Resolution Containing New Information . . . . .	81
7.1.2	The Number of Frames Needed for SR Reconstruction . . . . .	82
7.1.3	Cell Registration . . . . .	84
7.1.4	Conversions between HR and LR HT Frames . . . . .	86
7.1.5	HR Reconstruction Based on Iterated Back-Projection . . . . .	86
7.2	Discussion . . . . .	88
7.2.1	A Way to Reduce Computation Load . . . . .	88
7.2.2	Horizontal and Vertical Lines . . . . .	88
7.3	Experiments and Results . . . . .	89
7.3.1	HT Data Generated by the Proposed Method . . . . .	89
7.3.2	Straight Line Detection Errors . . . . .	90
7.3.3	Comparison for a Real Image . . . . .	90
<b>8</b>	<b>Line Positioning Based on HT Error Compensation</b>	<b>93</b>
8.1	The $\rho$ Value Detection Error of HT . . . . .	93
8.2	Shifting the Image Can Generate New Detection Errors . . . . .	94
8.3	Measuring the Detection Error via the Sequence of Detected $\rho$ Values of the Shifted Images . . . . .	95
8.4	High Precision $\rho$ Value Detection based on Error Compensation . . . . .	97
8.5	Experiments . . . . .	98
<b>9</b>	<b>An Assessment Tool for HTs – “Ideal” HT</b>	<b>101</b>
9.1	Expectations of the “Ideal” HT Data . . . . .	102
9.2	Calculation of the “Ideal” HT Data . . . . .	103
9.3	Evaluate the HT Data Generated by Specific Algorithm . . . . .	105
9.3.1	The Peak Height vs. the Segment Length . . . . .	106
9.3.2	The Quality of the Generated Butterfly . . . . .	106
9.3.3	Effect of Segment Parameters . . . . .	107
9.3.4	Evaluation of the SHT . . . . .	108
9.4	Weakness of the Proposed “Ideal” HT . . . . .	108
9.5	Conclusion . . . . .	108
<b>III</b>	<b>CONCLUSION AND FUTURE WORK</b>	<b>119</b>
<b>10</b>	<b>Conclusion</b>	<b>120</b>
<b>11</b>	<b>Future Work</b>	<b>122</b>
	<b>REFERENCES</b>	<b>123</b>

# LIST OF FIGURES

	PAGE
2.1 Unreliability of high resolution HT . . . . .	15
2.2 A straight line in a digital image . . . . .	16
2.3 Inappropriately high $\rho$ -resolution results in peak splitting . . . . .	17
2.4 Inappropriate high $\theta$ -resolution results in peak flatten . . . . .	18
2.5 Inappropriate high resolutions results in unreliable peaks . . . . .	19
2.6 3 patterns for digital images . . . . .	20
2.7 The discretisation error in the parameter space . . . . .	22
2.8 The case of a synthetic line . . . . .	24
2.9 The case of a real image . . . . .	25
4.1 The best resolution setting of HT. . . . .	35
4.2 The inflexion on error-resolution curves. . . . .	37
4.3 $\rho$ value of straight segments does not effect on the selection of best resolution . . . . .	38
4.4 $\theta$ value of straight segments does not affect on the selection of best resolution . . . . .	39
4.5 The length of segments affects on the selection of best resolution . . . . .	40
4.6 The width of segments affects on the selection of best resolution . . . . .	41
4.7 The area with small errors . . . . .	42
4.8 Approximating the area with small errors by upper and lower bounds . . . . .	43
4.9 Upper and lower bounds of various $\theta$ values of segments . . . . .	44
4.10 Upper and lower bounds of various $\rho$ values of segments . . . . .	44
4.11 Upper and lower bounds of various lengths of segments . . . . .	45
4.12 Upper and lower bounds of various widths of segments . . . . .	45
5.1 Geometric principle of HT . . . . .	47
5.2 Self-similarity of HT butterfly . . . . .	50
5.3 HT butterflies obtained by traditional method and proposed method under high resolutions ( $\Delta\rho = 0.05$ pixel and $\Delta\theta = 0.05^0$ ) . . . . .	52
6.1 The generation of the butterfly shape in HT . . . . .	55
6.2 Extend $\theta$ resolution of HT butterfly (centre part) . . . . .	57
6.3 Extend $\theta$ resolution of HT butterfly (wings) . . . . .	61
6.4 The length of intersection in the image space determines the density in the HT space . . . . .	62

---

6.5	Extending the HT resolution in $\rho$ direction . . . . .	65
6.6	Determine the votes in ends cases . . . . .	66
6.7	Computing complexity trends corresponding to the increase of resolution . . . . .	72
6.8	The peak is improved by the proposed method . . . . .	73
6.9	Comparison of the correlation with the theoretical butterfly . . . . .	74
6.10	Detection accuracy comparison . . . . .	75
6.11	The effect of resolutions on SHT and REHT detection accuracy . . . . .	76
6.12	Images contain straight line edge objects . . . . .	78
6.13	Edge images of Fig.6.12 . . . . .	79
7.1	Horizontally move a straight line . . . . .	83
7.2	Performance comparison for a synthetic straight line . . . . .	89
7.3	Detection error comparison for randomly generated straight lines . . . . .	91
7.4	The edges of the arrow mark to be detected . . . . .	92
8.1	The generation of $\rho$ value detection error in HT . . . . .	94
8.2	Comparison of detected position of given line . . . . .	99
8.3	Comparison of detected $\rho$ values of shifted straight lines . . . . .	99
8.4	Comparison of detection error . . . . .	100
9.1	The principle of ideal HT data . . . . .	103
9.2	The segment used to evaluate SHT . . . . .	105
9.3	Comparison of butterflies under the same resolutions ( $\Delta\theta = 1^\circ, \Delta\rho = 1\text{pixel}$ ) . . . . .	110
9.4	Peak height as the measurement of segment length . . . . .	111
9.5	The quality of butterflies . . . . .	112
9.6	The effect of segment $\theta$ value . . . . .	114
9.7	The effect of segment $\rho$ value . . . . .	116
9.8	The effect of segment length value . . . . .	118

# LIST OF TABLES

	<b>PAGE</b>
6.1 The operations intensively used in the SHT and the proposed Resolution Extended HT (REHT) . . . . .	70
6.2 The number of operations requested by the SHT and the proposed Resolution Extended HT (REHT) . . . . .	70
6.3 Memory storage requested by the SHT and the proposed method . . . . .	70
6.4 Comparison of detection errors . . . . .	78
7.1 Comparison of detection error . . . . .	92

# ABBREVIATIONS

<b>HT</b>	<b>Hough Transform</b>
<b>SHT</b>	<b>Standard Hough Transform</b>
<b>RHT</b>	<b>Randomised Hough Transform</b>
<b>SRHT</b>	<b>Super Resolution Hough Transform</b>
<b>REHT</b>	<b>Resolution Extended Hough Transform</b>
<b>LSHT</b>	<b>Low resolution Standard Hough Transform</b>
<b>HSHT</b>	<b>High resolution Standard Hough Transform</b>
<b>LS</b>	<b>Least Square</b>
<b>SR</b>	<b>Super Resolution</b>
<b>LR</b>	<b>Low Resolution</b>
<b>HR</b>	<b>High Resolution</b>
<b>LRHT</b>	<b>Low Resolution Hough Transform</b>
<b>HRHT</b>	<b>High Resolution Hough Transform</b>
<b>VFHT</b>	<b>Variable Filter Hough Transform</b>

# SYMBOLS

$x$	axes	pixel
$y$	axes	pixel
$\rho$	distance	pixel
$\theta$	angle	°
$\Delta\rho$	$\rho$ -direction resolution of parameter space	pixel
$\Delta\theta$	$\theta$ -direction resolution of parameter space	°
$R$	size of the retina	pixel
$l$	length of segment	pixel
$w$	width of segment	pixel
$V$	voting values of the parameter space	
$\Delta l$	intersection length of the straight line and the belt corresponding to the cell	pixel

*Dedicated to my husband, my son, my parents and sisters for all  
your support and patience. Thank you...*

# Overview of the thesis

This thesis consists of three parts. Part I is an introduction to the Hough Transform (HT) and covers the HT principle and research regarding its applications. Both positive and critical reviews are investigated to show the advantages of the HT and its potential improvements.

Chapter 1 introduces the progress of HT theoretical research. The applications and advantages of HT are demonstrated from positive viewpoints. In Chapter 2, critical reviews address the deficiencies of HT through geometry analysis, utilising a graphical method. The potential for solving these problems is the motivation for this research. Based on the ideas inspired by the critical reviews, Chapter 3 lists the contributions made towards higher performance HTs.

Although HT has the capacity to detect a variety of objects, this research focuses on the detection of straight lines and segments.

Part II, entitled Enhancements of the HT, introduces our efforts on improving the resolution and accuracy of HT.

Chapter 4 answered the question of “How to select good resolutions for HT?”. The “good” resolution is defined, followed by the study the relationship between the straight line detection errors and HT resolutions ( $\rho$ - and  $\theta$ - directions). The area containing “good” resolution settings is uncovered and modelled.

Chapter 5-6 improve the HT resolution by geometry analysis. In Chapter 5, the self-similarity of HT butterflies is discovered and used to obtain a reliable high resolution HT butterfly. Chapter 6 proposed a method to generate high resolution HT data from low resolution data, where the geometry principles are employed to discover the relationship between high and low resolution HT data.

Chapter 7 proposed super resolution method to improve HT resolution.

In Chapter 8, the line positioning errors are concerned. The error series when the image shifted are studied, and a error compensation method is proposed which greatly improved the detection accuracy.

Chapter 9 discusses the evaluation of HT butterflies generated by various methods. A method to generate the ideal HT butterfly is proposed.

Part III concludes the thesis.

## **Part I**

# **HOUGH TRANSFORM: LOVE IT OR LEAVE IT?**

# CHAPTER 1

## PROGRESS OF HT THEORETICAL RESEARCH AND APPLICATIONS

Nowadays, identifying objects from images is one of the important goals in image processing, computer vision and image analysis. Some of the popular methods for object recognition and detection are based on the edge features of the object. These methods initially extract the edge of the object and then use different algorithms for its identification. Among the algorithms commonly used, HT is an outstanding example. The HT is widely used to detect regular shapes such as lines, circles, ellipses and other parametric curves, including arbitrary shapes, in the image. Using HT to detect straight lines has received much attention due to its robustness.

### 1.1 The History of HT

HT is one of the most widely used and proven effective techniques for positioning objects in images. The HT was proposed by Hough [1] in 1962 and patented. This patent comprises five pages, including figures and descriptions, in order to explain the HT algorithm. There are no equations in the patent. The idea of this algorithm is “collinear points in the image plane can be identified by mapping them into geometric constructions (for Standard HT, straight lines) that intersect in the transform space”. However, it was not easy to use this geometry algorithm as a computer vision detection method at that time.

Hart [2] depicted the history of HT. Rosenfeld [3] gave the definition of HT in algebraic forms in his book in 1969. The definition is presented in the following slope-intercept equation

$$y = y_i x + x_i, \quad (1.1)$$

where  $x_i, y_i$  are feature points in the image space, and  $x$  and  $y$  are the axes of the transform plane. If these points  $(x_i, y_i)$  are collinear, then it is easy to prove that the corresponding lines in the transform plane will all pass through a single point. This is the first explicit algebraic form for the transform. A simple digital implementation of the transform space was defined as an array of counters. Initially, this idea was introduced to the computer science and computer vision community as an obscure analogue circuit based patent.

However, the discrete HT uses the slope-intercept parameters and thus, the parameter space is the two-dimensional slope-intercept plane. This method for the detection of straight lines suffers from horizontal and vertical line detection problems because the slope and the intercept are unbounded. To overcome this problem, it was suggested that each picture could be scanned twice at right angles. However, this results in excessive calculations and memory stores in computer processing.

Duda et al. [4] proposed to replace the slope-intercept parameters by angle-radius parameters. This method uses the polar (or normal) representation of straight lines as follows:

$$\rho = x \cos \theta + y \sin \theta, \quad (1.2)$$

where  $(x, y)$  is a feature point in the image space,  $\rho$  is the distance from the origin to the straight line, and  $\theta$  is the angle between the normal and the positive  $x$ -axis. The HT maps each point  $(x, y)$  in the image space to a sinusoidal curve in the parameter space. The HT space is quantised into many cells along the sinusoidal curve. Each cell can be confined to the region  $0 \leq \theta \leq \pi$ ,  $-R \leq \rho \leq R$ , where  $R$  is the size of the retina. The size of each cell is  $\Delta\rho$  and  $\Delta\theta$ . Each feature point in the image space will correspond to a curve according to Eq. (1.2), and the cell will obtain votes along the curve in the parameter space. If a number of feature points lie on the same straight line, their corresponding curves will intersect at one cell in the parameter space. This means that some cells will obtain most of the votes. The HT then searches for the cell with the most votes, that is, the peaks. In this way, the problem of detecting collinear points in image space is converted to the problem of finding peaks in parameter space.

This method overcomes the problem of horizontal lines and vertical lines. It also decreases the computation and memory stores, and is commonly referred to the Standard HT (SHT). In this thesis, if not specified, HT refers to this SHT.

## 1.2 Progress of HT Theoretical Research

### 1.2.1 Progress on Improving the Resolution and Accuracy

Due to the rounding operations in the voting process, the discretisation of image space and parameter space shows several problems regarding the accuracy and resolution of HT. These include peak splitting, flattening and resolution limitations. Many researchers have analysed the drawbacks of HT and suggested several methods to improve the accuracy and resolution.

The quantisation errors in both the image space and parameter space obviously affect the accuracy of straight line detection. Shapiro et al. [5] introduced graphical methods estimating HT performance for straight line detection in the presence of noise. They also demonstrated the effects of the quantisation errors on the accuracy of estimating the underlying set of collinear points. Veen et al. [6] analysed the influence of quantisation to the parameter and image spaces and the width of the line segments. It was reported that the accuracy of the HT was a function of the size of the cell ( $\Delta\rho$  and  $\Delta\theta$ ) and the width of the line segments. A method was proposed using a gradient weighting function in the transform to reduce peak scattering. Atiquzzaman et al. [7] stated that a spread of the peak will occur due to the quantisation of the parameter space when decreasing resolutions  $\Delta\rho$  and  $\Delta\theta$ . A non-iterative algorithm was proposed to detect straight line segments based on the analysis of HT data. This algorithm improves the efficiency of computing and obtains higher accuracy. Based on this algorithm, they also proposed another robust HT method [8] for the determination of the length and the endpoints of a line.

Other research focuses on the pre-treatment of HT data before the detection of the straight lines. Niblack et al. [9] reported a method to improve HT accuracy which smoothes the HT space prior to finding a peak location and interpolates this peak to find a final sun-bucket peak. Morimoto et al. [10] reported a high resolution HT based on a variable filter, in which the filter is designed and applied to the HT data before detecting the peak. Magli et al. [11]

proposed an algorithm based on interpolation and multi-scale matched filtering, in order to achieve high accuracy line detection from the HT.

The voting process is one of the hot topics that obtained intensive attention. Ji et al. [12] proposed a statistically efficient HT based on an analytical propagation of input errors. This method used a Bayesian probabilistic scheme to compute the contribution of each feature point to the accumulator. Thus, it improved accuracy and robustness. Shapiro et al. [13] summarised and proved the problem of discrete HT accuracy and adequacy to be the reason for the vote spreading problem. A non-voting Hough-Green transform was proposed to improve the accuracy of HT. Guo et al. [14] modified the HT voting scheme to suppress the impact of noise edges on the accumulation of votes in HT. They used surround suppression to assign the weights of votes for HT. This method improved the quality of detection results. Leandro et al. [15] presented an improved voting scheme for the HT that allowed a software implementation to achieve real-time performance, even with relatively large images. It improved the performance of the voting scheme and the robustness of HT.

The stochastic property of image space also raised concerns. A straight line segment recognising method was proposed using HT by Song et al. [16] This is reported as having the ability to overcome weaknesses when handling large-size images and being unaware of line thickness. Guo et al. [14] discussed the influence of the digital image space and proposed a method to improve the probabilistic HT by defining a suitable tolerance parameter as a function of  $\rho$  and  $\theta$ .

The structure of the parameter space is also considered. Cha et al. [17] developed an extension of the HT through a third parameter, the horizontal or vertical coordinate of the image space, to provide incremental information regarding the length of the lineal feature being sought. This method improved the accuracy of detection.

In this thesis, the nature and drawbacks of HT were analysed and summarised from a different point of view through experiments. Several ideas were generated to improve the accuracy and precision of HT, to achieve high resolution and to decrease the computation and memory requirements.

### 1.2.2 Progress on Decreasing the Computation Load and Storage Requirements

As the applications of straight line recognition obtained intensive attention, the computational cost and storage requirements became a concern.

According Eq. (1.2), the HT first transforms the feature points in the image space into sine curves in the parameter space. The parameter space is divided into an array of “accumulators”, and the accumulator receiving the largest number of votes along these curves is considered the peak. The position of the peak, that is,  $\theta$  and  $\rho$ , is used to interpret the dominant straight line in the image space. In this way, the HT requires large storage and computational requirements, which limit the applications of HT.

Therefore, methods to improve the detection speed and decrease the storage requirements in the HT process are being investigated. Avoiding unnecessary accumulators is the main method towards this goal. Li et al. [18] developed Fast HT (FHT) through an hierarchical approach. This approach divided the parameter space into hypercubes, from low to high resolutions. It performs the subdivision and subsequent “vote counting” only on hypercubes with votes exceeding a selected threshold. This greatly reduces both computation and storage. This method can also extend to more complex object detection. Illingworth et al. [19] introduced the Adaptive HT (AHT) for line and circle detection. This method used a small accumulator array and the idea of a flexible iterative “coarse to fine” accumulation. It utilised a search strategy to identify significant peaks in the Hough parameter spaces. The method increased efficiency and saved storage. Atiquzzaman et al. [20] addressed a multi-resolution implementation of the HT that reduced the computing time. Ben-Tzvi et al. [21] presented an algorithm for computing the HT using information available in the distribution of the image points, rather than depending solely on information extracted from the transform space. Hence, the processing of HT was calculated more efficiently.

Mapping only partial image space feature points to the parameter space is also helpful. Xu et al. [22] developed the Randomised HT (RHT) for detecting curves from a binary image. This method scans the binary image and obtains all of the feature points. Feature point pairs are then randomly selected from the image space and mapped to the parameter space. The method replaces the 1-to-n mapping in SHT. Its performance was analysed, [23, 24] and this demonstrated that the performance of the RHT was improved, and the speed

and storage requirements were reduced. Heikki et al. [25] wrote an overview on the comparison between probabilistic and non-probabilistic HTs and analysed some variants of the Randomised HT (RHT). They divided HT methods into two categories: probabilistic methods and non-probabilistic methods. An extension of the RHT method was proposed for high detection speed with low memory cost. Kiryati et al. [26] suggested an alternative approach to hasten HT computation. This method randomly selected a limited poll of feature points, rather than using full scale voting in the incremental stage of the HT. The method saved computation and improved accuracy. Gatos et al. [27] suggested a method to accelerate the detection of prevalent linear formations in binary images. An image is decomposed using rectangular blocks, and the contribution of each block to the HT space is evaluated, rather than the contribution of all the feature points in the image. Zhang et al. [28] presented a memory- and time-efficient HT algorithm for line segment detection. A set of small windows was used to determine the pairs of edge pixels. For each edge pixel, a window was defined, centring on this pixel. This method had two stages. Firstly, detecting line segments in each window and secondly, combining collinear and overlapping line segments into one.

Transforms in the parameter space are also reported. Ho et al. [29] outlined a fast and efficient method for the computation of the HT using Fourier methods. The maximum points generated in the Radon space, corresponding to the parameterisations of straight lines, can be enhanced with a post-transform convolutional filter. This can be applied as a 1D filtering operation on the re-sampled data in the Fourier space thus, further speeding up the computation. Additionally, any edge enhancement or smoothing operation on the input function can be combined into the filter and applied as a net filter function. Chung et al. [30] presented an affine transformation for line detection to improve memory utilisation and detection speed of the Hough space. This was based on slope intercept parameters.

### 1.3 Applications of HT

HT has been successfully used in various applications. It has the capacity to detect a wide spectrum of shapes such as straight lines, arcs, even arbitrary shapes, in computer vision and image processing.

A variety of extensions of HT have been investigated and applied in different fields. The HT has been widely used in medical imaging applications. Furen et al. [31] proposed a

procedure to measure midline shift by using HT to recognise the septum pellucidum within the given computed tomography (CT) study. Mauro et al. [32] used HT to detect special shapes in medical and astronomical images.

HT is also used in radar detection. Carlson et al. [33] proposed a method to track the target in multi-dimensional data space of the search radar. Moqiseh et al. [34] introduced a 3-D HT that detected linear trajectories in a 3-D data space of the radar.

HT is also helpful in agriculture to locate fruits. Eduardo et al. [35] detected the circular shape of berries using HT and obtained the position and radii of each berry. This algorithm serves as an automatic vision system that acquires images of wine grape clusters in the vineyard.

Several researchers used HT in other areas. Gao et al. [36] presented a method to detect dim manoeuvring targets using the Randomised HT. Pacey et al. [37] used HT to detect linear volcanic segments that constrained volcano distribution in the central Sunda Arc. Plob et al. [38] presented an approach to detect wavefront orientation with ultrasound-based flow measurement, using a modified HT. Davies [39] addressed an approach based on the Generalised HT for corner detection. This approach can locate corners of shapely defined metal objects, such as nuts and flanges, in industrial settings. Kang et al. [40] using HT, designed a method to detect corners in images.

## CHAPTER 2

# CRITICAL REVIEW AND PROBLEM

## DEFINITION

The HT suffers from a variety of problems stemming from its discretisation and voting processes. These seriously affect the performance of HT, regarding the resolution, accuracy, robustness, et cetera . It is commonly known that the discrete nature of the voting process causes peak generation problems in the HT space. These problems might split a peak into several peaks lying close to one another. It also possible for the peak to spread to several cells around the “true” position, causing the peak to be indistinct and hence, limit the accuracy of the HT. Different methods to improve the precision and resolution of the HT [4, 5, 7, 8, 16, 17, 41, 42, 43, 44, 45, 46] were reported. Most efforts focus on modifying the HT voting framework to increase the number of accumulators, in order to obtain higher precision and resolution. Another serious problem is uncovered and analysed in depth in this research, that is, the HT is sensitive to shifts of the input image. As a tool for object detection, it should be invariant to small shifts of the input image. A small shift of the input image should not lead to significant differences in HT data such as the height of the peak. However, because of the discretisation and rounding operations in the voting process, the output of the Standard HT (SHT) is very sensitive to minor input image shifts. For example, the peak height is affected quite considerably in this instance.

In this chapter, analysis based on the geometry principle of HT is intensively used to uncover the nature of HT problems and hence, inspire ideas for improvement. A critical review and analysis are the main components of this chapter. The following points will be discussed and demonstrated: (i) the robustness; (ii) the sources of the straight line detection errors; (iii)

the unreliability of image rotation and shift; (iv) the problems of votes splitting and peak flattening; (v) the difficulties for high resolution HTs. The problems of HTs will be critically reviewed and hence, the motivation for this research is derived. Some ideas emerging from the critical analysis are implemented in the later chapters of this thesis. These are the mean contributions of the research.

## 2.1 Expectations of HT

In existing literature, there are very few discussions regarding a rigorously theoretical framework for HT that consider performance, such as resolution, accuracy and robustness. This is the main barrier preventing HTs to be used as an object measurement tool rather than as an object detection tool. Shapiro [5] contributed to the relevant research by explicitly presenting the accuracy requirements of HTs as follows:

- Offset-independence. Straight lines collinearly shifted without distortion should yield equally high peaks in the parameter space.
- Isotropy. HT peak height should not depend on the straight line inclination.
- Discrete HT consistency as a measurement tool. Distance axioms should hold for measured line lengths. Specifically, for connected straight lines, the length should only depend on the distance between the endpoints and not on the line width.

Besides the requirements stated by Shapiro, [5] the following criteria are also critical for HT to be considered a measurement tool of straight lines and segments:

- Consistency between resolution and accuracy – Accuracy should increase with the increase in HT resolution.
- Appropriate high resolution – Sufficient resolution for a specific application should be available.
- Reliability independent to the resolution – The appropriate high resolution should not significantly affect the reliability of the geometric feature of the peak and its neighbourhood.

This thesis aims to uncover the gap between the expectations of HTs and the HTs themselves. Efforts are made to reduce this gap.

## 2.2 HT Problems

The main objective of HT is to divide the parameter space( $\rho, \theta$ ) into cells, where the size of each cell is  $(\Delta\rho, \Delta\theta)$ .  $\rho$  is the algebraic distance from the origin to a straight line and  $\theta$  is the angle between the normal and  $x$  axis. In this way, a feature point with coordinates  $(x, y)$  in the image space is mapped to a sinusoidal curve in the HT space. The curves corresponding to collinear points will intersect at a common cell, resulting in a peak on the accumulator matrix. Usually, the highest peak represents the most prominent straight line.

However, the Standard HT (SHT) suffers from a variety of problems stemming from its discretisation and voting process. [4, 5, 7, 8, 16, 17, 41, 42, 43, 44, 45, 46] Different methods were proposed to alleviate these problems. The HT voting framework was modified to increase the number of accumulators for higher precision and resolution. In fact, the discrete voting process is the main source of problems such as peak splitting (a peak is split into several peaks lying close to one another). The voting process also might spread the peak to several cells around the “true” position. These problems dim the peak and hence, affect detection accuracy and reliability.

In this thesis, the following HT problems are addressed:

### 2.2.1 The Precision Problem of Low Resolution HT

Lowering the HT resolution can alleviate the problems mentioned in section 2.2.2, but unfortunately with a loss of precision. For example, if the HT is applied to Fig. 2.1(a) with  $\Delta\rho = 1.5$  and  $\Delta\theta = 3$  respectively, the HT data obtained is as shown in Fig. 2.1(b). The problem of unreliability is greatly alleviated, that is, the only peak is more distinct and higher than the peaks shown in Fig. 2.1(d) to Fig. 2.1(f). However the ‘true’ straight line  $\rho = -10$ ,  $\theta = -63^\circ$  is detected as  $\rho = -10.62$ ,  $\theta = -63^\circ$ , where the  $\rho$  error is 0.62 pixel. This is not acceptable for certain applications such as remote sensing, in which a pixel represents a large area.

### 2.2.2 High Resolution HT Problems

It was recently demonstrated that the HT data around a peak, that is, the HT butterfly, could be used to derive a complete description of a line segment. [7, 46, 47, 52, 53, 54]. The butterfly features (width, intensity, orientation, uniformity, et cetera) are used to discover the parameters of a line segment. The resolution and reliability of the HT butterfly are hence, very important for the accuracy and the robustness of these HT butterfly- based techniques. However, the resolution of a traditional HT is limited by the vote spreading and peak splitting problems, which lead to unreliability in high resolution HTs. [5]. Resolution limitation is one of the main problems. If the  $\rho$  or  $\theta$  used is inappropriately high, the HT data suffers from unreliability. On the other hand, a low resolution HT presents low precision.

In practical image applications, resolution is very important. Occasionally high requirements of both resolution and precision are requested, which are mutually exclusive for the SHT. Fig. 2.1(a) shows a single-pixel-width straight line in the image space. Applying the high resolution SHT ( $\Delta\rho = 0.1$  and  $\Delta\theta = 0.1$ ) to this image, Fig. 2.1(c) shows a part of the HT data around the peak. It is obvious that several peaks appear in the HT data. The highest three peaks lie on  $(\rho = -11.5, \theta = -63.6)$ ,  $(\rho = -11.4, \theta = -63.3)$ , and  $(\rho = -10.7, \theta = -63.3)$  respectively. The heights of these peaks are very close, which leads to difficulties to determining the position of the “true” peak. The reason is that the fine quantisation of the HT space and the rounding operations during the voting process lead to the feature points simultaneously voting to several peak cells. This suppresses the height of the “true” peak and hence, the peak is not very distinct. Applying the SHT to Fig. 2.1(a) with different resolutions, the corresponding HT data obtained is shown in Fig. 2.1(d) to Fig. 2.1(f). It is clear that higher resolutions result in degradation of performance. Because of the discrete nature of the SHT, it is difficult to circumvent this problem.

Sharp distinct peaks are desired when mapping feature points from the image space to the HT space. Eq. (1.2) shows that collinear feature points in the image space correspond to a set of sinusoidal curves that intersect one another at a particular point in the HT space. In the computation, the HT space is sampled and represented as a discrete data structure, usually, as a 2-D array. If all the cells along these curves receive votes, then a peak exists in the accumulator array. Besides generating a peak, a butterfly-shaped spread of votes is also produced in the HT space. [47]. In fact, in the image space, a straight line is not usually smooth but split into horizontal or vertical short line segments in one of the grid directions.

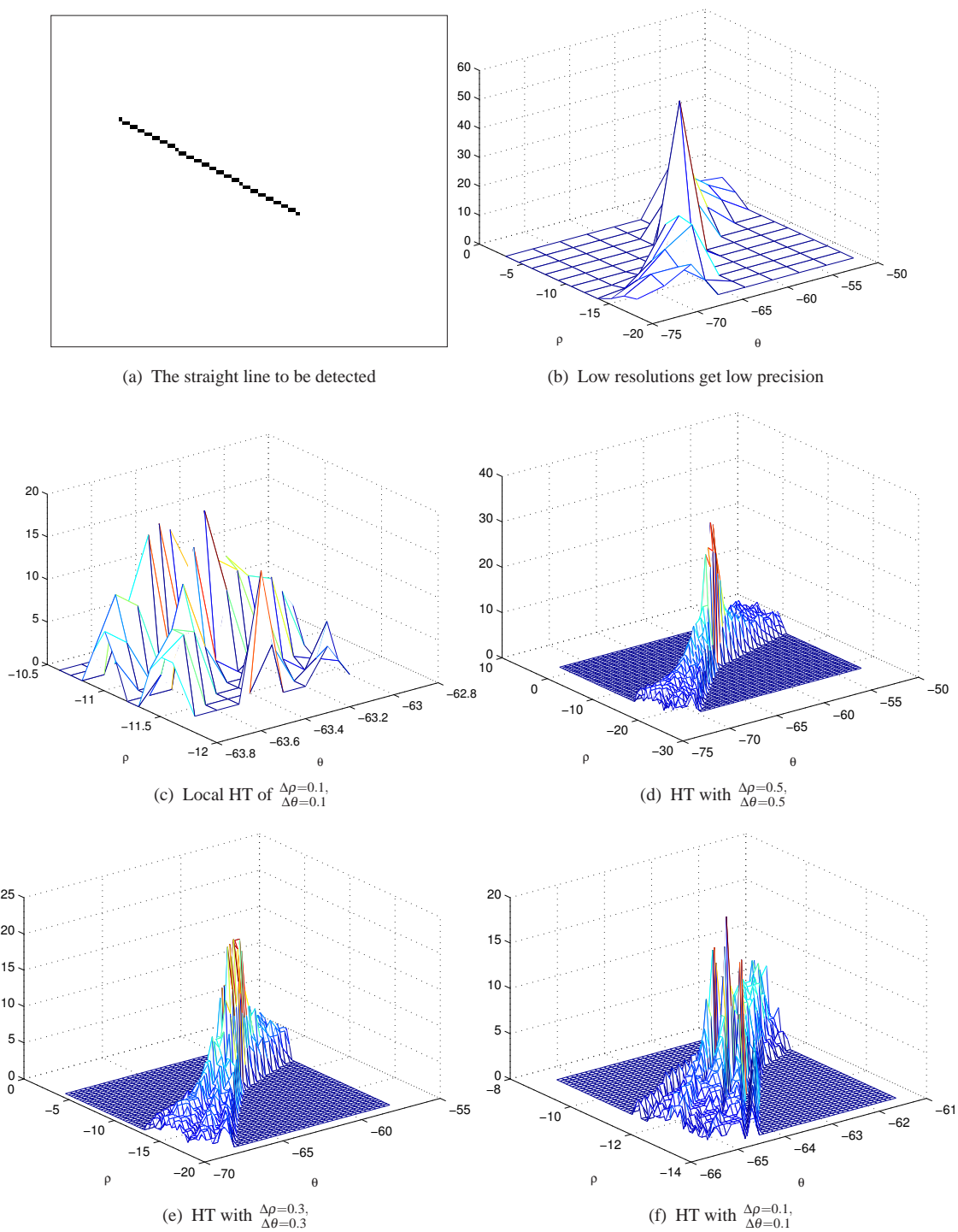


FIGURE 2.1: Unreliability of high resolution HT

This is shown in Fig. 2.2 where each square indicates one pixel. Quantisation and rounding operations in both the image and HT spaces result in HT voting and peak seeking errors. The inappropriately high resolution enlarges these errors and hence, makes the performances unacceptable.

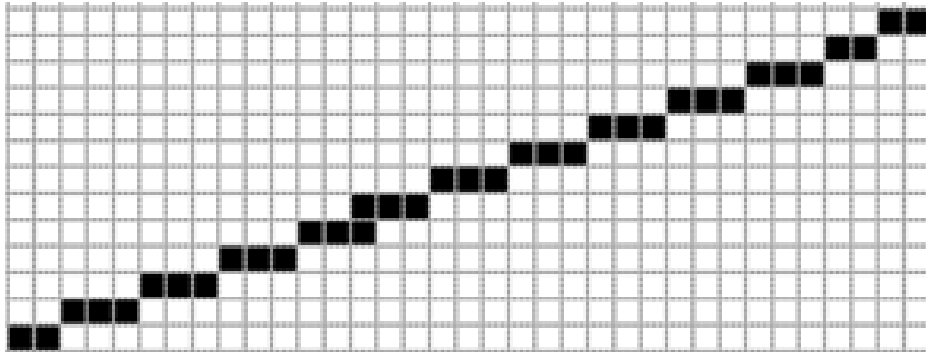


FIGURE 2.2: A straight line in a digital image

### 2.2.2.1 Inappropriate High $\rho$ -resolution ( $\Delta\rho$ ) Leads to Peak Splitting

When the straight line in an image is not  $\pm 45^\circ$ ,  $0^\circ$  or  $\pm 90^\circ$ , digital imaging technology approximates the straight line by using its nearest pixels. The inappropriate fine quantisation in the  $\rho$ -direction of the HT space will make these pixels vote to different straight lines and hence, two or more peaks will appear in the HT space, with each peak only receiving part of the votes. The example in Fig. 2.3 illustrates this problem. Fig 2.3(a) depicts how the straight line is represented by piece-wise horizontal short segments. Feature points of the straight line are in fact, contained in a bar with a specific width (denoted as  $d$  in the figure;  $d > 1$ ).

In the HT space, a cell corresponds to an infinite-length bar-shaped window at a distance  $\rho$  from the origin, of width  $\Delta\rho$ , and its normal making an angle  $\theta$  with the  $x$ -axis. In the image space, (Fig. 2.3(a)) if  $\Delta\rho$  is smaller than the line width  $d$ , feature points are separated into several bars (cells), resulting in several peaks in the HT space. For example, in Fig. 2.3(a), where  $\Delta\rho \leq \frac{d}{n}$  with  $n$  is a positive integer and  $n \geq 2$ , then the feature points of the straight line might generate at least two peaks, as shown in Fig. 2.3(b). The peaks may not lay close to one another, this causes difficulties in positioning the straight line, due to the position of its peak(s).

Another adverse effect of an inappropriately high  $\rho$ -resolution is the reduction of the peak height, since several other cells also share the votes from these feature points. The depressed peaks cause the straight line to be indistinctly represented in the HT space. As shown in Fig. 2.3(b), the peaks received four votes, even though the straight line had 36 pixels.

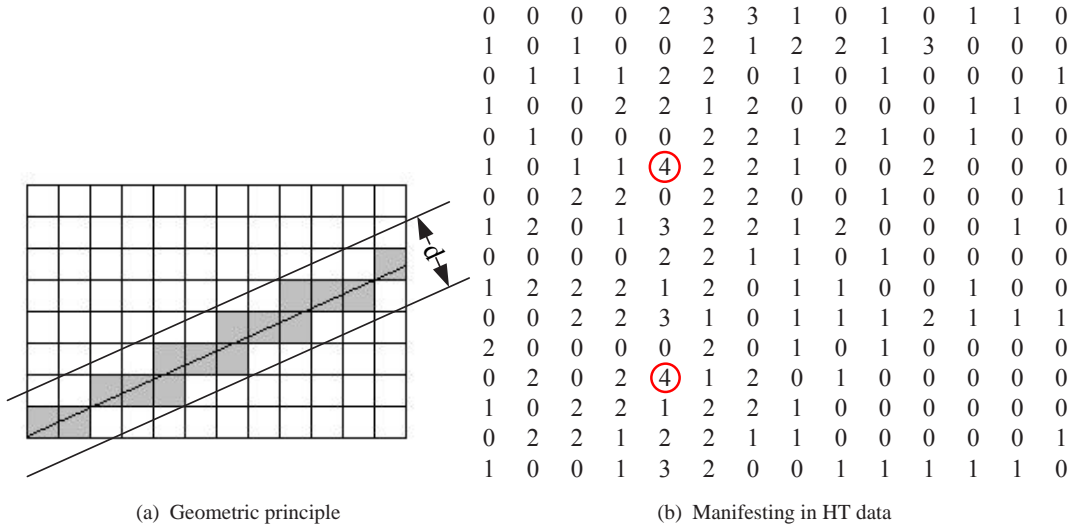


FIGURE 2.3: Inappropriately high  $\rho$ -resolution results in peak splitting

The peak-splitting problem severely affects the accuracy and reliability of the HT. However, a coarse quantisation of the HT space alleviates the problem since  $\Delta\rho > d$ , then one bar (corresponding to a cell in HT space) can contain all of the votes belonging to a line segment. This, however, comes at a loss in precision (accuracy).

### 2.2.2.2 Inappropriate High $\theta$ -resolution ( $\Delta\theta$ ) Leads to Peak Flattening

Even assuming that the straight line is continuous, that is, without any approximation errors in the image space, the HT still exhibits problems if the  $\theta$ -resolution is inappropriately high. To demonstrate this problem, two neighbouring bars  $(\theta_i, \rho_k)$  and  $(\theta_{i+1}, \rho_j)$  intersecting with a straight line are shown in Fig. 2.4(a). Their angles are  $\varphi_1$  and  $\varphi_2$  respectively, where

$$\varphi_1 + \varphi_2 = \Delta\theta. \quad (2.1)$$

If  $\varphi_1 = 0$  or  $\varphi_2 = 0$ , the straight line fully votes to the cell  $(\theta_i, \rho_k)$  or  $(\theta_{i+1}, \rho_j)$ . Otherwise it does not belong exclusively to any particular cell. If  $\Delta\theta$  is very small then the intersections

of the straight line with these neighbouring cells are so similar that all these bars get the same number of votes. This results in a plateau around the “true” peak, which makes the high  $\theta$  resolution HT valueless. Fig. 2.4(b) shows that every cell in a quite wide area in the  $\theta$ -direction of the HT space could be considered a peak. This causes difficulties when seeking the “true” peak to represent the straight line. This problem maybe not be so severe if  $\varphi_1 = 0$  or  $\varphi_2 = 0$ . However in the case of  $\varphi_1 \neq 0$  and  $\varphi_2 \neq 0$ , when the straight line is rather long, the problem may be more distinct.

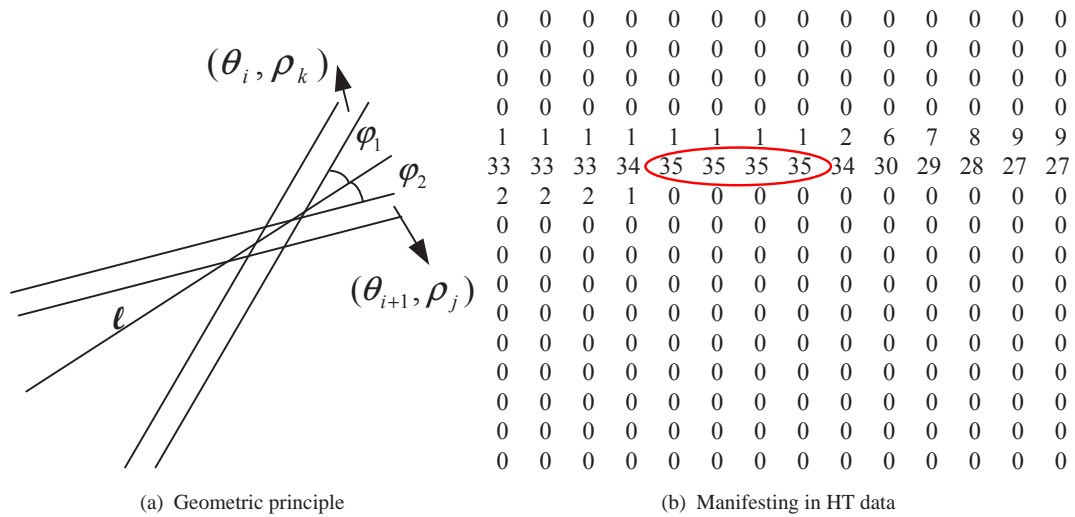


FIGURE 2.4: Inappropriate high  $\theta$ -resolution results in peak flatten

### 2.2.2.3 Inappropriate High Resolutions Result in Infeasible Peaks

When both  $\rho$ - and  $\theta$ -resolutions are inappropriately high, their adverse effects will combine as shown in Fig. 2.5. In fact the candidate line is considered as two dominant lines, because two independent butterflies are generated from the single straight line. This makes it difficult to determine which peak should represent the straight line. In this case even the method of filtering [11] cannot combine these peaks into a correct one. The methods of butterfly/peak enhancing [47, 48, 52, 53] are also ineffective in obtaining a distinct butterfly or peak, since each butterfly will be enhanced instead of combined.

Moreover, high resolutions lead to unacceptable computational load and memory storage requirements, as discussed in [5, 20].

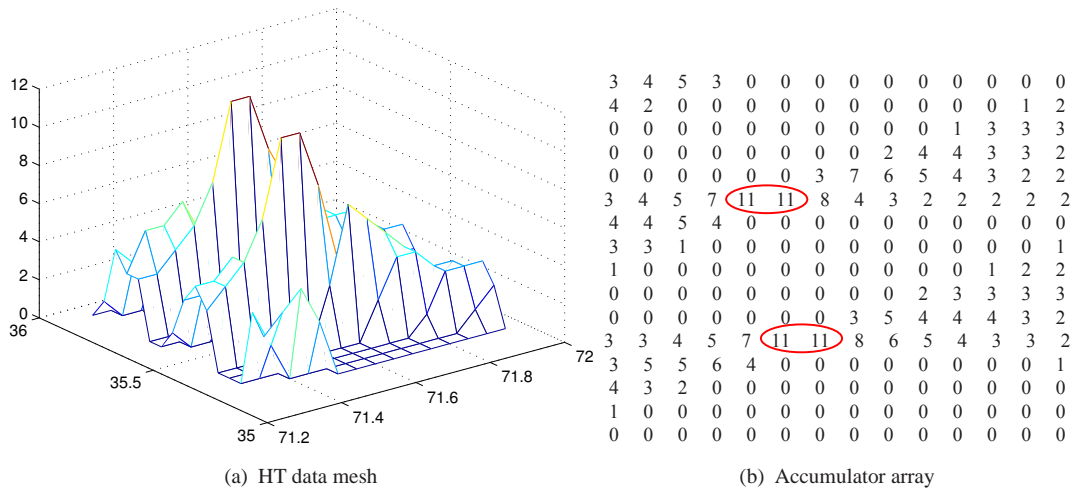


FIGURE 2.5: Inappropriate high resolutions results in unreliable peaks

## 2.3 Error Sources of HT

In HT, both the image space and the parameter space are discretised which introduces errors in the HT data. The image space discretisation errors are mainly manifested in the position biases of feature points (that is, the 1-pixels in the binary edging image), while the parameter space discretisation errors mainly affect the biases between the peak position and the “true” parameters of the segment. These errors are the main error sources of HT. Using a Bayesian scheme, Ji et. al [49] discussed how the input error, propagated to the detection error using Bayesian scheme. The following discussion will separate these errors and analyse how they affect the detection errors.

### 2.3.1 Discretisation Error in the Image Space

When an image is captured in digital imaging, the scene is divided into many square areas. Each of these square areas is stored as a pixel in the image. This process introduces discretisation errors in the image. For most digital image processing applications, the discretisation errors are unavoidable. In HT, these errors also seriously affect the quality of the generated HT data.

### 2.3.1.1 Pixel Position Errors

Generally, images are stored in the form of a pixel matrix. Pixels are usually considered as small squares connecting with eight neighbours, with four pixel-pair possible directions ( $0^\circ$ ,  $90^\circ$ , and  $\pm 45^\circ$ ). A straight line is composed of pixel-pairs with arbitrary angles that are approximated with available angles ( $0^\circ$ ,  $90^\circ$  and  $\pm 45^\circ$ ). This leads to biases in the pixel position. That is, the pixels composing a straight line are not always collinear. As shown in Fig. 2.6 the straight line segments are composed of various  $0^\circ$  and  $\pm 45^\circ$  pixel pairs when  $-45^\circ < \theta < 45^\circ$  (Fig. 2.6(a)), and  $90^\circ$  and  $\pm 45^\circ$  pixel pairs when  $\theta > 45^\circ$  or  $\theta < -45^\circ$  (Fig. 2.6(b)). Position errors due to this problem are common in almost all digital image algorithms and applications such as [42].

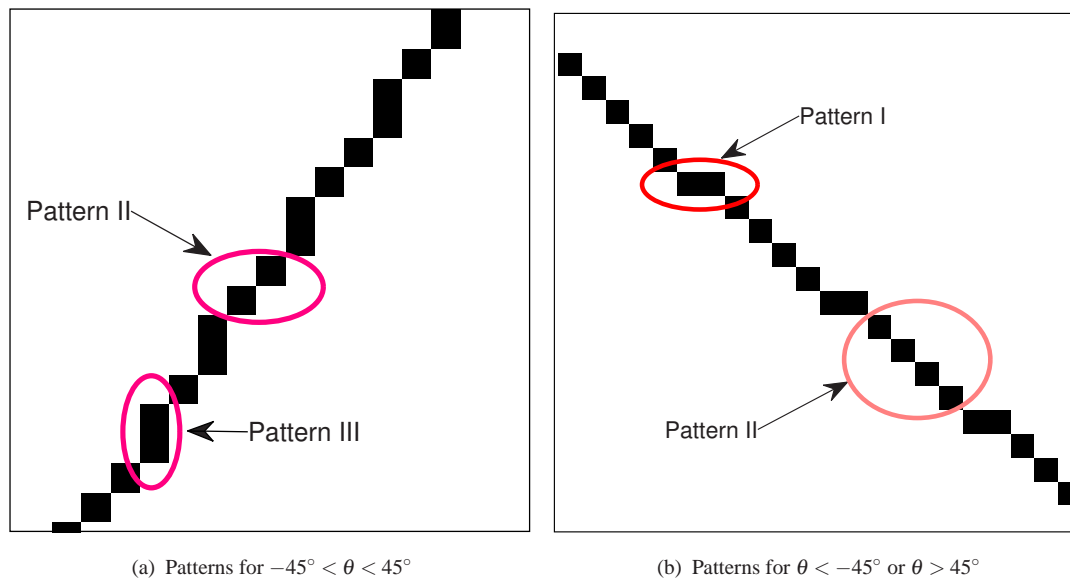


FIGURE 2.6: 3 patterns for digital images

### 2.3.1.2 Pixel Numbers vs. Length of Straight Lines

It would be desirable for the number of pixels to represent the length of the straight line. However, this is not always possible in digital images, since the pixels are considered small squares, and straight lines are composed of piece-wise horizontal and/or vertical segments. Only the length of the vertical and horizontal segments can be directly and accurately represented by their number of pixels. The number of pixels in all the other segments is approximately equal to the length of their projection in the horizontal direction (for  $\theta > 45^\circ$

or  $\theta < -45^\circ$ ) or vertical direction (for  $-45^\circ \leq \theta \leq 45^\circ$ ). Unfortunately, most HT methods, such as SHT, do not address this problem. This is the main obstacle when considering HT as a segment measurement tool.

### 2.3.2 Discretisation Error in the Parameter Space

In HT, the parameter space is quantified to a matrix of cells or a similar structure. In SHT, a matrix of cells represents the parameter space; and the RHT parameter structure is a binary linked list where each node (similar to a cell in SHT) represents a straight line. FHT uses a k-tree to represent the parameter space and each node is similar to a cell in SHT. The size of a cell or node is called the “resolution”. A series of angles (or slopes) is predefined, and for each feature point in the image space, these angles (or slopes) are substituted to Eq. (1.2) or its equivalent, in order to calculate the other parameters, such as  $\rho$  or intercept, the calculated values are rounded to a predefined grid point. Votes to the corresponding cells (or nodes) are counted. During this process, the predefined angles or slopes are accurate, but the calculated values are rounded to the nearest quantified cells or nodes. This rounding error is the main source of parameter space error, especially when the resolution is high (the size of a cell or node is very small). The image space position errors also negatively affect the parameter space errors. For example, in Fig. 2.7, the cell corresponding to the solid line bounded image area will obtain votes from the feature points contained in the area. However, considerable votes are missed because of the feature point position biases and rounding errors. This leads to low peaks even for long segments.

### 2.3.3 Sensitivity to Input Image Shifts

Another serious problem of SHT is addressed in this research, that is, the HT is sensitive to small shifts of the input image. As a tool for object detection, it should be invariant to small shifts of the input image. That is, a small shift of input images should not lead to a significant difference in the HT data. However, because of the discretisation and rounding operations in the voting process, the output of the Standard HT (SHT) is very sensitive to minor input image shifts. For example, the peak height is affected quite considerably.

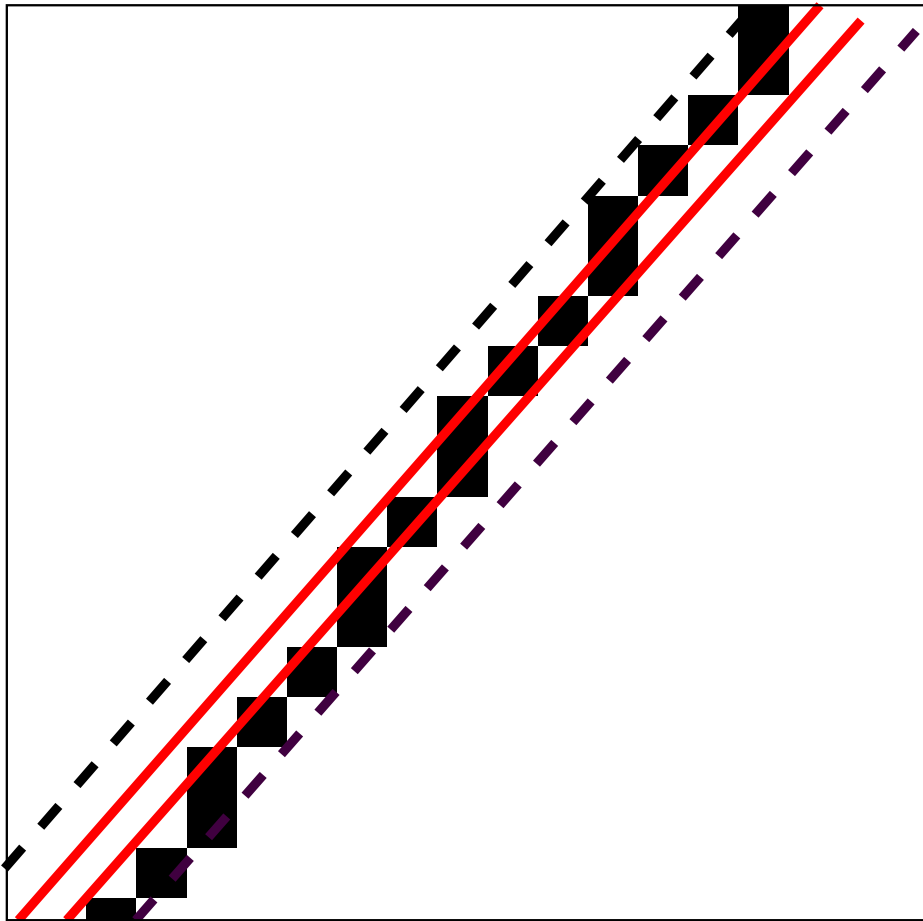


FIGURE 2.7: The discretisation error in the parameter space

For an image containing a synthetic straight line, the peak heights detected by a SHT with  $\Delta\rho = 1, \Delta\theta = 1$  are shown in Figs. 2.8(a) and 2.8(b), when the image is shifted pixel by pixel. Theoretically, these differences should only shift the peak by 1 HT cell at most if the image is shifted by one pixel, these differences should only shift the peak by one HT cell at most, and the height of the peak (in most cases representing the number of pixels lying on the straight line) should be similar. However, the peak heights shown in Figs. 2.8(a) and 2.8(b) change quite distinctly with minor shifts of the input image. It is therefore, reasonable to expect that the number of votes obtained by the cells around the peak is also considerably by the shift of the image, because the voting process does not distinguish the peak from the other cells. This means the global SHT output is sensitive to the shift of the input image. This does not only occur with synthetic images. Fig. 2.9 illustrates an example of a real image, where the HT peak of the most dominant straight line is considered. Figs. 2.9(c) and

**2.9(d)** demonstrate similar features to the example of the synthetic image shown in Fig. **2.8**.

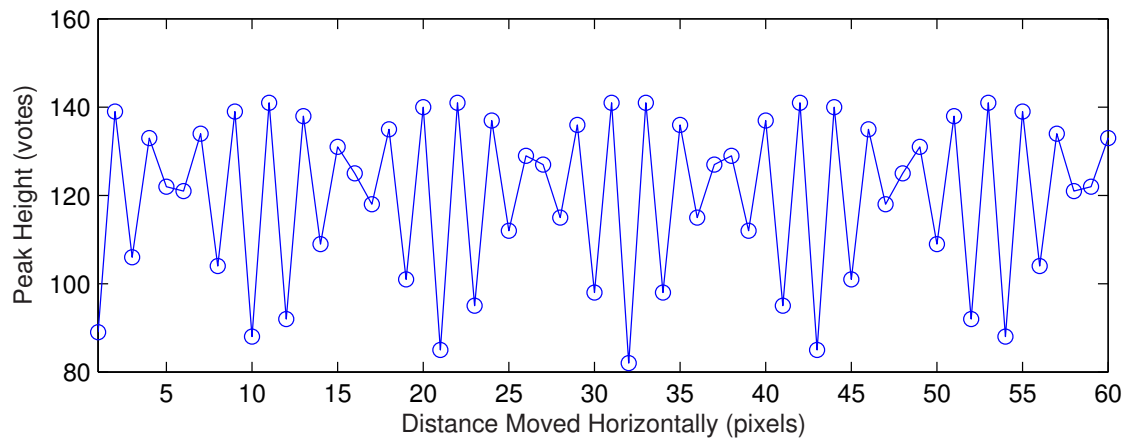
In the situation of two images containing the same scene but with minor shift, the outputs of the SHT for each are quite different, and it is difficult to state that one output is more correct than the other. Therefore, this sensitivity degrades the reliability of SHT because the positions of the feature points are randomly located for a given image. That is, straight lines can locate at any position in the image. The reason for the sensitivity is that shifting the image leads to the rearrangement of the feature points in the rounding operations and the voting process. That is, the votes of the feature points are re-split and re-rounded, according to their new positions and hence, new sub-pixel information is generated.

Another interesting feature depicted in Figs. **2.8(a)**, **2.8(b)**, **2.9(c)** and **2.9(d)** is pseudo-periodicity, that is, similar peak heights can be expected to by shift the image by a fixed number of pixels. This means it is not necessary to enumerate all possibilities of shifting an image to obtain enough “new” information for high resolution HT data reconstruction. The low resolution HT data frames (denoting the HT data obtained from a single shifted image as a frame) within one “period” contain most of the “new” information generated by shifting the input image. This is valuable for the super-resolution reconstruction of high resolution HT data from low resolution HT data frames.

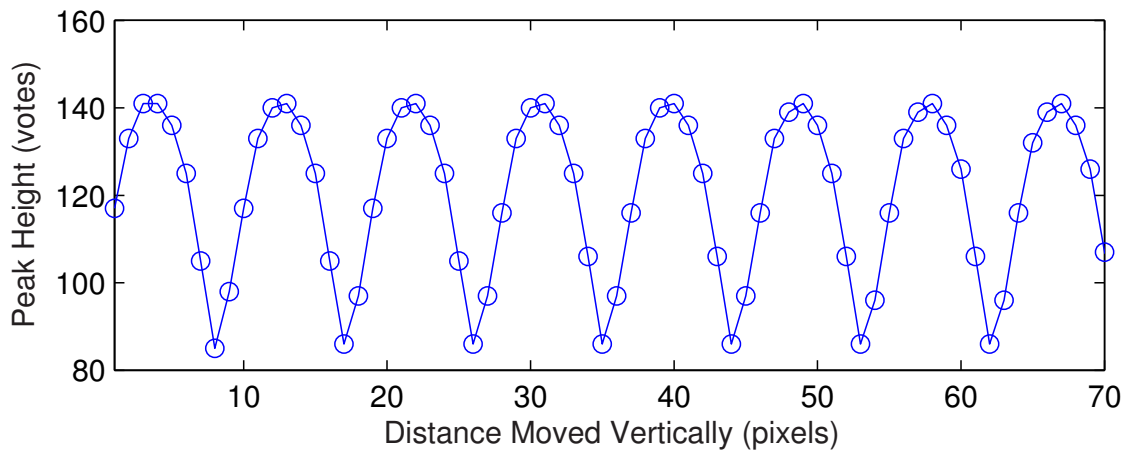
## **2.4 HT Butterflies are More Meaningful than the Peak**

In the HT, each feature point  $(x,y)$  of a straight line is mapped to a sine curve via (1.2). By discretising the parameter space by resolutions  $\Delta\theta$  and  $\Delta\rho$ , an array of accumulators (cells) is generated with each cell corresponding to a belt in the image space. During the voting process, not only is the peak generated, but also a large area is also built, composed of curves corresponding to all the feature points of the straight line. By considering the area around the peak, a butterfly shape area (denoted by HT butterfly in this thesis) is obtained.

Due to errors arising in the digital imaging and voting process, [6], HT peaks are not robust. For instance, the peak position, especially the height of the peak, has considerable biases from the “true” values, which degrades the HT peak as a measure of the segment length [5]. Fortunately, the butterflies are more robust to noise and the aforementioned errors because the segment parameters are manifested by a group of cells, instead of a single cell representing



(a) Peak height changes with the image horizontally shift



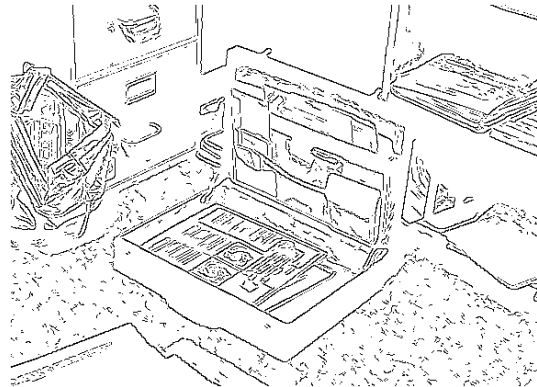
(b) Peak height changes with the image vertically shift

FIGURE 2.8: The case of a synthetic line

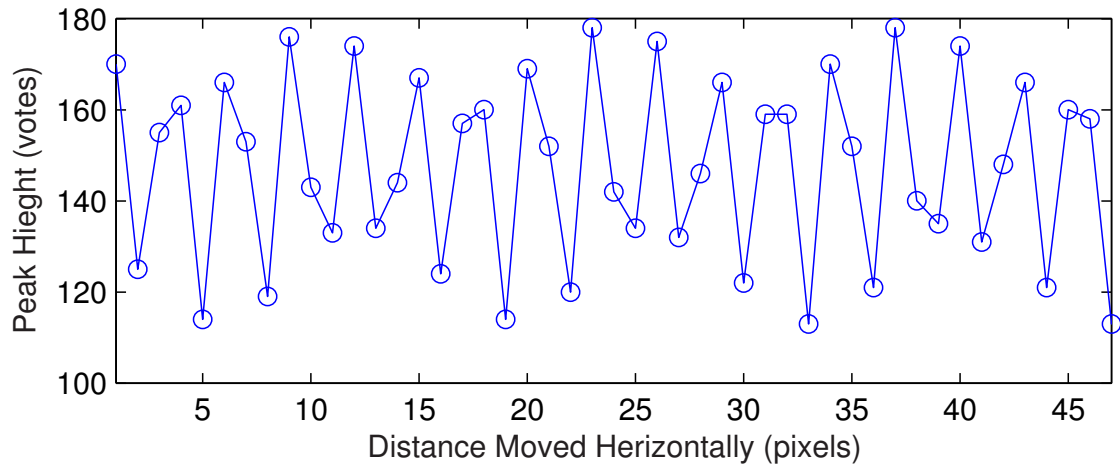
the peak. [41, 50] The results from a variety of applications demonstrated that HT butterflies provide more detail of the segments, such as the length, the position of the endpoints, the width and the smoothness (uniformity). These are not achievable if only the HT peaks are used. Due to this fact, various HT butterfly based segment detection methods were proposed, [7, 8, 41, 50, 51, 52, 53] with the aim of obtaining a robust and high resolution butterfly. [41, 50, 51, 52, 53] However, it is known that SHT high resolutions might lead to problems such as peak splitting, flattening [5] and high computation load. [45], Therefore, reliable high resolution butterflies cannot be obtained by simply increasing the resolutions of SHT. Acquiring reliable high resolution butterflies is still a problem, with little success reported.



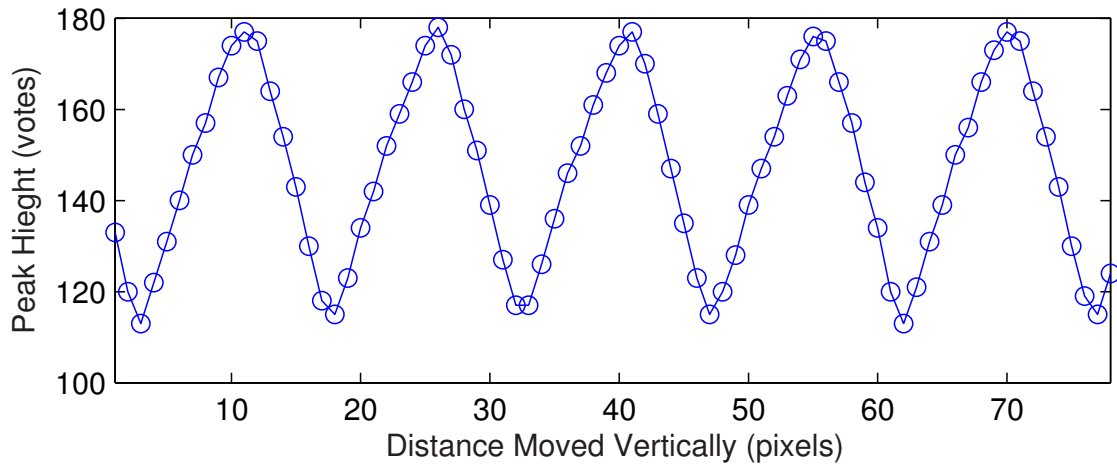
(a) Briefcase



(b) Edges of briefcase



(c) Peak height changes with the image horizontally shift



(d) Peak height changes with the image vertically shift

FIGURE 2.9: The case of a real image

## CHAPTER 3

# CONTRIBUTIONS TOWARDS SOLVING THE HT PROBLEMS

This thesis focuses on the HT butterflies rather than the global HT data. In this thesis various ideas are proposed and implemented to improve the resolution, accuracy and computational load.

### 3.1 Criteria of HT Resolution Selection

As discussed in Sections 2.2 and 2.3, the detection error is closely related to the resolutions. Desirable resolution selections are determined by the straight parameters, and this makes it complex to select a suitable resolution when different objects are to be detected in images. The research problems of whether the best resolutions for a straight segment exist, and which factors determine the best resolutions are discussed. Experiential criteria of resolution selection are depicted in this thesis.

### 3.2 Self-similarity of the HT Butterfly

In the situation of zooming into the centre of an HT butterfly by applying the appropriate higher  $\rho$ - and  $\theta$ -resolutions (keeping the ratio of  $\frac{\Delta\rho}{\Delta\theta}$ ), similar butterflies are found if the dimensions are ignored. That is, if an accumulator matrix is given without dimensions, then the resolutions used to generate the data are unknown.

This scale-free property of HT butterflies, initially discovered in this research, is called self-similarity. This interesting self-similarity is demonstrated using geometrical analysis. Based on this scale-free property, a simple method is proposed to obtain very high resolution and a very reliable HT butterfly, without the adverse effects of vote spreading and peak splitting.

### 3.3 Super Resolution Method

Due to the sensitivity of the HT butterflies on the image shifting, as explained in Section 2.3.3, it became apparent that “new information” in the HT data is generated during this shifting process and the consequent HT operations on the shifted images. To reconstruct a higher resolution HT butterfly by making use of this “new information”, a super resolution reconstruction method, based on iterated back-projection, is proposed. High resolution HT butterflies are obtained from low resolution HT data sequences. Details of the steps to implement the proposed method are discussed, such as generating/observing multiple low resolution HT frames, registering cells, converting between low and high resolution HT frames, et cetera. A constrained function is employed in our iterative algorithm to guarantee non-negative votes. The proposed method aims to conquer HT resolution and precision problems.

### 3.4 Extend Resolution in HT Butterflies through Geometry Analysis

Geometry Principles of HT show the relationship between the low and high resolution HT data. Based on this relationship, a method is proposed to obtain high resolution HT butterflies directly from a single low resolution HT butterfly. These high resolution HT butterflies are obtained without the problems, such as peak splitting and flattening, caused by the inappropriate high resolution settings of Standard HT (SHT). Compare with the self-similarity method, this idea frees the high resolution HT butterflies from the fixed ratio of resolutions ( $\frac{\Delta\rho}{\Delta\theta}$ ).

### 3.5 Error Compensation for Straight Line Detection

Since the HT space is discretised with given resolutions, the positioning error is generated when the  $\rho$  value of a line is not equal to  $n\Delta\rho$  ( $n$  is a nonnegative integer). This is very common if the straight line is not vertical ( $\theta = 0^\circ$ ) or horizontal ( $\theta = \pm 90^\circ$ ). This error is omitted during the voting process and hence, it is unknown if the straight line is detected by seeking the peak. In the example of a straight line that is not vertical or horizontal, if the image is shifted by one pixel in the  $x$ - or  $y$ - axis then the  $\rho$  value of the line will be changed by an amount less than one pixel. The exact value of the change can be obtained by simple geometric analysis. The  $\rho$  value of the shifted line is composed of three parts: (i) the  $\rho$  value of the original line detected by seeking the HT peak ( $\rho_0^{\text{HT}} = n\Delta\rho$ , which is known); (ii) the detection error of the original line ( $e_{\rho_0}$  which is unknown); (iii) the change in the  $\rho$  value due to the shift ( $\delta\rho$  which is known). By employing HT on the shifted image, a new discretisation error is generated for the shifted line if the third part is not equal to the integer times of  $\Delta\rho$ . The new detection error is derived, and it is relevant to the one before shifting. After shifting the image times, a chain of detection errors is obtained. Based on the analysis of this error chain, the estimation of  $e_{\rho_0}$  is derived. A high-precision line positioning method is proposed by compensating for the estimated detection error.

### 3.6 Ideal HT: One Useful Tool to Evaluate the HT Butterflies

Because the HT butterflies contain important information regarding straight lines in the image, the quality of HT butterflies is critical for detecting these objects. The resolution settings, the various methods for HT butterfly generation and the straight line parameters have considerable impact on the butterfly quality. However, very few criteria for butterfly qualification evaluation are reported in existing literature. This research addresses the “ideal” HT data calculation, which is independent of the HT methods, digital discretisation errors in the image space and errors due to the voting and verifying processes. The generated HT data is dependent only on the physical facts, that is, the endpoints of the segment. The ideal HT data can be employed to evaluate the data generated by the HT varieties. Given a specific

segment detection method, the ideal HT data may also be used to evaluate the performance improvement potential.

## **Part II**

# **EFFORTS FOR ENHANCING THE HT**

Part II focuses on improving the performance of HT. Due to the digitalisation error of images and the discretisation error of HT, the resolution limitation is a considerable constraint for SHT when employed in actual applications. Inappropriately high  $\rho$ - or  $\theta$ - resolution leads to unreliability of the HT data. Conversely, a low resolution HT results in runs on low precision.

This research on the improvement of the HT performance includes the following aspects:

- How to select “good” resolutions for HT;

The “good” resolution is defined, followed by the study the relationship between the straight line detection errors and HT resolutions ( $\rho$ - and  $\theta$ - directions). The inflexion of the error-resolution curve is uncovered. To study the location of the inflexion comprehensively, the effects of several factors are considered, such as the positions ( $\rho$  and  $\theta$ ), the widths and lengths of straight segments, noise level and the ratio of resolutions. An error surface, according to  $\rho$ - and  $\theta$ - resolutions, is obtained to guide the search for the best resolutions. The area containing “good” resolution settings is uncovered and modelled.

- Improvement of the resolution by geometry analysis

SHT is based on simple and clearly defined geometrical mapping, that is, the conversion between the rectangular coordinate system and the polar coordinate system. The HT data has well-defined geometric meanings in both the image space and the parameter space. This property makes it possible to improve the resolution using geometry analysis on the HT data.

- Observations show that accumulator arrays (butterflies) in the parameter space exhibit self-similar properties. This is theoretically proved through geometry analysis. A very high resolution HT is proposed based on this property. This method reliably overcomes the peak splitting and vote spreading problems associated with traditional high resolution HTs.
- The relationship between the low and high resolution HT data is derived from the geometric principles of SHT. Based on this relationship, a method is proposed to obtain high resolution HT butterflies directly from low resolution HT data. The high resolution HT butterflies are obtained without the problems caused by infeasible high resolutions, such as peak splitting and flattening.

- Super resolution method.

Super resolution (SR) techniques are successful for normal optical images, such as surveillance videos and satellite images. However, the techniques have never been considered for the improvement of the resolution of HT data. In fact, multiple HT data frames can be easily obtained by shifting the original image. Super resolution HT data might be constructed, based on these frames. In this research, the generation of “new information” in multiple HT data frames, the difference between HT data frames and normal optical images, the specific cell registration and the conversion between high and low resolution frames are considered. A Super Resolution HT (SRHT) is proposed.

- A high precision line positioning method based on HT detection error compensation

The accuracy of HT is been considered as a common concern [5, 6, 11, 12, 26, 43, 54, 55, 57, 58, 59] because of discretisation. Given the HT resolutions, the positioning error is generated when the  $\rho$  value of a line is not equal to  $n\Delta\rho$  ( $n$  is a nonnegative integer). This is prevalent in straight line detection if the straight line is not vertical ( $\theta = 0^\circ$ ) or horizontal ( $\theta = \pm 90^\circ$ ). This error is omitted during the voting process and hence, it is unknown in detection of the straight line by seeking the peak. For a straight line that is not vertical or horizontal, if the shift is one pixel in the  $x$ - or  $y$ -axis, then the change in its  $\rho$  value will be smaller than one pixel (the exact value of the change can be calculated through simple geometric principles). The  $\rho$  value of the shifted straight line is composed of three parts: 1. the  $\rho$  value of the original line detected by seeking the HT peak ( $\rho_0^{\text{HT}} = n\Delta\rho$ , which is known); 2. the detection error of the original line ( $e_{\rho_0}$ , which is unknown); 3. the change of  $\rho$  value due to the shift ( $\delta\rho$ , which is known). By employing HT, a new detection error is generated for the shifted straight line, if point 3 is not equal to the integer times of  $\Delta\rho$ . This means the detection error of the shifted straight line has some relationship with the error of the original straight line. If the straight line is shifted many times, a chain of detection errors results. These detection errors are unknown, but the detected values provide a clue to estimate the errors. In this research, it was discovered that the chain of detection errors is an increasing/decreasing arithmetical series. Furthermore, a method to estimate  $e_{\rho_0}$  by studying the detected  $\rho$  value of shifted straight lines was derived, and a high-precision line positioning method proposed.

## CHAPTER 4

# GOOD RESOLUTIONS FOR HT

For straight line detection, the parameter space is represented by a matrix of cells with the resolutions in  $\theta$ - and  $\rho$ - directions, that is,  $\Delta\theta$  and  $\Delta\rho$  respectively. The setting of resolutions received intensive study recently with much research proposed on collinear segment detection[41, 50], high accuracy [9, 53], high precision[51], nonuniform quantisation [43, 49, 57] et cetera. It is shown that this quantisation leads to compromised; finer  $\rho$  quantization, that is, higher precision with regards to  $\rho$  is paid with the decreased robustness. [5] Zhang [58] determined the resolution  $\Delta\rho$  in the  $\rho$  direction considering the digitisation of the spatial domain, and then calculated the resolution  $\Delta\theta$  based on the length of the straight line  $l$  and  $\Delta\rho$ . The nonlinear relationship between  $\Delta\rho$  and  $\Delta\theta$  was studied and a non-uniform quantisation on the  $\rho$  direction was proposed in [42], where  $\Delta\rho$  was determined according to the value of  $\theta$ .

It is commonly accepted that the detection error is closely related to the resolution, and therefore, desirable resolutions are determined by the object parameters. This makes it complex to select a suitable resolution with different objects in images. The research problems of this chapter are “whether the *best* resolutions exist for a straight segment” and “which factors determine the best resolutions.”

This chapter demonstrates the relationship between straight line detection errors and resolutions ( $\rho$ - and  $\theta$ - directions) and then uncovers the inflexion of the error-resolution curve. To study the location of the inflexion comprehensively, the effects of several factors are considered, such as the positions ( $\rho$  and  $\theta$ ), the widths and lengths of straight segments, the noise level, and the ratio of resolutions. An error surface according to  $\rho$ - and  $\theta$ - resolutions

is obtained in this research, in order to guide the research the best resolutions. The area containing “good” resolution settings is uncovered and modelled.

## 4.1 What are “Good” Resolutions of HT?

The principle of HT is to map the image space feature points to the parameter space and build a peak for a certain pattern. Therefore, a distinguishable peak is a very important criterion for whether the resolution setting is “good” or not.

*Definition 1 (“Good” resolutions).* A “good” resolution setting should build a peak for a certain patten, satisfying the following criteria:

1. A distinguishable peak exists for a certain pattern only.
2. The cell corresponding to the peak should obtain the most possible votes from the feature points of the certain patten.
3. The cells around the peak should obtain the least possible votes from the feature points of the certain patten.

As shown in Fig. 4.1, there is a segment in the image space with length  $l$  and width  $w$ , centred on the straight line  $(\theta_0, \rho_0)$ . Assuming the cell  $(\theta_i, \rho_j)$  is the peak, then the resolution setting is “good” only if the image space belt corresponding to the peak  $(\theta_i, \rho_j)$  contains the most possible feature points of the segment, and the belts corresponding to the other cells around the peak, such as  $(\theta_{i-1}, \rho_j)$  and  $(\theta_i, \rho_k)$ , contain the least possible feature points of the segment.

*Definition 2 (The “best” resolutions setting).* The “best” resolution setting is the “good” resolution that has the smallest detection error.

Assume the resolutions of HT in  $\theta$ - and  $\rho$ -direction are  $\Delta\theta$  and  $\Delta\rho$  respectively. Let  $V_{i,m}$  denote the maximum voting values in column  $i$  of the parameter space, that is the column corresponding to  $\theta_i = i\Delta\theta + 90$ .  $n_{i,m}$  denotes the number of cells in column  $i$  obtaining the

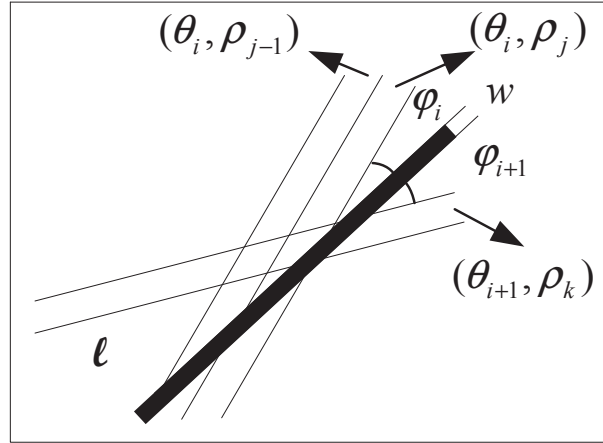


FIGURE 4.1: The best resolution setting of HT.

maximum voting values  $V_{i,m}$ . Therefore,  $n_{i,m}$  is the number of peaks if the column  $i$  contains the global maximum voting cell(s). By geometry analysis, one finds that

$$V_{i,m} = \begin{cases} \frac{w\Delta\rho}{\sin\varphi_i}, & l \sin\varphi_i \geq \Delta\rho \\ lw, & l \sin\varphi_i \leq \Delta\rho, \varphi_i < \tan^{-1} \frac{w}{l}, w < \Delta\rho \\ l\Delta\rho, & l \sin\varphi_i \leq \Delta\rho, \varphi_i < \tan^{-1} \frac{w}{l}, w \geq \Delta\rho \\ lw, & l \sin\varphi_i \leq \Delta\rho, \varphi_i \geq \tan^{-1} \frac{w}{l} \end{cases} \quad (4.1)$$

and

$$n_{i,m} \leq \begin{cases} \lfloor \frac{l \sin\varphi_i}{\Delta\rho} \rfloor, & l \sin\varphi_i \geq \Delta\rho \\ 1, & l \sin\varphi_i \leq \Delta\rho, \varphi_i < \tan^{-1} \frac{w}{l}, w < \Delta\rho \\ \lfloor \frac{w}{\Delta\rho} \rfloor, & l \sin\varphi_i \leq \Delta\rho, \varphi_i < \tan^{-1} \frac{w}{l}, w \geq \Delta\rho \\ 1, & l \sin\varphi_i \leq \Delta\rho, \varphi_i \geq \tan^{-1} \frac{w}{l} \end{cases} \quad (4.2)$$

where  $\varphi_i = \theta_i - \theta_0$ .

Since the  $\theta$  value of  $(\theta_i, \rho_j)$  is possibly slightly different to the “true”  $\theta$  value of  $l$ , in order to satisfy criterion 2 of “good” resolution, that is containing the most possible feature points of the segment, the belt must have enough width ( $\Delta\rho$ ). However, a big  $\Delta\rho$  results the belts corresponding to the cells around the peak  $(\theta_i, \rho_j)$  to also contain considerable feature points of the segment which disobey criterion 3. This means the  $\rho$ -resolution cannot be too high or too low. It is similar when the  $\theta$ -resolution is considered. when  $\Delta\theta$  is high, the difference between  $\theta_i$  and the “true”  $\theta$  value of  $l$  can be substantial, and it is therefore, difficult to satisfy criterion 2. However, a low  $\Delta\theta$  leads to the difference of  $\theta_{i+1}$  being slight which results the

cells around the peak obtain high votes, thus, disobeying criterion 3. A low  $\Delta\theta$  also might disobey criterion 1, that is several peaks appearing around the peak in the direction of  $\theta$ .

From the above discussion, it is clear that resolution settings that are “better” than others for a given pattern must exist. The following sections focus on demonstrating the existence of “better” resolution settings and seeking the factors that determine the “good” resolution settings.

## 4.2 Inflexion of Error-Resolution Curves

It is clear that low resolutions for the Standard HT (SHT) detects the straight segments with low precision, and with an increase in the resolutions, the detection precision is improved. However, inappropriately high resolutions lead to the problems of robustness reduction, vote spread and peak splitting and hence, increases the detection error. Therefore, an inflexion on the error-resolution curve should exist when the resolutions increase to infeasible values. The inflexion indicates a “good” resolution value with a small detection error. This section aims to study the existence of the inflexion and the factors that affect the inflexion when a series of resolution settings are applied.

Various images containing straight segments with various parameters, such as the length, the width and the  $(\rho, \theta)$  values are considered. Series experiments are implemented with difference resolution settings and the detection errors are recorded. Each error-resolution curve has similar features as shown in Fig. 4.2 (the resolutions are  $\Delta\theta = 0.1^\circ, \Delta\rho = 0.1, 0.2, \dots, 2$ ), where the detection error initially decreases with the decrease of  $\Delta\rho$ , and then increases after a certain point. A global minimum and several local minimums exist on the curve. The resolution corresponding to the global minimum is considered as the inflexion. Obviously, it is valuable if the inflexion is known before HT is employed. The following section aims to study the factors that affect the inflexion.

## 4.3 The Factors Affecting the Inflexion

Eqs. (4.1) and (4.2) demonstrate that the peak in an HT space is related to the parameters of a segment, that is, the  $\rho_0, \theta_0, w$  and  $l$ . The inflexions on error-resolution curves, according

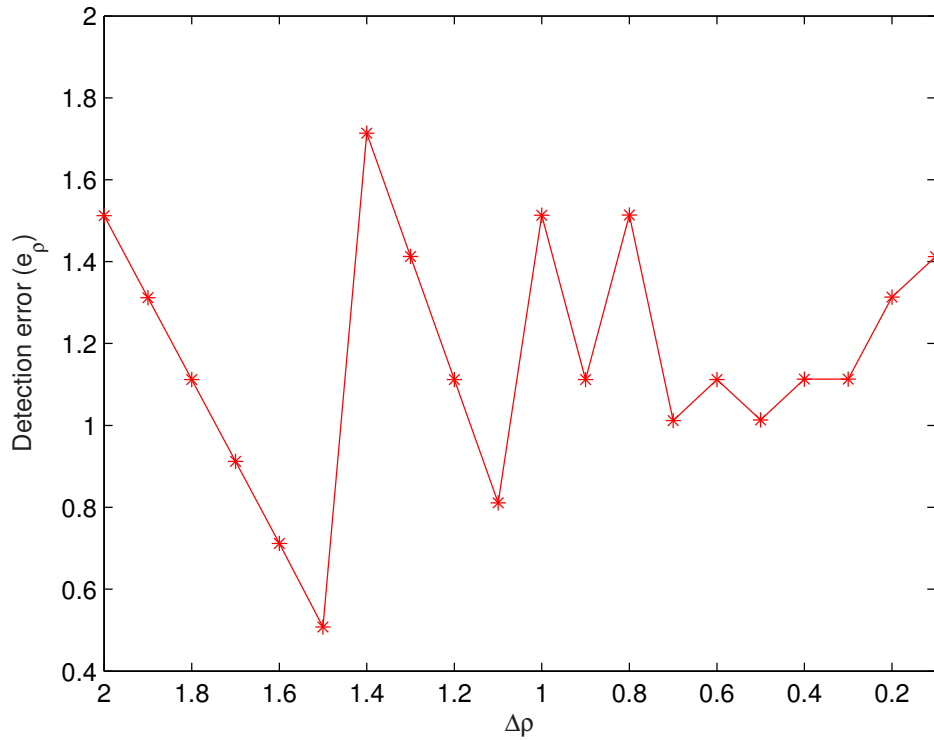


FIGURE 4.2: The inflexion on error-resolution curves.

to the changes of these factors, are considered.

### 4.3.1 The Effect of the Straight Segment Position ( $\theta_0$ and $\rho_0$ ) on the Inflexion

To study the effect of  $\rho_0$  on the inflexion, SHT is implemented to a series of images containing a single segment having the same  $\theta_0$ ,  $w$  and  $l$ , but different  $\rho_0$ . Various settings of  $\Delta\rho \in [0.001 \quad 1]$  and  $\Delta\theta \in [0.001 \quad 1]$  are employed. The detection error corresponding to every  $\Delta\theta$  and  $\Delta\rho$  combination is recorded. Fig. 4.3 shows the inflexions of the curves corresponding to the combinations of resolutions ( $\Delta\theta = 0.1^\circ, \Delta\rho = 0.1, 0.2, \dots, 2$ ) crossing the images containing segments  $\rho_0 \in [30 \quad 120]$ . Fig. 4.3 shows that the change of  $\rho_0$  does not affect the inflexion.

Fig. 4.4 demonstrate the inflexion on curves  $\Delta\theta = [0.1^\circ, \dots, 1^\circ], \Delta\rho = [0.1, 0.2, \dots, 5]$  while  $\theta_0$  changes from  $20^\circ$  to  $80^\circ$ .

Fig. 4.4 shows that the inflexion is not affected by the change of  $\theta_0$ .

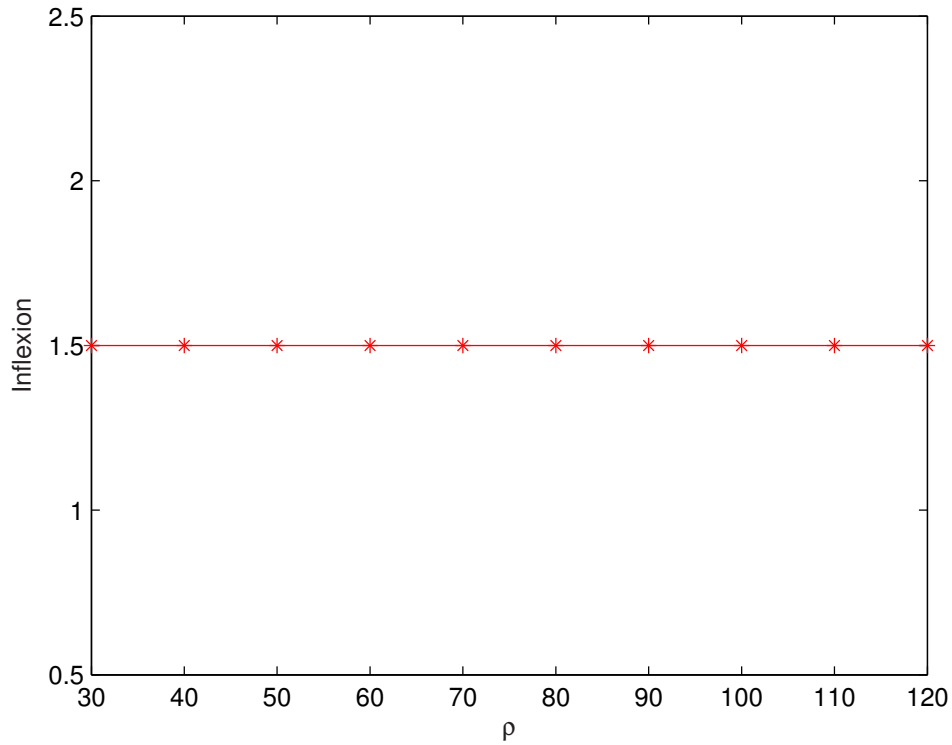


FIGURE 4.3:  $\rho$  value of straight segments does not effect on the selection of best resolution

Figs. 4.3 and 4.4 demonstrate that the position of straight segments ( $\rho_0$  and  $\theta_0$ ) does not affect the selection of the “best” resolution setting. This means that estimating the “best” resolutions, these parameters can be omitted. This reduces the complexity of determining feasible resolutions.

### 4.3.2 The Effect of Straight Segment Length ( $l$ ) on the Inflexion

If  $\theta_0$ ,  $\rho_0$  and  $w$  are fixed  $l$  is changed, a series of segments result. The employment of HT with various  $\Delta\theta$  and  $\Delta\rho$  combinations can obtain the “best” resolution settings for different segment lengths.

Fig. 4.5 shows the inflexion changes with different segment lengths. It is clear that when the segment is long the inflexion is not affected. However, when the segment is short, the inflexion is significantly altered. This is because the  $\tan^{-1}\frac{w}{l}$  in Eqs. (4.1) and (4.2) becomes considerable when  $l$  is short, which makes the  $V_{i,m}$  and  $n_{i,m}$  frequently switch between different cases.

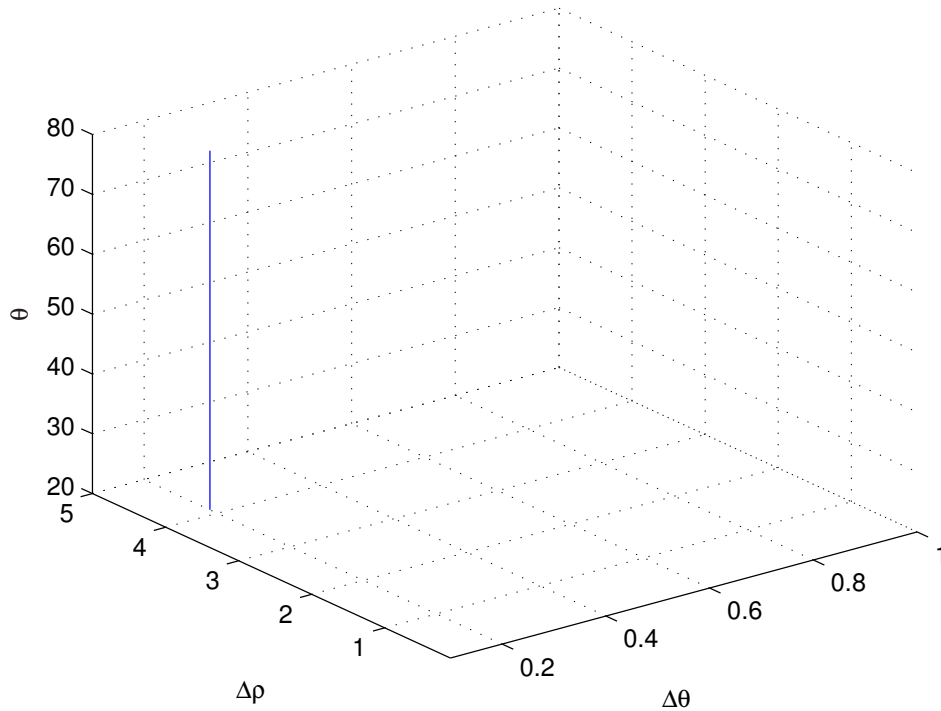


FIGURE 4.4:  $\theta$  value of straight segments does not affect on the selection of best resolution

### 4.3.3 The Effect of Straight Segment Width ( $w$ ) on the Inflexion

A similar result is obtained in the case of fixed  $\theta_0$ ,  $\rho_0$  and  $l$  values but changed  $w$  value. Fig. 4.6 shows that the width of the segment affects the inflexion.

## 4.4 A Global View of “Good” Resolutions

In Section 4.2, the inflexion of the error-resolution curves, that is, the resolution settings having the least detection errors were studied, according to the segments with specified parameters. The inflexion is affected by certain parameters of the segments, but in fact, initially, the parameters are unknown, and these uncertainties of the segment parameters exist in images as well. Therefore, detecting the “best” resolution setting according to the inflexion is not always practical or reliable. Hence, the area of “good” resolutions is more valuable than the single “best” point. This section aims to demonstrate the areas containing “good” resolutions, that is, having acceptable detection errors.

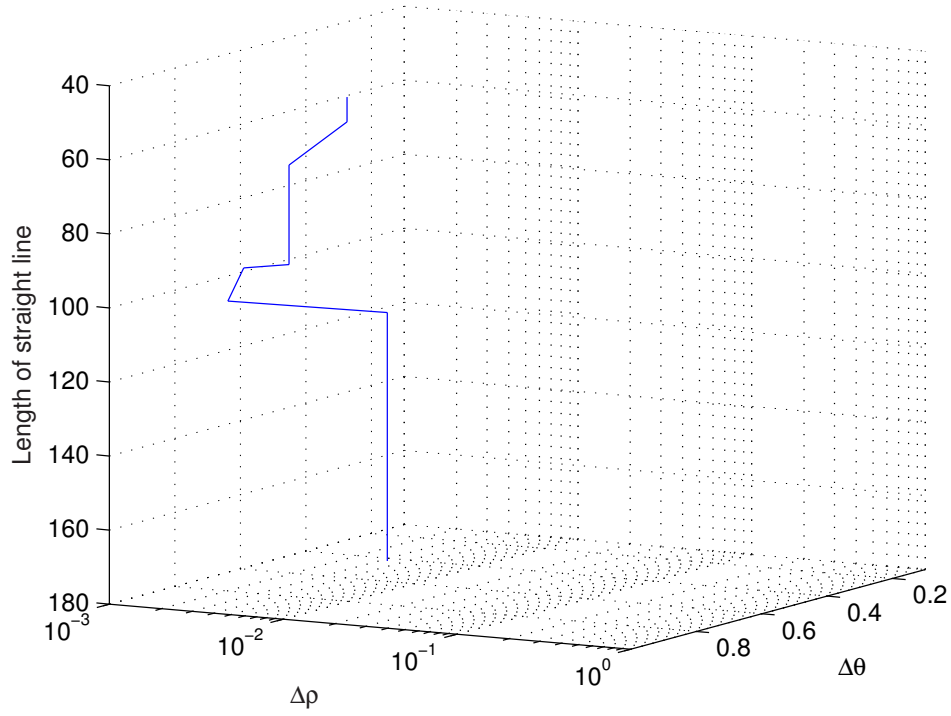


FIGURE 4.5: The length of segments affects on the selection of best resolution

As reported in [51], the ratio of resolutions,  $\frac{\Delta\rho}{\Delta\theta}$ , is related to the detection error of HT. This section considers the detection error as the function of  $\Delta\theta$ , and this ratio is denoted as  $a$ . For example, given a specific segment, the detection errors according to various  $a$  and  $\Delta\theta$  values, are shown in Fig. 4.7. When  $\Delta\theta$  and  $a$  are both inappropriately high, the detection errors are substantial. A decrease in  $\Delta\theta$  and  $a$  causes a decrease in the detection error. However, as discussed in Section 4.2 the detection error will increase after a certain point. Fig. 4.7 shows the global view of the detection error. The inflexion order is allocated in a valley with its considerable vicinity having very small detection errors. It is clear that if the area is obtained before HT, one can select a “good” resolution for a certain scope of segments.

To study the “good” resolution area, isolines are drawn in Fig. 4.8. The bounds of the valley are effectively approximated by curves

$$\Delta\theta = \frac{b_1}{a + c_1} + d_1 \quad (4.3)$$

and

$$\Delta\theta = \frac{b_2}{a + c_2} + d_2. \quad (4.4)$$

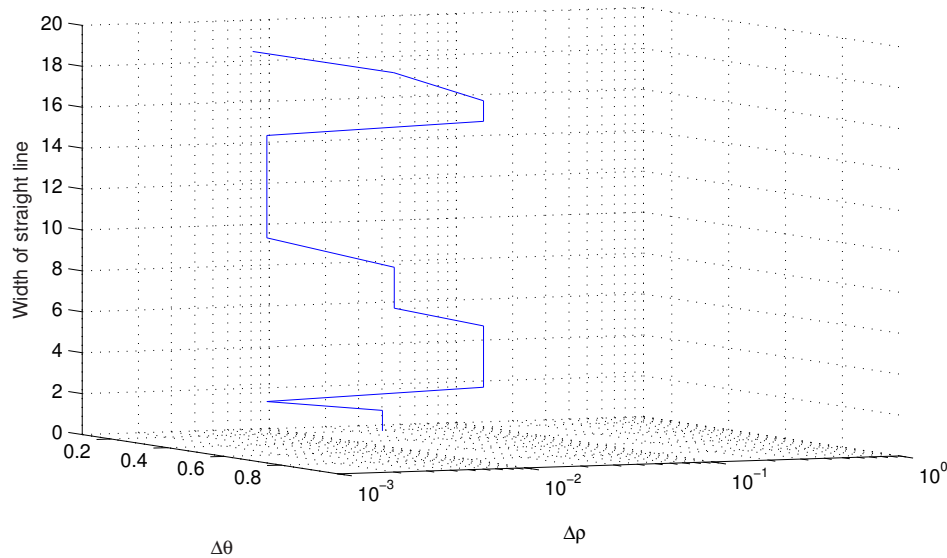


FIGURE 4.6: The width of segments affects on the selection of best resolution

After many experiments for various segment parameters, it was found that  $c_1 = c_2 = 1$  and  $d_1 = d_2 = 0.03$  are always fixed,  $b_1$  and  $b_2$  change, according to the parameters of the segments. This greatly alleviates the complexity of finding the “good” resolution area. It is possible to obtain the relationship for a parameter with the bounds of the valley, and figs. 4.9-4.12 demonstrate how these bounds are affected by segment parameters. If partial information regarding the segments to be detected is known, then it is possible to obtain the nest of “good” resolutions before HT is employed. This is helpful in increasing the detection accuracy without adding extra computation loads.

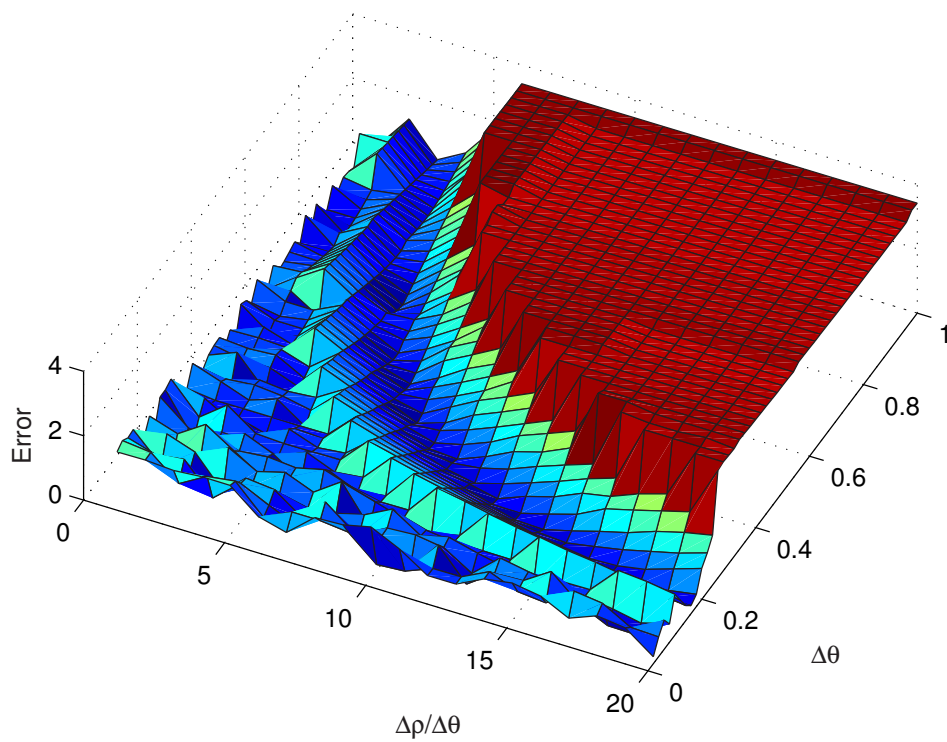


FIGURE 4.7: The area with small errors

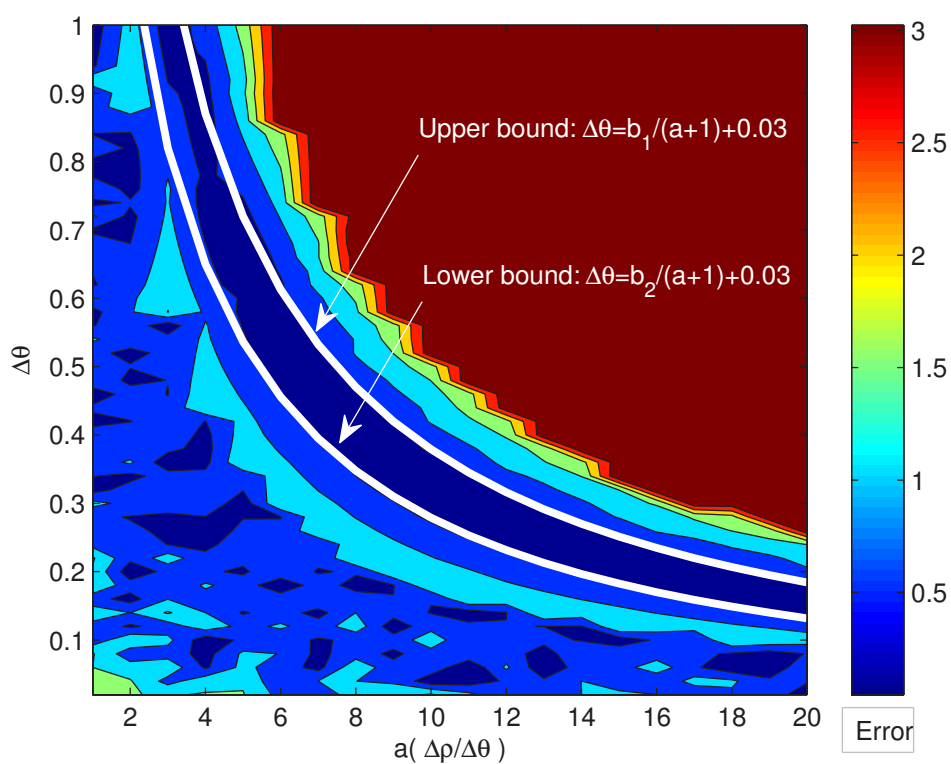


FIGURE 4.8: Approximating the area with small errors by upper and lower bounds

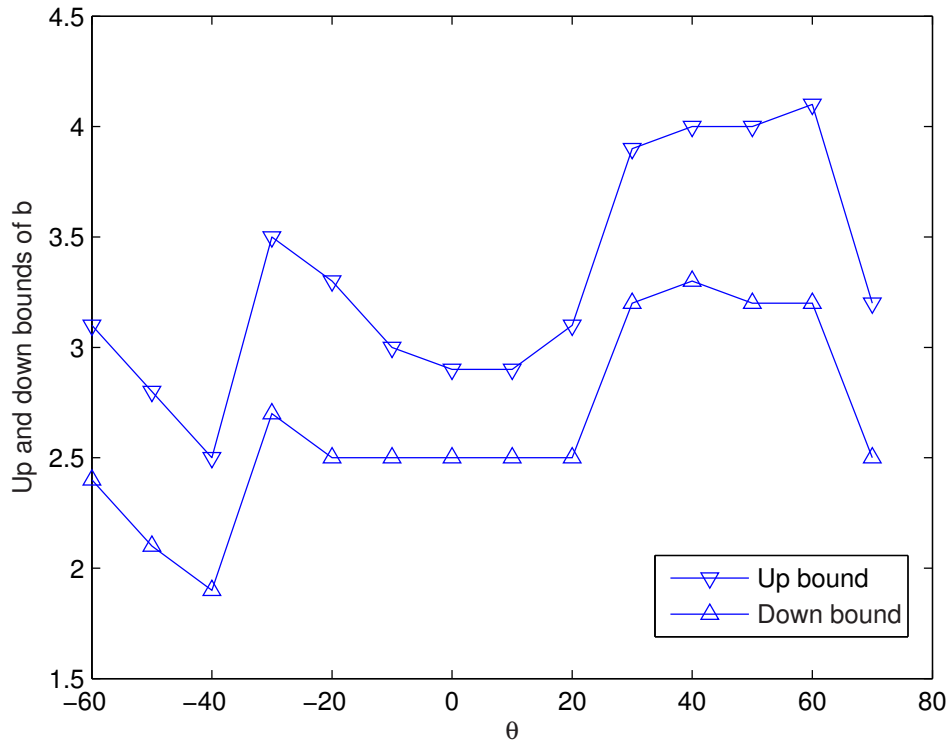


FIGURE 4.9: Upper and lower bounds of various  $\theta$  values of segments

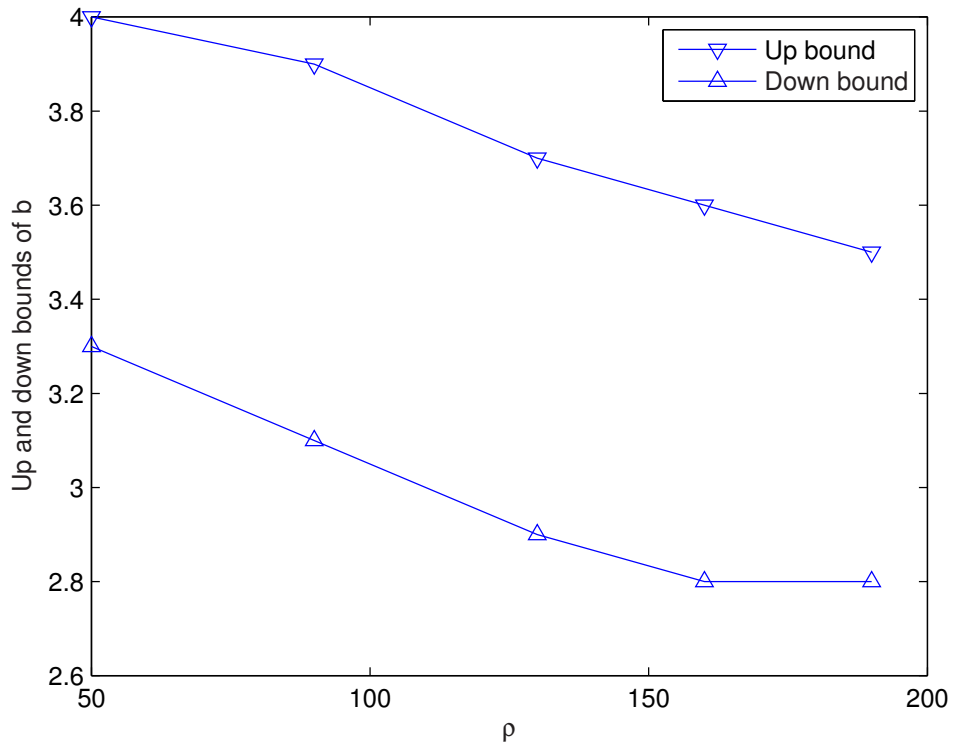


FIGURE 4.10: Upper and lower bounds of various  $\rho$  values of segments

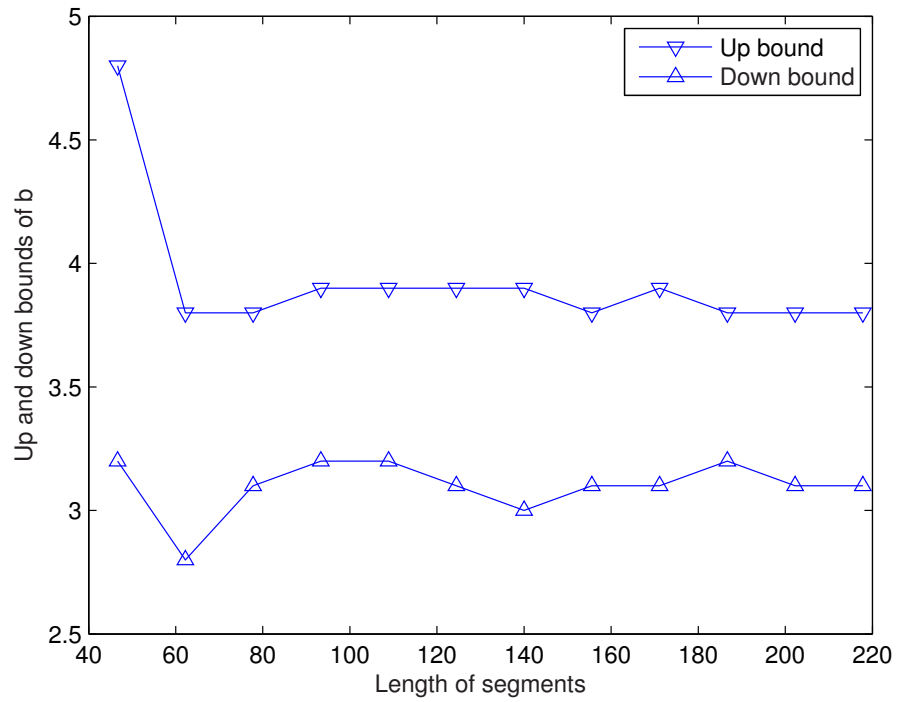


FIGURE 4.11: Upper and lower bounds of various lengths of segments

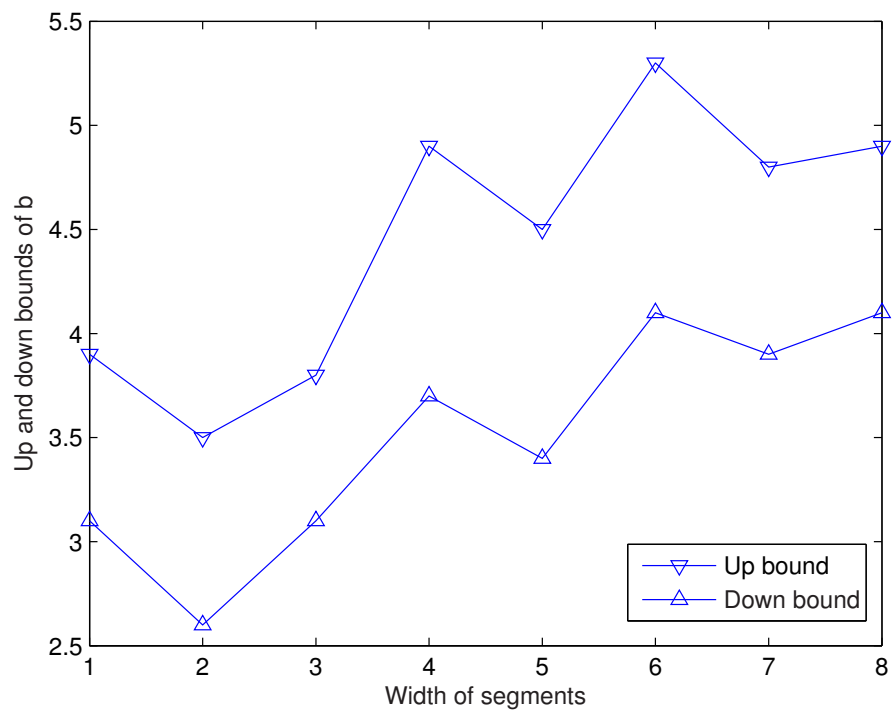


FIGURE 4.12: Upper and lower bounds of various widths of segments

## CHAPTER 5

# HIGH RESOLUTION HT BASED ON BUTTERFLY SELF-SIMILARITY

### 5.1 Self-similarity

In the HT, each feature point  $(x,y)$  of a straight line is mapped to a sine curve via

$$\rho = x \cos \theta + y \sin \theta. \quad (5.1)$$

By discretising the parameter space by resolutions  $\Delta\theta$  and  $\Delta\rho$ , an array of accumulators (cells) is generated with each cell corresponding to a belt in the image space. The feature point  $(x,y)$  votes to the cells located on the curve of Eq. (5.1). The position of the most voted cell, or peak, is considered as the  $(\rho, \theta)$  values of the straight line. During the voting process, not only is the peak generated, but also a large area is also built, composed of curves corresponding to all the feature points of the straight line. By considering the area around the peak, a butterfly is obtained.

The intensity of each cell in the butterfly is in proportion to the intersection length ( $\Delta l$ ) of the straight line and the belt corresponding to the cell. Fig. 5.1(a) demonstrates,

$$\Delta l = \frac{\Delta\rho}{\sin \varphi} \quad (5.2)$$

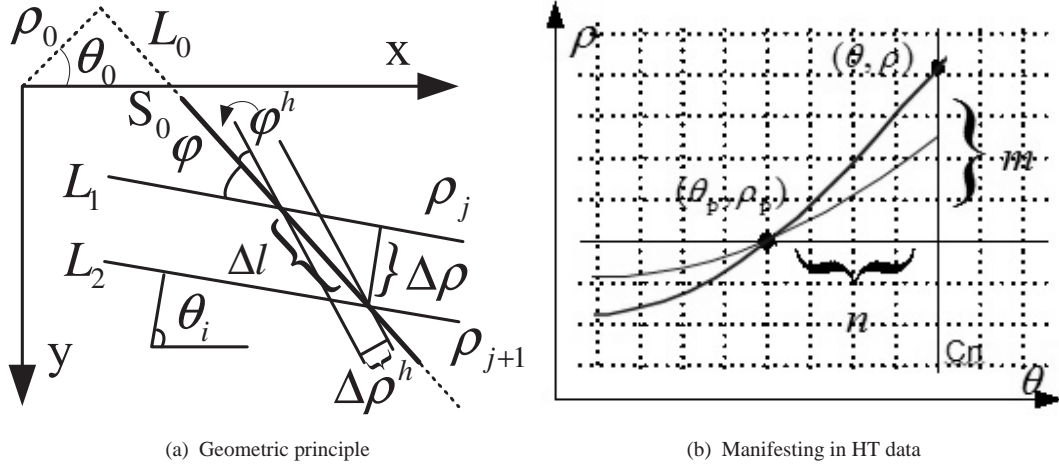


FIGURE 5.1: Geometric principle of HT

where  $\varphi$  is the angle between the segment and the belt. In HT space accumulators, the slope of the segment is approximated by  $\theta_p$  (the  $\theta$  value of the peak). Therefore,

$$\varphi \approx \theta_p - \theta_i = n\Delta\theta \quad (5.3)$$

that is,

$$\Delta l \approx \frac{\Delta\rho}{\sin(n\Delta\theta)}. \quad (5.4)$$

where  $n$  is a positive integer. Eq. (5.4) demonstrates that for the column  $C_n$  (as shown in Fig. 5.1(b)) where both  $\Delta\rho$  and  $n$  are small, the result is

$$\Delta l \approx \frac{\Delta\rho}{(n\Delta\theta)} = \frac{1}{n} \frac{\Delta\rho}{\Delta\theta}, \quad (5.5)$$

This proves  $\Delta l$  is not determined by  $\Delta\rho$  or  $\Delta\theta$  but by their ratio. This means for high and low resolution HT, if they have the same resolution ratio  $\frac{\Delta\rho}{\Delta\theta}$ , then their ideal intensity of cells in the column having the same distance ( $n$ ) to the peak, is similar.

Fig. 5.1(a) considers the position of cells obtaining votes in column  $C_n$ .

$$\rho_0 = x \cos \theta_0 + y \sin \theta_0 \quad (5.6)$$

$$\rho = x \cos(\theta_0 - \varphi) + y \sin(\theta_0 - \varphi) \quad (5.7)$$

$$\begin{aligned}
\rho - \rho_0 &= x(\cos(\theta_0 - \varphi) - \cos \theta_0) + y(\sin(\theta_0 - \varphi) - \sin \theta_0) \\
&= 2 \sin(-n\Delta\theta/2)(-x \sin(\theta_0 - n\Delta\theta/2) + y \cos(\theta_0 - n\Delta\theta/2)) \\
&\approx -n\Delta\theta(-x \sin(\theta_0 - n\Delta\theta/2) + y \cos(\theta_0 - n\Delta\theta/2))
\end{aligned} \tag{5.8}$$

$$\begin{aligned}
m &= (\rho - \rho_0)/\Delta\rho \\
&\approx -n\Delta\theta/\Delta\rho(-x \sin(\theta_0 - n\Delta\theta/2) + y \cos(\theta_0 - n\Delta\theta/2))
\end{aligned} \tag{5.9}$$

$$\begin{aligned}
m^h &= (\rho^h - \rho_0)/\Delta\rho^h \\
&\approx -n\Delta\theta^h/\Delta\rho^h(-x \sin(\theta_0 - n\Delta\theta^h/2) + y \cos(\theta_0 - n\Delta\theta^h/2))
\end{aligned} \tag{5.10}$$

where  $m$  and  $m^h$  is the  $\rho$ -distance from the cell to the peak in low and high resolution HT space respectively. Since

$$\alpha = \Delta\theta/\Delta\rho = \Delta\theta^h/\Delta\rho^h \tag{5.11}$$

$$\begin{aligned}
m - m^h &\approx -n\alpha[-x(\sin(\theta_0 - n\Delta\theta/2) - \sin(\theta_0 - n\Delta\theta^h/2)) \\
&\quad + y(\cos(\theta_0 - n\Delta\theta/2) - \cos(\theta_0 - n\Delta\theta^h/2))] \\
&\approx 2n\alpha \sin(n(\Delta\theta - \Delta\theta^h)/4)[-x \cos(\theta_0 - n(\Delta\theta + \Delta\theta^h)/4) \\
&\quad + y \sin(\theta_0 - n(\Delta\theta + \Delta\theta^h)/4)]
\end{aligned} \tag{5.12}$$

when the column is close to the peak, that is,  $n\Delta\theta$  is small, hence

$$\sin(n(\Delta\theta - \Delta\theta^h)/4) \approx 0 \tag{5.13}$$

results in,

$$m \approx m^h \tag{5.14}$$

Eq. (5.14) demonstrates that in the columns close to the peak, the cells obtaining votes in the high and low resolution HT space have a similar relative position to the peak.

From the above analysis, it is shown that in a given segment, the shape of the butterflies in the high and low resolution HT spaces should be similar. When zooming into the centre of a butterfly by applying appropriate higher  $\rho$ - and  $\theta$ -resolutions, then similar butterflies can be expected if the dimensions are ignored. That is if an accumulator is given without dimensions, the resolutions used to generate the butterfly are unknown. Fig. 5.2 demonstrates

that the HT butterflies of a segment under different resolutions are similar, with the exception of the  $\rho$ - and  $\theta$ -dimensions.

## 5.2 Method for High Resolution HT

The self-similarity in the HT butterfly discovered in Section 5.1 inspires a method to obtain a very high resolution HT butterfly from a low resolution butterfly, without the effects of peak splitting and vote spreading. Because of the similarity in the areas close to the peak in high and low resolution HT spaces, high resolution data can be obtained by copying corresponding cells from low resolution data. It should be noted that although the peak is in the centre of the butterfly, its position is not accurate in low resolution data. Some methods aiming to determine the position of the peak accurately from low resolution HT data (such as the filtering method in [11]) should be employed in these instances to obtain an accurate peak ( $\theta_p^h \approx \theta_0$ ,  $\rho_p^h \approx \rho_0$ ) from the low resolution data. Self-similarity is then used to build the small area around the obtained peak. Clearly for the columns that are not so close to the peak, that is  $\varphi = n\Delta\theta$  where  $n$  is relatively high, Eqs. (5.4), (5.8 to 5.10), (5.12 to 5.20) will not hold. In this case, for a given cell in high resolution HT space, its corresponding cell in the low resolution data should be considered. Similar to Eq. (5.2),

$$\Delta l^h = \Delta \rho^h / \sin \varphi^h \quad (5.15)$$

where

$$\varphi^h = \theta_p^h - \theta^h \quad (5.16)$$

Obviously if  $\Delta l^h \geq \Delta \rho$ , i.e.

$$\varphi^h \leq \arcsin(\Delta \rho^h / \Delta \rho) \quad (5.17)$$

Therefore, in the low resolution belt, there must exist a belt that has a similar intersection with the segment, as shown in Fig. 5.1(a).

Note: There is no belt in the a low resolution HT space corresponding to the high resolution belt when  $\varphi^h > \arcsin(\Delta \rho^h / \Delta \rho)$ . However, an HT butterfly in the scope defined by Eq. (5.17) is wide enough for segment detection. For example ( $\Delta \rho = 1, \Delta \theta = 1,$ ) and ( $\Delta \rho =$

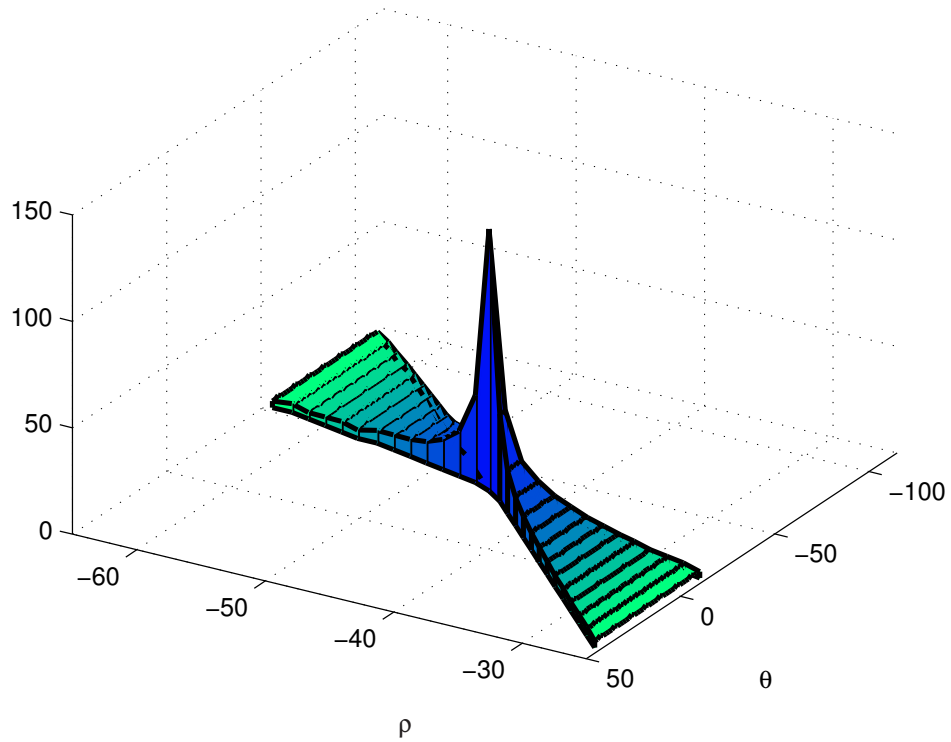
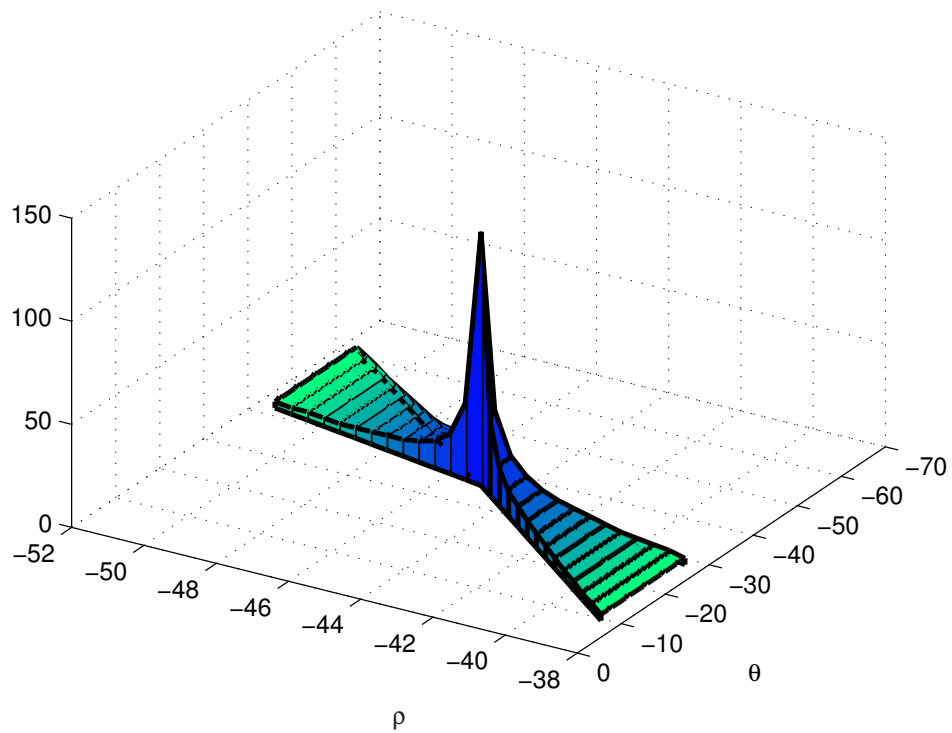
(a) HT butterfly under  $\Delta\rho = 1.5$  pixel and  $\Delta\theta = 1.5^\circ$ (b) HT butterfly under  $\Delta\rho = 0.5$  pixel and  $\Delta\theta = 0.5^\circ$ 

FIGURE 5.2: Self-similarity of HT butterfly

0.1,  $\Delta\theta = 0.1$ ,) the scope determined by Eq. (5.17) is about  $\arcsin(0.1) = 5.73^\circ$ , which means the high resolution butterfly has about  $5.73/0.1 \times 2 \approx 115$  columns.

From Eqs. (5.2) and (5.15), for a given high resolution cell  $(\theta^h, \rho^h)$

$$\varphi = \arcsin(\sin \varphi^h \Delta\rho / \Delta\rho^h) \quad (5.18)$$

Similar to Eq. (5.7)

$$\rho^h = x \cos(\theta_0 - \varphi^h) + y \sin(\theta_0 - \varphi^h) \quad (5.19)$$

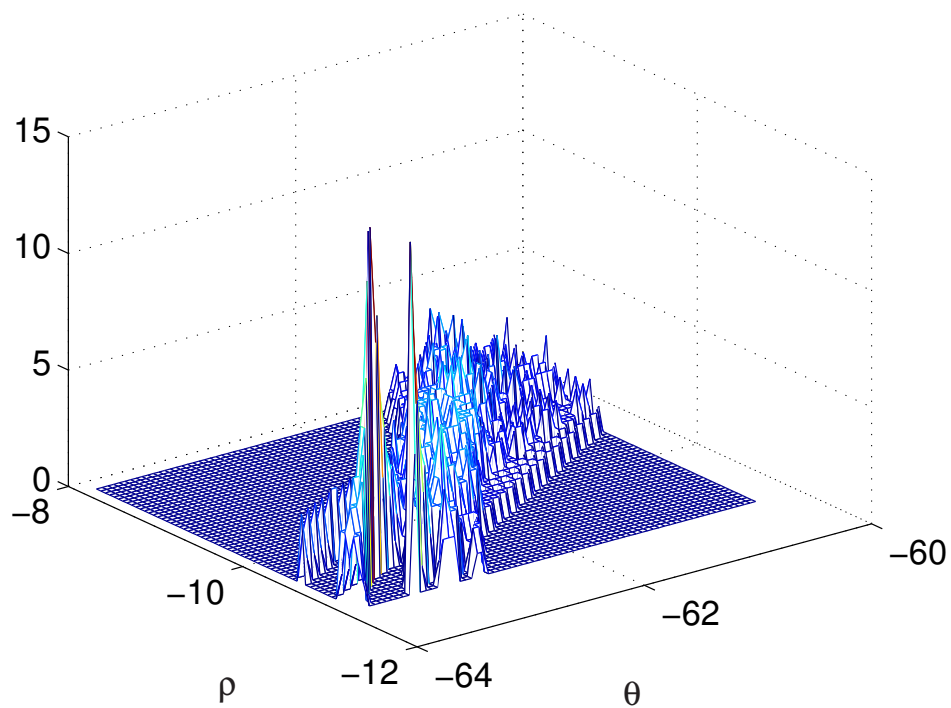
By solving the system of equations given by Eqs. (5.6), (5.7), (5.18), (5.19), one finds the  $\rho$  value of the low resolution cell as follows:

$$\rho = (\rho_p \sin(\varphi - \varphi^h) + \rho^h \sin(-\varphi)) / \sin(-\varphi^h) \quad (5.20)$$

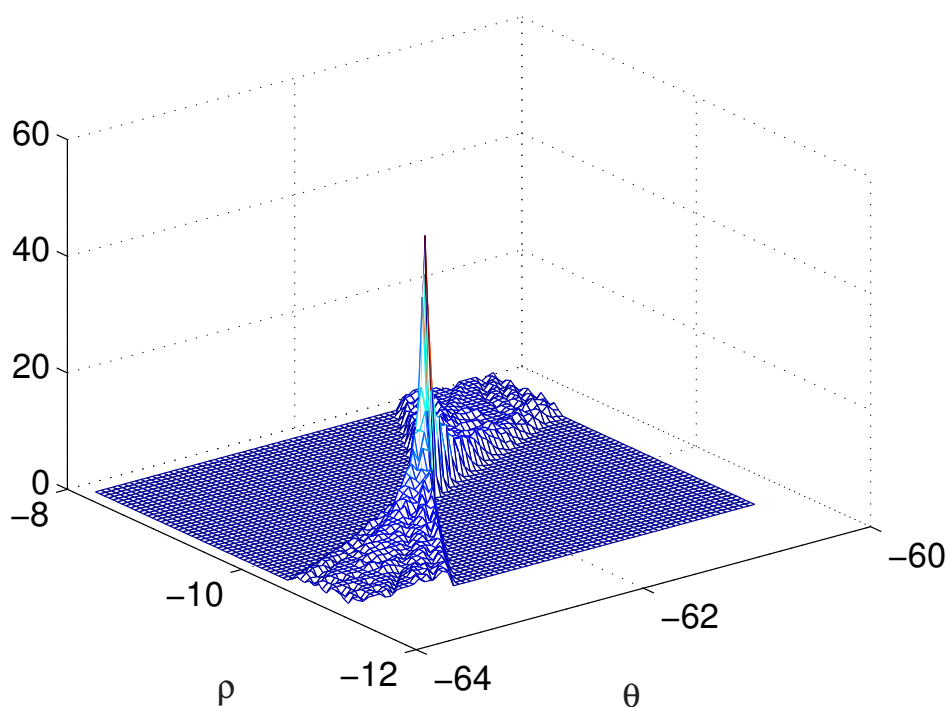
It should be noted that when solving the system of equations,  $\theta_0$  and  $\rho_0$  are approximated by  $\theta_p^h$  and  $\rho_p^h$ , respectively.

### 5.3 Results

Fig. 5.3 demonstrates the butterflies obtained by the traditional HT and the proposed method under high resolutions. It is very clear that the proposed method outperforms the traditional method regarding both the peak height and votes distribution.



(a) Traditional method



(b) Proposed method (local)

FIGURE 5.3: HT butterflies obtained by traditional method and proposed method under high resolutions ( $\Delta\rho = 0.05$  pixel and  $\Delta\theta = 0.05^\circ$ )

## CHAPTER 6

# GENERATING HIGH RESOLUTION HT BUTTERFLIES

### 6.1 Generating High Resolution HT Butterflies

For HT-based line detection methods, the detection precision benefits from precise and distinct peaks in the HT space. However, the peak alone cannot provide fully accurate straight line information, such as the length, width and midpoint. Fortunately, this information is contained in the low resolution HT butterfly areas around the peaks. [7, 8, 20, 41, 50] Nevertheless, the low resolution SHT cannot provide precise peaks or high resolution HT butterflies. Also, the high resolution SHT is not feasible because of the problems mentioned in previous chapters.

An interesting self-similarity method to generate high resolution HT data within a small vicinity of the peak is presented. In this chapter, generating high resolution HT (HT) butterflies for straight line detection, based on low resolution HT data around the peak, is addressed. This method is considered free from the constraints of the range. Geometric principles show the relationship between the low and high resolution HT data. According to the normal equation of HT, shown in Eq.(1.2), the smoothness of the trigonometric functions enables the increase of resolution in the  $\theta$ -direction by the interpolation method to be carried out with high accuracy. From the physical position of a cell in the parameter space, one finds that in the column with the same  $\theta$  value, high resolution HT data can be generated by splitting the cell of the low resolution HT data in the  $\rho$ -direction.

Based on this relationship, a method is proposed to obtain high resolution HT butterflies directly from low resolution HT data. The high resolution HT butterflies are obtained without the problems such as peak splitting and flattening, which are caused by the infeasible high resolution settings of the Standard HT (SHT). Since only the desired butterfly-shape area around the peak is needed, it is possible to reduce the computational cost and memory storage by generating the desired area only.

Before discussing the relationship between low and high resolution HT data, the generation of butterfly areas is initially demonstrated. Assume a straight line segment  $S_0$  lies on straight line  $L_0(\rho_0, \theta_0)$  in the image space. As shown in Fig. 6.1(a), a bar  $(\theta_k, \rho_i)$  contains the segment  $S_0$ , that is  $\theta_0 \in [\theta_k - \Delta\theta/2, \theta_k + \Delta\theta/2)$  and  $\rho_0 \in [\rho_i - \Delta\rho/2, \rho_i + \Delta\rho/2)$ , which means the cell  $(\theta_k, \rho_i)$  corresponding to this bar obtains all the votes from the segment feature points, that is the cell is the peak. As shown in Fig. 6.1(b), if the bar intersects with the straight line segment  $S_0$ , and the angle between them is  $\varphi$ , this implies that the bar contains part of the feature points of  $S_0$ . The cell corresponding to the bar will only receive part of the votes during the voting process. When  $\varphi$  becomes larger (the cell moves far from the peak in the  $\theta$ -direction of the HT space), the number of bars intersecting with  $S_0$  increases (the butterfly width in the  $\rho$ -direction increases), and the feature points contained in each bar decreases (the votes received by each cell decreases). A butterfly shaped voting area is therefore, generated around the peak as shown in Fig. 6.1(c). For clarity,  $\text{HT}(\Delta\rho, \Delta\theta)$  denotes the HT data with resolutions  $\Delta\rho$  and  $\Delta\theta$  in  $\rho$ - and  $\theta$ - directions respectively, and the ranges of  $\rho$  and  $\theta$  are  $[-\sqrt{W^2 + H^2} \quad \sqrt{W^2 + H^2})$  and  $[-90^\circ \quad 90^\circ)$  respectively, where  $W$  and  $H$  are the width and the height of an image.

### 6.1.1 Extending the $\theta$ -resolution of Butterflies: $\text{HT}(\Delta\rho, \Delta\theta) \implies \text{HT}(\Delta\rho, \frac{\Delta\theta}{n})$

By using geometric analysis on the generation of the butterfly around the HT peak, the relationship between low and high resolution HT data is demonstrated, and hence, a high resolution HT butterfly based on this relationship is obtained.

Firstly, the  $\theta$ -resolution is extended while keeping  $\Delta\rho$  fixed, that is,

$$\Delta\theta^h = \frac{\Delta\theta}{n} \quad (6.1)$$

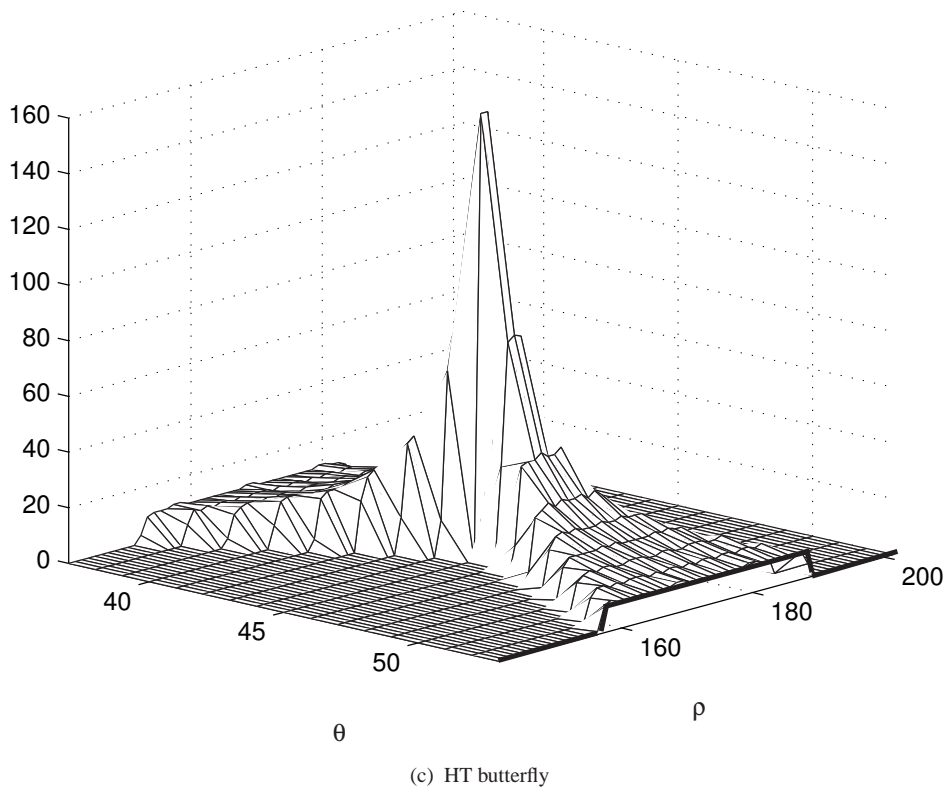
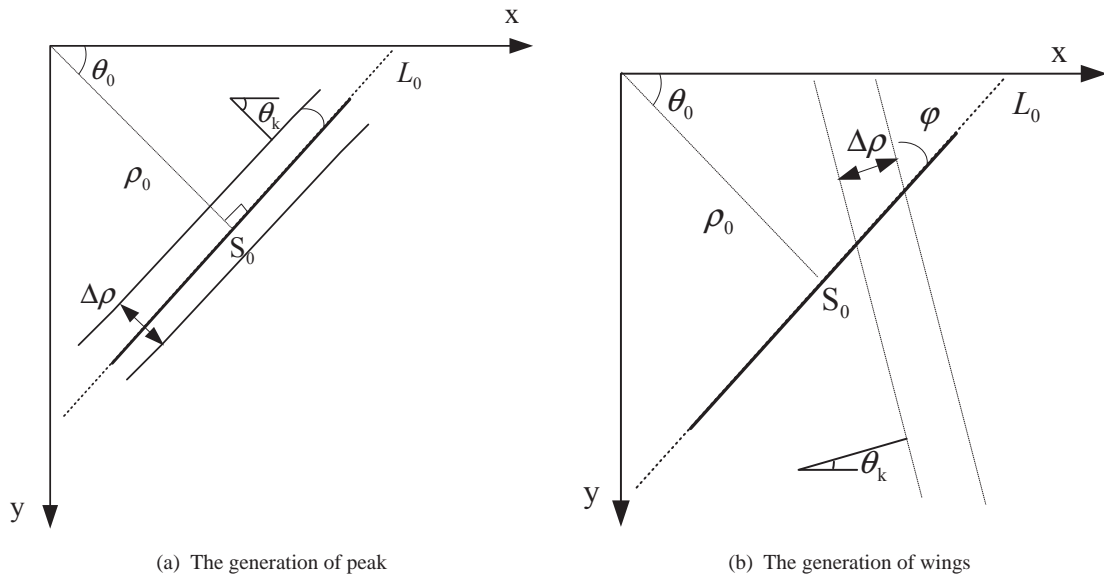


FIGURE 6.1: The generation of the butterfly shape in HT

$$\Delta\rho^h = \Delta\rho \quad (6.2)$$

where  $\Delta\theta$  and  $\Delta\rho$  are the low HT resolutions,  $\Delta\theta^h$  and  $\Delta\rho^h$  are the improved resolution, and  $n$  is a positive integer by which the  $\theta$ -resolution is multiplied.

$$\begin{aligned} \theta_k &= -90^\circ + k\Delta\theta \\ &= -90^\circ + kn\Delta\theta^h \\ &= \theta_{nk}^h, \end{aligned} \quad (6.3)$$

As a result, the centre of the cell  $(\theta_k, \rho)$  in the low resolution HT corresponds to the centre of the cell  $(\theta_{nk}^h, \rho)$  in the high resolution HT. Note that these two cells correspond to the same bar in the image space. Hence, when only the  $\theta$ -resolution is extended, the low resolution data in the  $\theta_k$  column and the high resolution data in the  $\theta_{nk}^h$  column are identical. That is, the high resolution column  $\theta_{nk}^h$  can be obtained by copying the low resolution column  $\theta_k$  for  $k = 0, 1, \dots, N_\theta - 1$ , where  $N_\theta = \lceil \frac{180}{\Delta\theta} + 1 \rceil$  is the number of columns in the low resolution HT and “ $\lceil \quad \rceil$ ” is the ceiling function.

After  $\theta_{nk}^h$  ( $k = 0, 1, \dots, N_\theta$ ), the columns of high resolution HT data are obtained and the calculation of the columns between the  $\theta_{nk}^h$  and  $\theta_{n(k+1)}^h$  columns is discussed.

#### 6.1.1.1 Determining the Cells receiving Votes when the Peak is included between $\theta_{nk}^h$ and $\theta_{n(k+1)}^h$ Columns

From Eq. (6.1) one finds the  $\theta$  value of the  $i$ -th column between the  $\theta_{n(k-1)}^h$  and  $\theta_{nk}^h$ -th columns is

$$\begin{aligned} \theta_{n(k-1)+i}^h &= \theta_{n(k-1)}^h + i\Delta\theta^h \\ &= \theta_{n(k-1)}^h + \frac{i}{n}\Delta\theta, \end{aligned} \quad (6.4)$$

where  $i = 1, \dots, n - 1$ . And for the  $j$ -th column between  $\theta_{nk}^h$  and  $\theta_{n(k+1)}^h$ -th columns is

$$\begin{aligned} \theta_{nk+j}^h &= \theta_{nk}^h + j\Delta\theta^h \\ &= \theta_{nk}^h + \frac{j}{n}\Delta\theta, \end{aligned} \quad (6.5)$$

where  $j = 1, \dots, n - 1$ .



Fig. 6.2 shows the sine curves bounding the butterfly shape around the peak (that is, the intersecting point of the curves). If the peak falls between two neighbouring columns in the low resolution HT data, the peak column (that is,  $\theta_k$  column in Fig. 6.2(a)) might not include the “true” peak, but it is generally quite close to the peak. In this situation, the votes are usually distributed over very few cells, sometimes over only one cell. However, this peak should not be considered the “true” peak in the high resolution HT space, and hence, the position of this peak should be re-considered. In this case, three neighbouring columns, that is,  $\theta_{k-1}$ ,  $\theta_k$  and  $\theta_{k+1}$ , from the low resolution HT data are taken, as shown in Fig. 6.2(b). Because  $\rho_{k-1}^1$ ,  $\rho_{k-1}^2$ ,  $\rho_{k+1}^1$ ,  $\rho_{k+1}^2$ ,  $\theta_{k-1}$ , and  $\theta_{k+1}$  are known from the low resolution HT data, we can calculate  $\hat{\theta}_p^h$  and  $\hat{\rho}_p^h$ , that is, the position of the peak in the high resolution HT space. Since  $\Delta\theta$  is very small,  $AC$  and  $BD$  can be considered straight lines intersecting at  $P(\hat{\theta}_p^h, \hat{\rho}_p^h)$ .

Because  $ABP$  and  $CDP$  are similar triangles, the following is obtained:

$$\frac{PI}{PI'} = \frac{AB}{CD}, \quad (6.6)$$

that is,

$$\frac{\hat{\theta}_p^h - \theta_{k-1}}{\theta_{k+1} - \hat{\theta}_p^h} = \frac{\rho_{k-1}^1 - \rho_{k-1}^2}{\rho_{k+1}^1 - \rho_{k+1}^2}, \quad (6.7)$$

resulting in

$$\hat{\theta}_p^h = \frac{\theta_{k+1}(\rho_{k-1}^1 - \rho_{k-1}^2) + \theta_{k-1}(\rho_{k+1}^1 - \rho_{k+1}^2)}{\rho_{k+1}^1 - \rho_{k+1}^2 + \rho_{k-1}^1 - \rho_{k-1}^2}, \quad (6.8)$$

Therefore, the peak lies on the  $\left(\left\lceil \frac{(\hat{\theta}_p^h + 90^\circ)n}{\Delta\theta} \right\rceil + 1\right)$ -th column in the high resolution HT space. Similarly,  $AIP$  and  $CI'P$  are similar triangles and considering Eq. (6.6), the following is obtained:

$$\frac{AI}{CI'} = \frac{PI}{PI'} = \frac{AB}{CD}, \quad (6.9)$$

that is,

$$\frac{\hat{\rho}_p^h - \rho_{k-1}^2}{\rho_{k+1}^1 - \hat{\rho}_p^h} = \frac{\rho_{k-1}^1 - \rho_{k-1}^2}{\rho_{k+1}^1 - \rho_{k+1}^2}, \quad (6.10)$$

resulting in

$$\hat{\rho}_p^h = \frac{\rho_{k-1}^2(\rho_{k+1}^1 - \rho_{k+1}^2) + \rho_{k+1}^1(\rho_{k-1}^1 - \rho_{k-1}^2)}{\rho_{k+1}^1 - \rho_{k+1}^2 + \rho_{k-1}^1 - \rho_{k-1}^2} \quad (6.11)$$

Consequently, the peak lies on the cell  $\left( \left\lceil \frac{(\hat{\theta}_p^h + 90^\circ)n}{\Delta\theta} \right\rceil, \left\lceil \frac{\hat{\rho}_p^h + \sqrt{W^2 + H^2}}{\Delta\rho} \right\rceil \right)$  in the high resolution HT space.

After the position of the new peak is determined, the columns between  $\hat{\theta}_p^h$  and  $\theta_{n(k+1)}^h$  and  $\theta_{n(k-1)}^h$  and  $\hat{\theta}_p^h$  can be obtained using the principle of similar triangles.

Since PEF and PAB are similar triangles, for the column  $\theta_{n(k-1)+i}^h$  between  $\theta_{n(k-1)}^h$  and  $\hat{\theta}_p^h$ , shown in Fig.6.2(b)), where EF represents the cells receiving votes, the following is obtained:

$$\frac{\hat{\rho}_p^h - \rho_{n(k-1)+i}^h}{\hat{\rho}_p^h - \rho_{k-1}^h} = \frac{\hat{\theta}_p^h - \theta_{n(k-1)+i}^h}{\hat{\theta}_p^h - \theta_{k-1}^h} \quad (6.12)$$

that is,

$$\rho_{n(k-1)+i}^h = \hat{\rho}_p^h - \frac{(\hat{\rho}_p^h - \rho_{k-1}^h)(\hat{\theta}_p^h - \theta_{n(k-1)+i}^h)}{\hat{\theta}_p^h - \theta_{k-1}^h}, \quad (6.13)$$

and

$$\frac{\hat{\rho}_p^h - \rho_{n(k-1)+i}^h}{\hat{\rho}_p^h - \rho_{k-1}^h} = \frac{\hat{\theta}_p^h - \theta_{n(k-1)+i}^h}{\hat{\theta}_p^h - \theta_{k-1}^h} \quad (6.14)$$

that is,

$$\rho_{n(k-1)+i}^h = \hat{\rho}_p^h - \frac{(\hat{\rho}_p^h - \rho_{k-1}^h)(\hat{\theta}_p^h - \theta_{n(k-1)+i}^h)}{\hat{\theta}_p^h - \theta_{k-1}^h}, \quad (6.15)$$

where  $\theta_{k-1}^h, \rho_{k-1}^h, \rho_{k-1}^h$  are known from the low resolution HT data,  $\theta_{n(k-1)+i}^h$  is obtained from Eq.(6.4) and  $\hat{\rho}_p^h$  and  $\hat{\theta}_p^h$  are obtained from Eqs. (6.11) and (6.8) respectively.

Similarly, as shown in Fig. 6.2(b), one can obtain the column  $\theta_{nk+j}^h$  where GH represents the cells receiving votes as:

$$\rho_{nk+j}^h = \hat{\rho}_p^h - \frac{(\hat{\rho}_p^h - \rho_{k+1}^h)(\hat{\theta}_p^h - \theta_{nk+j}^h)}{\hat{\theta}_p^h - \theta_{k+1}^h}, \quad (6.16)$$

and

$$\rho_{nk+j}^h = \hat{\rho}_p^h - \frac{(\hat{\rho}_p^h - \rho_{k+1}^h)(\hat{\theta}_p^h - \theta_{nk+j}^h)}{\hat{\theta}_p^h - \theta_{k+1}^h}, \quad (6.17)$$

Where  $\theta_{k+1}^h, \rho_{k+1}^h, \rho_{k+1}^h$  are known from the low resolution HT data,  $\theta_{nk+j}^h$  is obtained from Eq. (6.5) and  $\hat{\rho}_p^h$  and  $\hat{\theta}_p^h$  are obtained from Eqs. (6.11) and (6.8) respectively.

### 6.1.1.2 Determining the Cells Receiving Votes When the Peak is Not Included between the $\theta_{nk}^h$ and $\theta_{n(k+1)}^h$ Columns

From Eq. (6.1) one finds that the  $\theta$  value of the  $i$ -th column between  $nk$ -th and  $n(k+1)$ -th columns is

$$\begin{aligned}\theta_{nk+i}^h &= \theta_{nk}^h + i\Delta\theta^h \\ &= \theta_{nk}^h + \frac{i}{n}\Delta\theta^h,\end{aligned}\quad (6.18)$$

where  $i = 1, \dots, n-1$ . If a rectangle is used to intersect the area of the wings between the columns  $\theta_{nk}^h$  and  $\theta_{n(k+1)}^h$ , points A, B, C, and D can be obtained, as shown in Fig. 6.3(a). Since  $\Delta\theta$  is small, AD and BC lying on the sine curves can be regarded as straight edges. It is possible to zoom into this area as shown in Fig. 6.3(b). The values  $\rho_k^1, \rho_k^2, \rho_{k+1}^1, \rho_{k+1}^2$  shown in Fig. 6.3(b) are known in the low resolution HT data, but  $\rho_{nk+i}^{h1}$  and  $\rho_{nk+i}^{h2}$  in the high resolution HT are unknown. From Fig. 6.3(b), the following is observed:

$$\frac{BI}{CI'} = \frac{FI}{FI'} \quad (6.19)$$

therefore

$$\frac{\rho_k^1 - \rho_{nk+i}^{h1}}{\rho_{nk+i}^{h1} - \rho_{k+1}^1} = \frac{i\Delta\theta^h}{(n-i)\Delta\theta^h} \quad (6.20)$$

From Eq. (6.20) the following is obtained

$$\rho_{nk+i}^{h1} = \frac{(n-i)\rho_k^1 + i\rho_{k+1}^1}{n}. \quad (6.21)$$

Similarly, since

$$\frac{AJ}{DJ'} = \frac{EJ}{EJ'}, \quad (6.22)$$

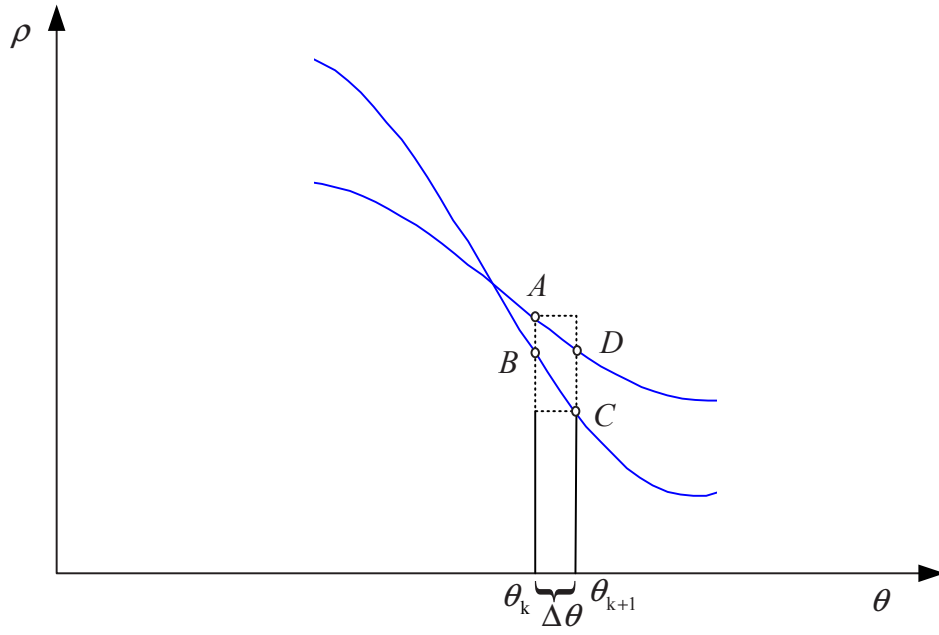
the results in

$$\frac{\rho_k^2 - \rho_{nk+i}^{h2}}{\rho_{nk+i}^{h2} - \rho_{k+1}^2} = \frac{i\Delta\theta^h}{(n-i)\Delta\theta^h}. \quad (6.23)$$

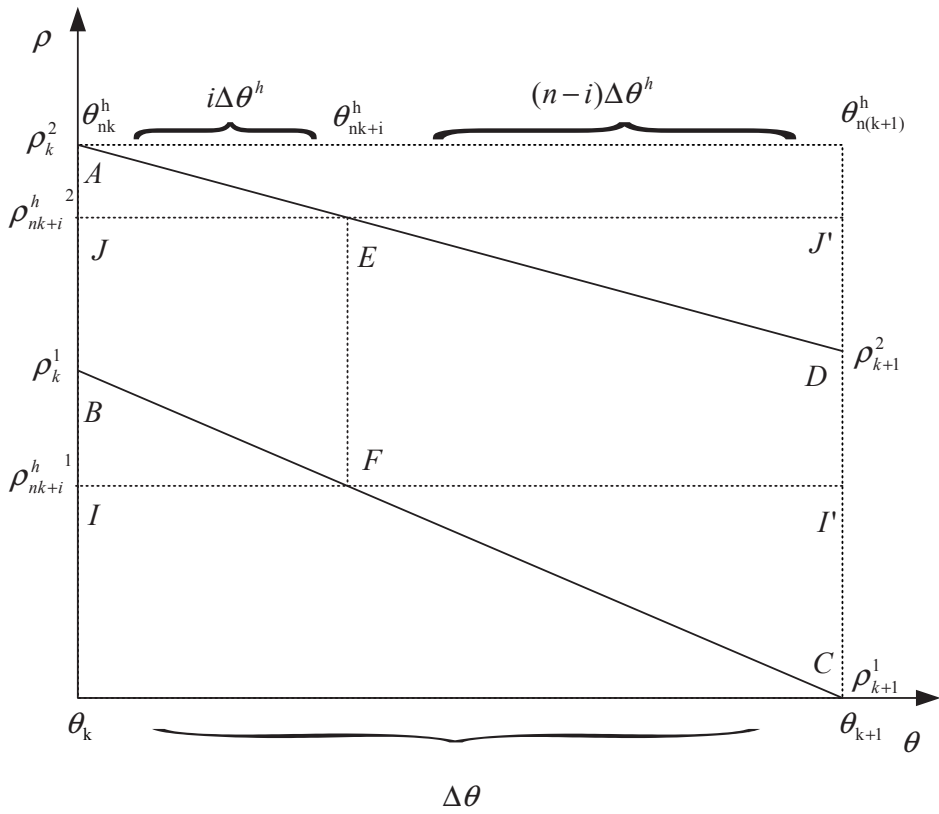
From Eq. (6.23) the following is obtained

$$\rho_{nk+i}^{h2} = \frac{(n-i)\rho_k^2 + i\rho_{k+1}^2}{n}. \quad (6.24)$$

From Eqs. (6.21) and (6.24) show that in the  $\theta_{nk+i}^h$  column of the high resolution HT, the cells between  $(\theta_{nk+i}^h, \rho_{nk+i}^{h1})$  and  $(\theta_{nk+i}^h, \rho_{nk+i}^{h2})$  obtained votes. After the cells that received votes



(a) Butterfly beyond the peak



(b) The parts of butterfly beyond the peak (local)

FIGURE 6.3: Extend  $\theta$  resolution of HT butterfly (wings)

are obtained, the number of votes obtained by each cell is discussed.

### 6.1.1.3 Determining the Number of Votes Received by Each Cell in $HT(\Delta\rho, \frac{\Delta\theta}{n})$

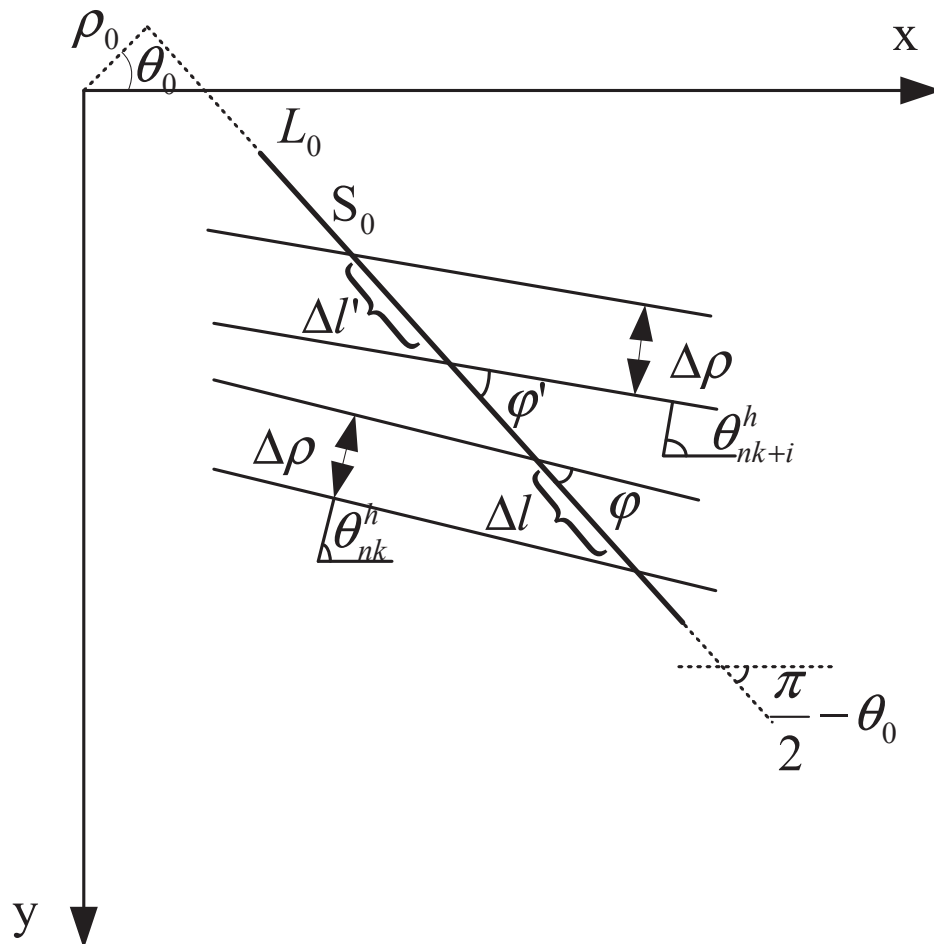


FIGURE 6.4: The length of intersection in the image space determines the density in the HT space

In the low resolution HT,  $\Delta\rho$  is assumed to be sufficiently large (larger than the width of the candidate straight lines). It is clear that if the bar corresponding to the low resolution HT peak  $(\theta_k, \rho)$  contains the straight line in the image space then the cell  $(\theta_{nk}^h, \rho)$  should also contain the same straight line since the bars corresponding to them are identical. In this case, the peak obtains votes from all the straight line feature points, and its neighboring cells in the same column receive no votes from the straight line. Therefore the height of the low and high resolution HT peaks are also the height of the “true” peak. If the bar  $(\theta_k, \rho)$  does not contain the complete straight line, that is it shares the votes with its parallel neighbouring

bars  $(\theta_k, \rho + p\Delta\rho)$ , where  $p = \pm 1, \pm 2, \dots$ . The height of the “true” peak should be the sum of the votes received by the peak cell and its parallel neighbours, that is the cells in the same column close to the peak. This “true” peak height is considered the height of the peak in the high resolution HT space in the proposed method.

For the columns not containing the peak, as shown in Fig. 6.4, the straight line segment  $S_0$  lies on the straight line  $L_0(\rho_0, \theta_0)$ , and two bars belonging to columns  $\theta_{nk}^h$  and  $\theta_{nk+i}^h$  ( $0 < i < n - 1$ ) intersect with  $S_0$  respectively. The acute angles between them and  $L_0$  are  $\varphi$  and  $\varphi'$  respectively. The length of their intersection with  $S_0$  are denoted as  $\Delta l$  and  $\Delta l'$ .  $\Delta l$  and  $\Delta l'$ , and they determine the number of votes obtained by these two cells. It is clear that

$$\Delta l = \frac{\Delta\rho}{\sin\varphi}, \quad (6.25)$$

$$\Delta l' = \frac{\Delta\rho}{\sin\varphi'}, \quad (6.26)$$

$$\varphi = \theta_{nk}^h - \theta_0, \quad (6.27)$$

$$\varphi' = \theta_{nk+i}^h - \theta_0. \quad (6.28)$$

By substituting Eq. (6.18) into Eq. (6.28), the following is obtained

$$\begin{aligned} \varphi' &= \theta_{nk}^h + i\Delta\theta^h - \theta_0 \\ &= \theta_{nk}^h - \theta_0 + i\Delta\theta^h \end{aligned} \quad (6.29)$$

Considering both Eq. (6.27) and Eq. (6.29),

$$\varphi' = \varphi + i\Delta\theta^h \quad (6.30)$$

From Eqs. (6.25), (6.26) and (6.30), the following is obtained

$$\begin{aligned} \frac{\Delta l}{\Delta l'} &= \frac{\sin\varphi'}{\sin\varphi} \\ &= \frac{\sin(\varphi + i\Delta\theta^h)}{\sin\varphi} \\ &= \frac{\sin\varphi \cos(i\Delta\theta^h) + \cos\varphi \sin(i\Delta\theta^h)}{\sin\varphi} \\ &= \cos(i\Delta\theta^h) + \sin(i\Delta\theta^h) / \tan\varphi. \end{aligned} \quad (6.31)$$

Since  $i\Delta\theta^h < \Delta\theta$  is very small, we obtain  $\cos(i\Delta\theta^h) \approx 1$  and  $\sin(i\Delta\theta^h) \approx i\Delta\theta^h$ . Therefore from Eq. (6.31) the following is obtained

$$\frac{\Delta l}{\Delta l'} \approx 1 + i\Delta\theta^h / \tan \varphi, \quad (6.32)$$

where  $\Delta\theta^h$  is constant, and  $\varphi$  is constant for  $i = 1, \dots, n-1$  (that is the columns between  $\theta_{nk}^h$  and  $\theta_{nk+n}^h$ ). From Eq. (6.32) it is seen that  $\frac{\Delta l}{\Delta l'}$  is a simple linear function of  $i$ .

Considering the nature of digital images, all straight lines are represented by piece-wise connected horizontal or vertical short segments. The number of pixels comprising a straight line equals its projection on the  $X$  (when  $|\theta_0| > 45^\circ$ ) or  $Y$  (when  $|\theta_0| \leq 45^\circ$ ) axis. Therefore, for the cells in the  $\theta_{nk}^h$  column whose corresponding bars intersect with the segment, the following is seen:

$$V(\rho, \theta_{nk}^h) = \begin{cases} \Delta l \cos \theta_0, & |\theta_0| > 45^\circ \\ \Delta l \sin \theta_0, & |\theta_0| \leq 45^\circ \end{cases}, \quad (6.33)$$

In this equation,  $V(\rho, \theta_{nk}^h)$  denotes the number of votes received by the cell  $(\theta, \rho)$ , where  $\rho$  is an appropriate value making the bar corresponding to this cell intersect with the segment. In theory, the votes received by each cell in the same column are identical, with the exception of the cells at the two ends, this depends on whether the cell can receive votes, since its bar intersects with the segment by the same length, that is,  $\Delta l$ .

The following denotes the cells in the  $\theta_{nk+i}^h$  column that receive votes:

$$V(\rho, \theta_{nk+i}^h) = \begin{cases} \Delta l' \cos \theta_0, & |\theta_0| > 45^\circ \\ \Delta l' \sin \theta_0, & |\theta_0| \leq 45^\circ, \end{cases} \quad (6.34)$$

resulting in

$$\frac{V(\rho, \theta_{nk}^h)}{V(\rho, \theta_{nk+i}^h)} = \frac{\Delta l}{\Delta l'} \approx 1 + i\Delta\theta^h / \tan \varphi. \quad (6.35)$$

Since the  $\theta_{nk}^h$  column is copied from the  $\theta_k$  column in the low resolution HT data,

$$V(\rho, \theta_{nk}^h) = V(\rho, \theta_k) \quad (6.36)$$

and therefore,

$$V(\rho, \theta_{nk+i}^h) \approx \frac{V(\rho, \theta_k)}{1 + i\Delta\theta^h / \tan \varphi} \quad (6.37)$$

can be calculated. It should be noted that due to rounding errors, the cells in the column of a butterfly do not usually receive exactly the same number of votes. Therefore, the value of  $V(\rho, \theta_k)$  in Eq. (6.37) is obtained by averaging the number of votes received by the cells in the column  $\theta_k$  of the low resolution HT butterfly.

### 6.1.2 Extending the $\rho$ -resolution: $\mathbf{HT}(\Delta\rho, \frac{\Delta\theta}{n}) \implies \mathbf{HT}(\frac{\Delta\rho}{m}, \frac{\Delta\theta}{n})$

Section 6.1.1, described the method to obtain a high  $\theta$ -resolution HT. In this section, the  $\theta$ -resolution is kept constant at  $\frac{\Delta\theta}{n}$ , and increase the  $\rho$ -resolution is increased.

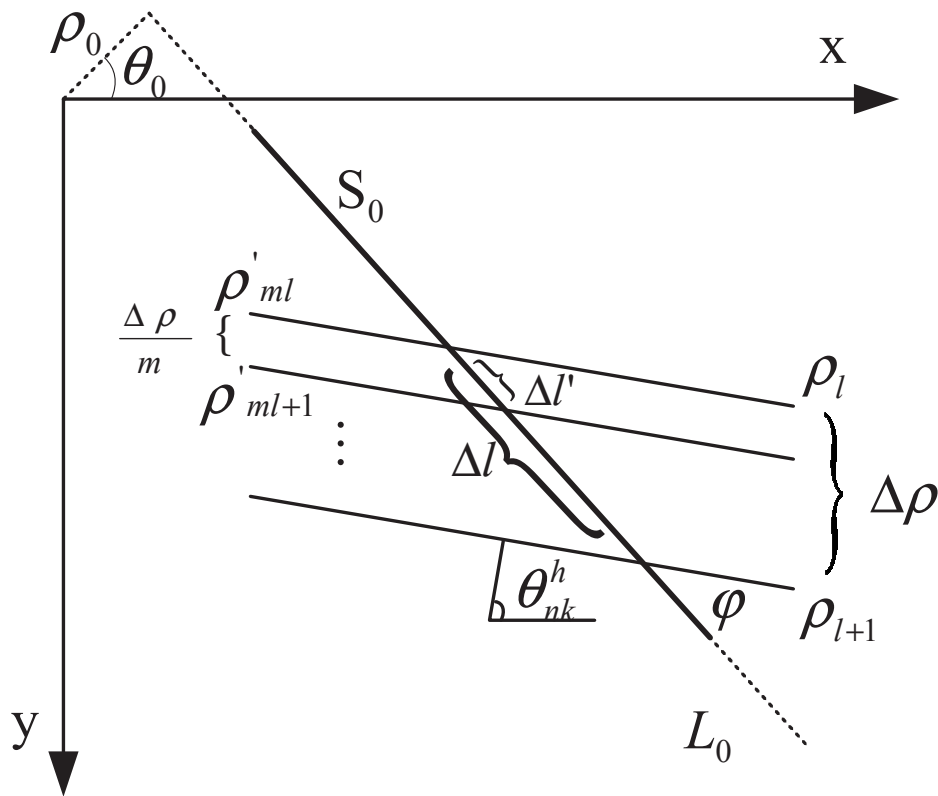


FIGURE 6.5: Extending the HT resolution in  $\rho$  direction

Assume the  $\rho$ -resolution to be increased  $m$  times the low  $\rho$ -resolution, where  $m$  is a positive integer. This means a cell in  $\mathbf{HT}(\Delta\rho, \frac{\Delta\theta}{n})$  is split into  $m$  cells in the  $\rho$ -direction, as shown in Fig. 6.5.

$$\Delta\theta^h = \frac{\Delta\theta}{n}, \quad (6.38)$$

$$\Delta\rho^h = \frac{\Delta\rho}{m}, \quad (6.39)$$

and

$$\begin{aligned} \rho_l &= -\sqrt{M^2 + N^2} + l\Delta\rho \\ &= -\sqrt{M^2 + N^2} + ml\Delta\rho^h \\ &= \rho_{ml}^h. \end{aligned} \quad (6.40)$$

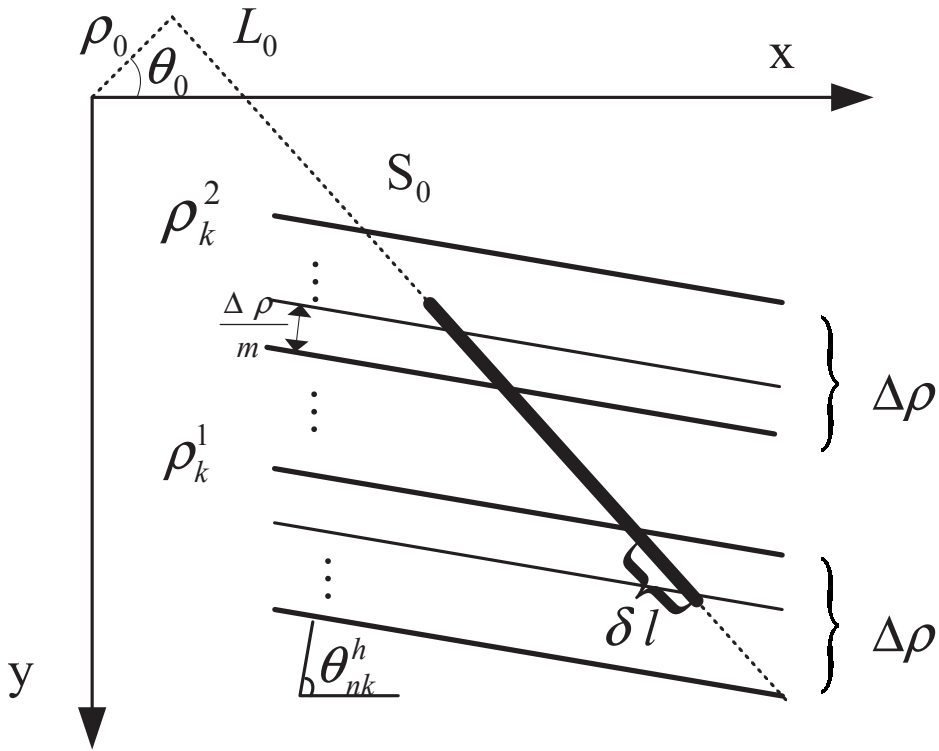


FIGURE 6.6: Determine the votes in ends cases

In Fig. 6.5, the bar corresponding to the cell  $(\theta_{nk}^h, \rho_l)$  in  $\text{HT}(\Delta\rho, \frac{\Delta\theta}{n})$  is split into  $m$  bars corresponding to  $m$  cells in  $\text{HT}(\frac{\Delta\rho}{m}, \frac{\Delta\theta}{n})$ .  $\Delta l$  is the length of the intersection of the segment  $(S_0)$  and a bar of  $\text{HT}(\Delta\rho, \frac{\Delta\theta}{n})$ , and  $\Delta l'$  is the length of the intersection of the segment and a bar of  $\text{HT}(\frac{\Delta\rho}{m}, \frac{\Delta\theta}{n})$ .

$$\Delta l' = \frac{\Delta l}{m}. \quad (6.41)$$

Considering the simple, directly proportional relationship between the length of the intersection and the number of votes received by the cell as shown in Eq. (6.33), each high resolution cell receives  $\frac{1}{m}$  votes of the low resolution cell, with the exception of the cells intersecting

with the segment at one of its endpoints. That is,

$$V(\rho_{ml+i}^h, \theta_{nk+i}^h) = \frac{1}{m} V(\rho_l, \theta_{nk+i}^h). \quad (6.42)$$

Fig. 6.6 illustrates the first and the last bars. Using the first bar  $(\theta_{nk}^h, \rho_k^1)$  as an example, assume the length of the segment included in this bar is  $\delta l$ .

$$\frac{V(\rho_k^1, \theta_{nk}^h)}{V(\rho, \theta_{nk}^h)} = \frac{\delta l}{\Delta l} = \frac{m' \Delta \rho^h}{m \Delta \rho^h}, \quad (6.43)$$

therefore,

$$m' = m \frac{V(\rho_k^1, \theta_{nk}^h)}{V(\rho, \theta_{nk}^h)} \quad (6.44)$$

where  $\rho$  is an appropriate value causing the corresponding bar to intersect with the segment in the middle, in order for it to obtain an intersection of  $\Delta l$  length.

Therefore, the first cell in the  $\theta_{nk}^h$  column of  $\text{HT}(\frac{\Delta \rho}{m}, \frac{\Delta \theta}{n})$  receiving votes are obtained as

$$\rho_{nk}^{h1} = \rho_k^1 + m' \Delta \rho^h. \quad (6.45)$$

Similarly, one can find the first cell in the column receiving votes as well. The number of votes obtained by each of these cells is equal to the votes in the middle of the segment, as shown in Eq. (6.42).

## 6.2 Summary and Discussion of the Proposed Method

### 6.2.1 Steps to Implement the Proposed Method:

1. Apply low resolution HT on the image to obtain  $\text{HT}(\Delta \rho, \Delta \theta)$ .
2. Detect the peaks in  $\text{HT}(\Delta \rho, \Delta \theta)$  and for each peak:
  - (a) Take out the window  $H_w(\Delta \rho, \Delta \theta)$  with the scopes:  $\theta_p - w \Delta \theta \leq \theta \leq \theta_p + w \Delta \theta, \rho_p - h \Delta \rho \leq \rho \leq \rho_p + h \Delta \rho$ ;

- (b) Extend the  $\theta$ -resolution of the window  $H_w(\Delta\rho, \Delta\theta)$  to get  $H_w(\Delta\rho, \frac{\Delta\theta}{n})$  using the following steps:
- i. Copy columns  $\{p+i\}$  of  $H_w(\Delta\rho, \Delta\theta)$  to the columns  $\{p+i \times n\}$  of  $H_w(\Delta\rho, \frac{\Delta\theta}{n})$  where  $i = -w, -w+1, \dots, 0, \dots, w-1, w$  and  $p$  indicates the column containing the peak;
  - ii. For each column between the columns  $p+i \times n$  and  $p+(i+1) \times n$  of  $H_w(\Delta\rho, \frac{\Delta\theta}{n})$  where  $i \geq 1$  or  $i < -1$ , do:
    - A. Determine the cells obtain votes in the column according to Eqs. (6.21) and (6.24);
    - B. Determine the votes got by each of these cells according to Eq. (6.37).
  - iii. For each columns between the columns  $p-n$  and  $p+n$  of  $H_w(\Delta\rho, \frac{\Delta\theta}{n})$ ,
    - A. Determine the cells obtaining votes in the column according to Eqs. (6.16) and (6.17);
    - B. Determine the votes received by each of these cells according to Eq. (6.37).
  - iv. Build the peak of  $H_w(\Delta\rho, \frac{\Delta\theta}{n})$ :
    - A. Calculate the position of the high resolution peak according to Eqs. (6.8) and (6.11);
    - B. Assign the number of votes to the new peak by summing the votes received by the “old” peak in  $H_w(\Delta\rho, \Delta\theta)$  and its  $\rho$ -direction neighboring cells.
- (c) Extend the  $\rho$ -resolution of  $H_w(\Delta\rho, \frac{\Delta\theta}{n})$  to obtain  $H_w(\frac{\Delta\rho}{m}, \frac{\Delta\theta}{n})$ :
- i. For the column  $p$  of  $H_w(\frac{\Delta\rho}{m}, \frac{\Delta\theta}{n})$ , keep the peak  $(\hat{\theta}_p^h, \hat{\rho}_p^h)$  but insert 0’s to the remaining cells of the column;
  - ii. For the column  $p+i$  of  $H_w(\frac{\Delta\rho}{m}, \frac{\Delta\theta}{n})$  where  $i = p-nw, p-nw+1, \dots, p-1, p+1, p+nw$ ,
    - A. Split each cell  $(\theta_i^h, \rho_k)$  in the column of  $H_w(\Delta\rho, \frac{\Delta\theta}{n})$  except the first and the last non-zero voted cells into  $m$  cells of  $H_w(\frac{\Delta\rho}{m}, \frac{\Delta\theta}{n})$  with the number of votes equal to the  $\frac{1}{m}V(\rho_k, \theta_i^h)$ ;
    - B. For the first and the last none-zero voted cells in this column, split the cell into  $m$  cells of  $H_w(\frac{\Delta\rho}{m}, \frac{\Delta\theta}{n})$  and determine the cells receiving votes, according to Eq. (6.44) Assign the votes to these cells as per the middle cells.

## 6.2.2 Running Time and Memory Storage

To compare the computational complexity of the proposed method and the Standard HT, the following symbol definitions are used:

$H$ : the height of image;

$W$ : the width of image;

$R$ :  $\sqrt{H^2 + W^2}$ ;

$h$ : the height of butterfly area considered;

$w$ : the width of butterfly area considered;

$C$ : the number of feature points;

$D$ : the number of straight lines;

$n$ : the extension factor in  $\theta$  direction;

$m$ : the extension factor in  $\rho$  direction;

$\Delta\theta_0$ : low resolution in  $\theta$  direction;

$\Delta\theta$ : high resolution in  $\theta$  direction ( $\Delta\theta_0 = n\Delta\theta$ );

$\Delta\rho_0$ : low resolution in  $\rho$  direction;

$\Delta\rho$ : high resolution in  $\rho$  direction ( $\Delta\rho_0 = m\Delta\rho$ );

$N_0$ :  $\lceil \frac{180^\circ}{\Delta\theta_0} \rceil$ ;

$N$ :  $\lceil \frac{180^\circ}{\Delta\theta} \rceil$ ;

$M_0$ :  $\lceil \frac{2R}{\Delta\rho_0} \rceil$ ;

$M$ :  $\lceil \frac{2R}{\Delta\rho} \rceil$ .

Therefore,

$$N = nN_0, \quad (6.46)$$

and

$$M = mM_0. \quad (6.47)$$

The operations intensively used in the SHT and the proposed Resolution Extended HT (REHT) are listed in Table 6.1. Table 6.2 lists the number of operations requested by the proposed REHT and the SHT.

When the resolutions are increased, the running time and memory requirements are related to the resolution extension factors,  $n, m$ . To demonstrate this comparison, an example is given with the following parameters:

TABLE 6.1: The operations intensively used in the SHT and the proposed Resolution Extended HT (REHT)

Op	SHT	REHT
Additions(A)	Used in Eq. (1.2) and updating the number of votes obtained by a cell in HT	Used in Eqs. (6.10, 6.13, 6.15, 6.17, 6.18, 6.19, 6.23, 6.26, 6.39)
Products(P)	Used in Eq. (1.2)	Used in Eqs. (6.10, 6.13, 6.15, 6.17, 6.18, 6.19, 6.23, 6.26, 6.39)
Look Up Table access(L)	Used in Eq. (6.1) to access the values of $\sin \theta_k$ and $\cos \theta_k$ stored in look up tables	Used in Eqs. (6.1, 6.39) to access the values of $\sin \theta_k$ , $\cos \theta_k$ and $\tan \varphi$ stored in look up tables
The HT space memory access(PA)	Used during updating the number of votes obtained by a cell in HT	Used during updating the number of votes obtained by a cell in HT
Divisions(D)	n/a	Used in Eqs. (6.10, 6.13, 6.15, 6.17, 6.18, 6.19, 6.23, 6.26, 6.39)

TABLE 6.2: The number of operations requested by the SHT and the proposed Resolution Extended HT (REHT)

Op	SHT	REHT
A	$CN$	$\frac{CN}{n} + D(4n(4+w) - w - 7)$
P	$2CN$	$\frac{2CN}{n} + D(nw(h+4) - hw - 4n - 2)$
L	$2CN$	$\frac{2CN}{n} + Dw$
PA	$CN$	$\frac{CN}{n} + D(mnhw)$
D	0	$D((2w-2)n - 2 - \frac{hw}{2} + mnhw)$

TABLE 6.3: Memory storage requested by the SHT and the proposed method

Storage/Methods	SHT	REHT
Integer	$MN$	$(\frac{MN}{mn} + Dh w)$
Single	$2N$	$\frac{2N}{n} + Dw$

$H = 100$  pixels;  $W = 100$  pixels;  $R = 141$  pixels;  $h = 10$  cells;  $w = 10$  cells;  $C = 1000$ ;  $D = 10$ ;  $\Delta\theta_0 = 1^\circ$ ;  $\Delta\rho_0 = 1$  pixel;  $M_0 = 180$ ;  $N_0 = 283$ .

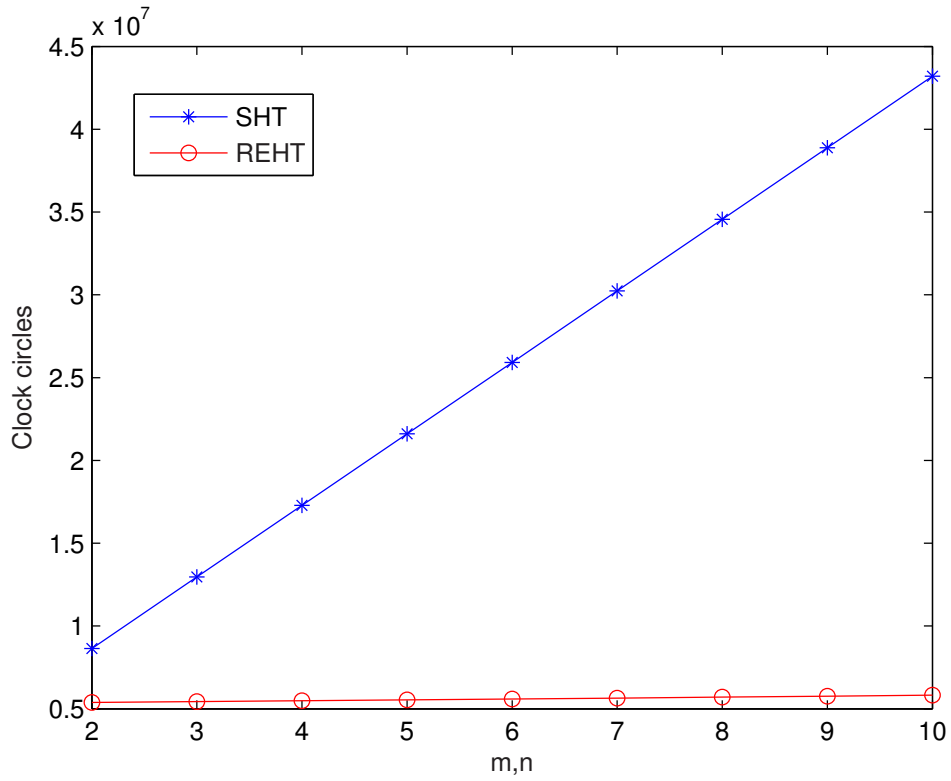
The running time (clock cycles) and memory storage (32bit units) are shown in Fig. 6.7(a) and Fig. 6.7(b). It is clear that the proposed REHT runs faster and needs less memory than the SHT. The running time and memory requirements of the proposed method increase with the increase of  $n$  and  $m$ . However, the requirements related to SHT escalate greatly, especially memory storage, which increases exponentially.

It should be noted that the running time of the SHT is only related to the  $\theta$  resolution, that is, the number of columns of HT data that should be built. The  $\rho$  resolution does not affect the running time, as demonstrated with Eq. (1.2). This denotes that for each feature point in the image space, only one cell in each column of the HT space obtains the vote. The position of the voted cell depends on the  $\rho$  value obtained from Eq. (1.2), and the vote is assigned to the nearest cell. Consequently the number of cells in a column does not affect the running time at all. Therefore, the running time is directly proportional to the  $\theta$  resolution, but the memory storage is proportional to the cell number in the HT space.

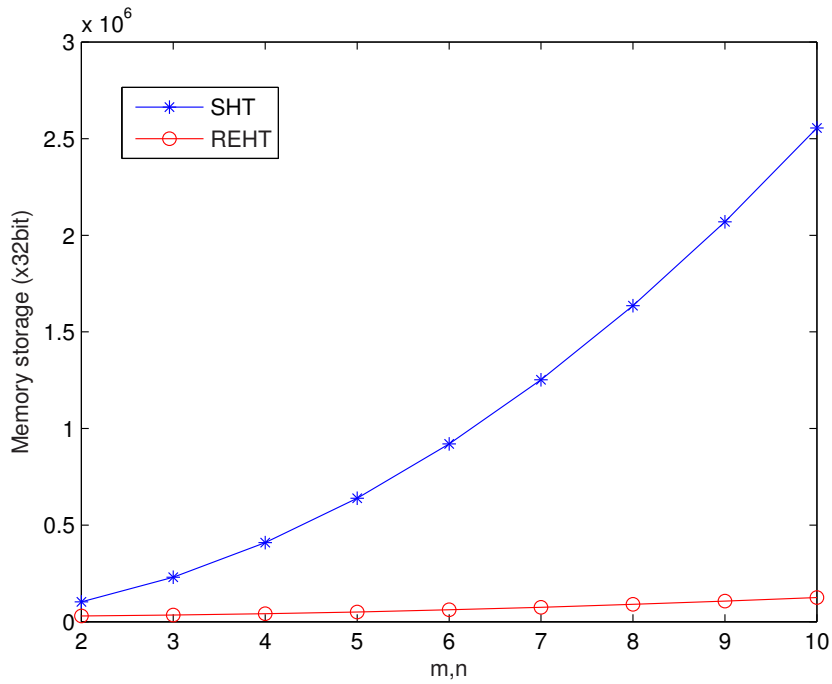
## 6.3 Experiments

### 6.3.1 The Peak Becomes More Distinct

This experiment demonstrates the distinct peak generated by the proposed method. The same resolutions, that is,  $\Delta\theta = 0.4^\circ$  and  $\Delta\rho = 0.4$  pixel, are applied in both the SHT and the REHT methods. Fig. 6.8(a) shows a line in an image used as input to the SHT and the proposed REHT. Fig. 6.8(b) is the butterfly generated by the SHT and Fig. 6.8(c) is butterfly generated by the REHT. It is very clear that the peak generated by the proposed method is far more distinct than the peak of the SHT. Fig. 6.8(d) and Fig. 6.8(e) display the HT space array around the peaks, which enhances the comparison.

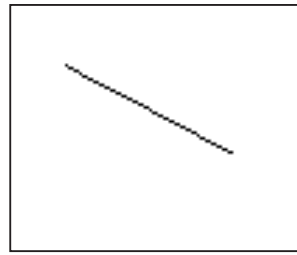


(a) Running time

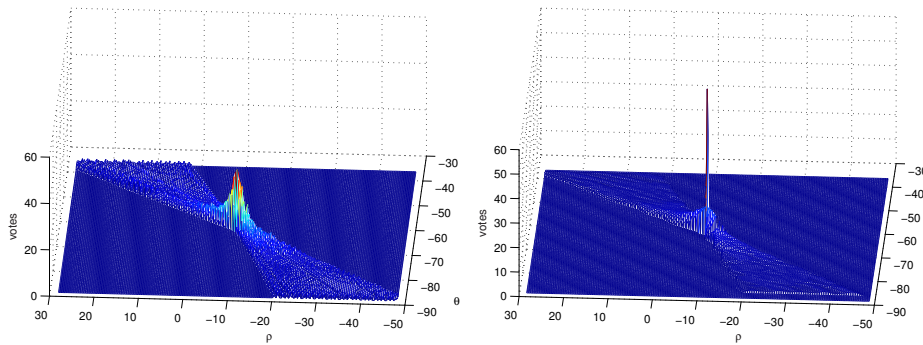


(b) Memory

FIGURE 6.7: Computing complexity trends corresponding to the increase of resolution

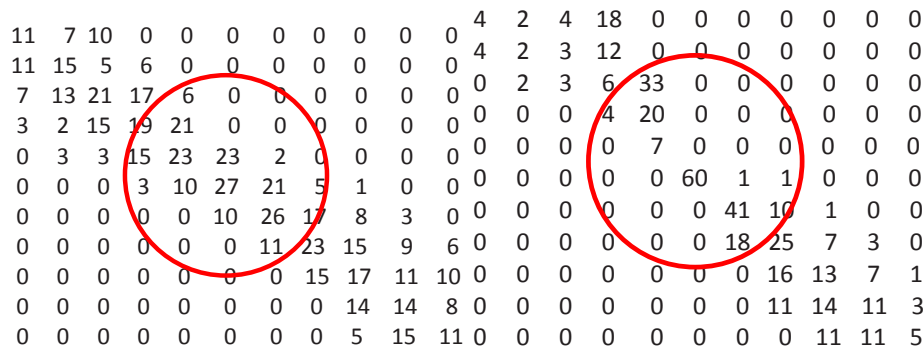


(a) The segment



(b) SHT butterfly( $\Delta\rho=0.4$ ,  $\Delta\theta=0.4$ )

(c) REHT butterfly( $\Delta\rho=0.4$ ,  $\Delta\theta=0.4$ )



(d) SHT peak( $\Delta\rho=0.4$ ,  $\Delta\theta=0.4$ )

(e) REHT peak( $\Delta\rho=0.4$ ,  $\Delta\theta=0.4$ )

FIGURE 6.8: The peak is improved by the proposed method

### 6.3.2 Comparison of the “Ideal” HT Butterfly

To evaluate the HT butterfly generated by the proposed method, a theoretical HT butterfly is calculated. To calculate the theoretical HT butterfly, the endpoints (denoted as  $(x_1, y_1)$  and  $(x_2, y_2)$ ) of a segment are assumed known. The exact normal parameters (that is,  $\theta_p$  and  $\rho_p$ ) are obtained, and the height of the peak is assigned to the length of the segment.

For each cell in the parameter space, the density is the length of the intersection between the segment and the image space bar corresponding to the cell.

It is clear that a butterfly is superior if it is close to the theoretical butterfly. Therefore, the correlation with the theoretical butterfly is used as the criterion to evaluate a butterfly. The correlation of butterflies under different resolutions are depicted in Fig. 6.9, where the butterflies generated by the proposed method have very high correlation coefficients with the theoretical butterfly. This demonstrates that the proposed method generates high quality butterflies. It should be noted that the quality of SHT butterflies decreases quickly with the increase in resolution.

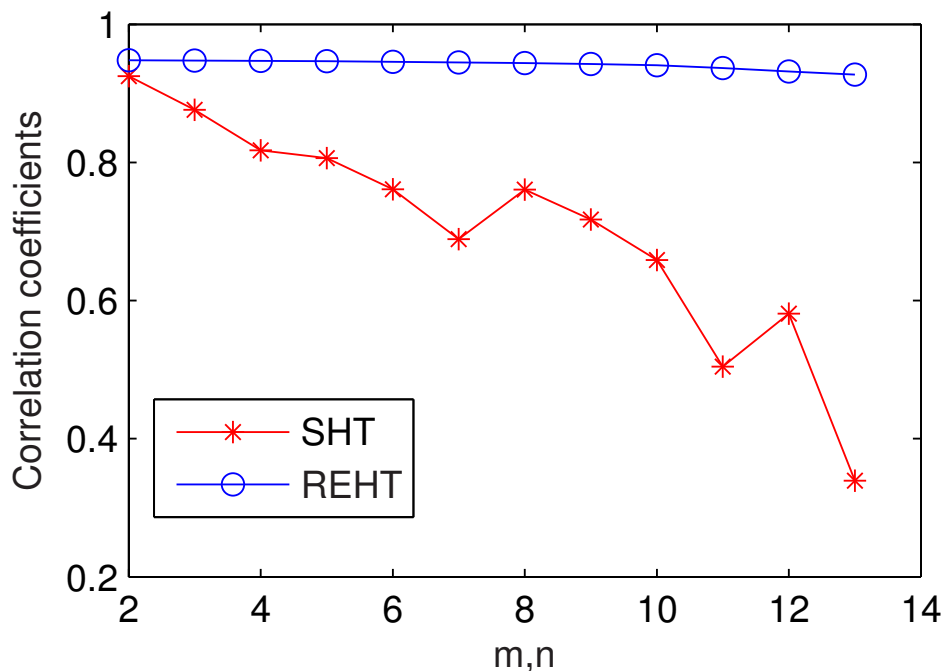
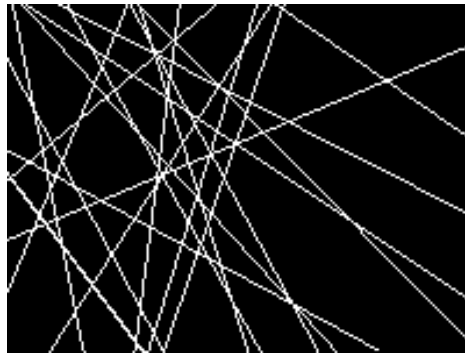


FIGURE 6.9: Comparison of the correlation with the theoretical butterfly

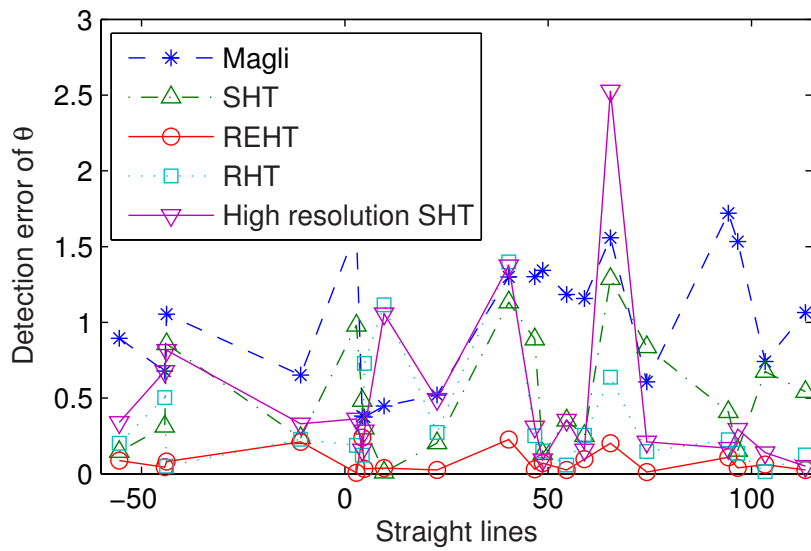
### 6.3.3 Straight Line Positioning Accuracy (the Accuracy of the Generated Peak)

#### 6.3.3.1 Example of Synthetic Images

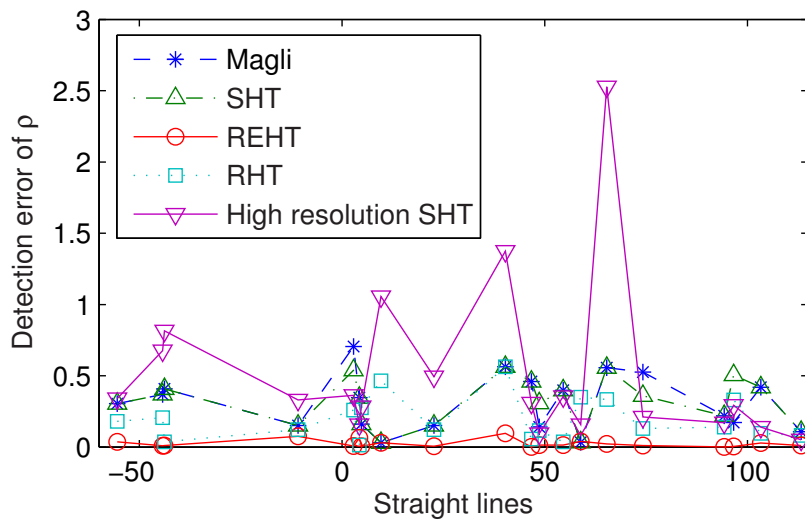
In this experiment, many straight lines are randomly generated (with random  $\rho$  and  $\theta$ ) to verify the detection accuracy of the proposed method. Fig. 6.10(a) shows the random lines.



(a) Randomly generated lines



(b) The detection error of  $\theta$



(c) The detection error of  $\rho$

FIGURE 6.10: Detection accuracy comparison

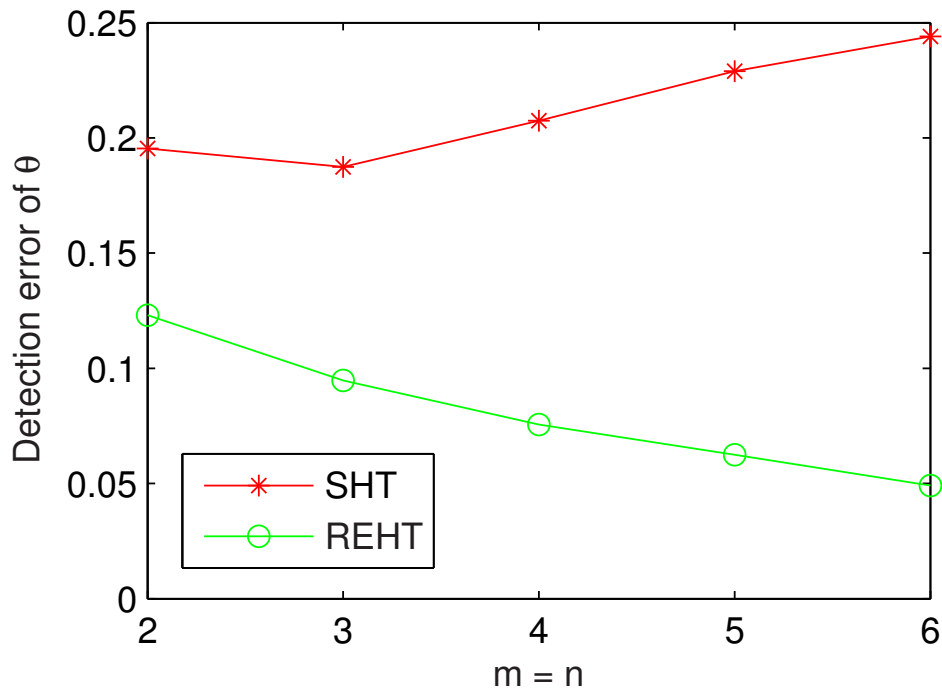
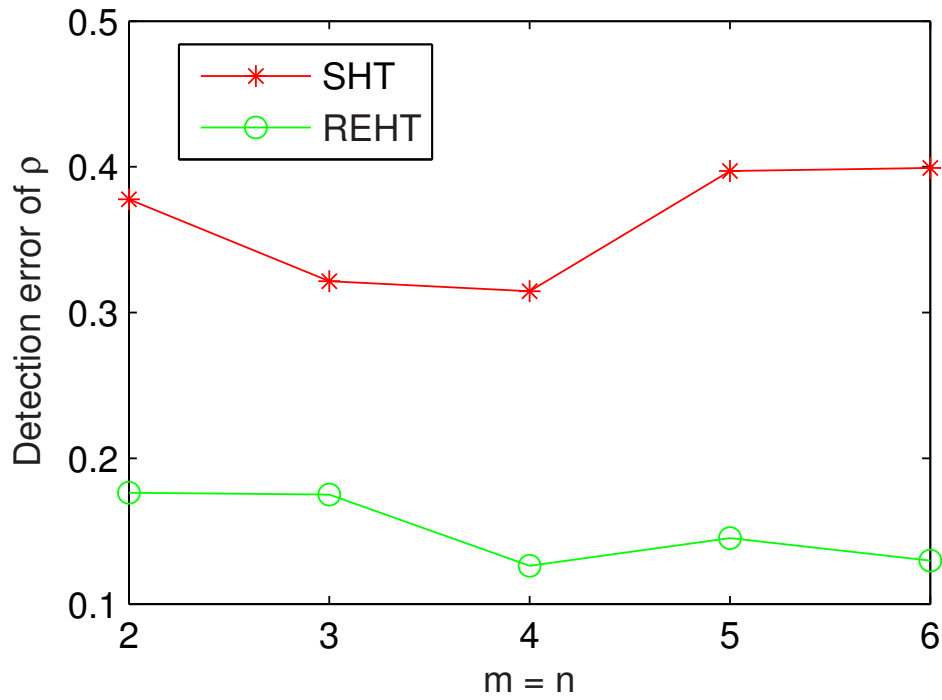
(a) The detection error of  $\theta$ (b) The detection error of  $\rho$ 

FIGURE 6.11: The effect of resolutions on SHT and REHT detection accuracy

The SHT ( $\Delta\theta = 1^\circ$  and  $\Delta\rho = 1$  pixel), the SHT with higher resolutions ( $\Delta\theta = 0.1^\circ$  and  $\Delta\rho = 0.1$  pixel), the method proposed in [11], the Randomised HT [22], and the proposed REHT are employed to compare the performances. The detection accuracy comparison is demonstrated in Fig. 6.10(b) and Fig. 6.10(c) where it is shown that the proposed method has a higher detection accuracy than all other compared methods. It should be noted that the straight lines are sorted by their  $\theta$  values in Fig. 6.10(b) and Fig. 6.10(c).

To study the effects of resolutions ( $\Delta\theta$  and  $\Delta\rho$ ) on detection accuracy, the trend of detection errors according to the increase of  $m$  and  $n$ , is demonstrated in Fig. 6.11(a) and Fig. 6.11(b). The detection errors in Fig. 6.11(a) and Fig. 6.11(b) are the average values of the detection errors of all the randomly generated straight lines, as shown in Fig. 6.10(a). Clearly, there is a decrease in detection errors in the proposed method. However, for the SHT, the detection errors might increase with an increase in resolutions, due to the problems of peak splitting and flattening.

### 6.3.3.2 Example of Real Images

In this experiment, several real images Fig. 6.12 are employed using different straight line detection methods. The SHT of feasible resolutions (denoted as LSHT) and infeasible high resolutions (denoted as HSHT), the multi-scale filtering method [11] (denoted as Magli), Randomised HT [22] (denoted as RHT), and the proposed method (denoted as REHT) are employed to compare detection performance. All the images in Fig. 6.12 and their edges shown in Fig. 6.13 come from the World Wide Web ([http://marathon.csee.usf.edu/edge/edge\\_detection.html](http://marathon.csee.usf.edu/edge/edge_detection.html)). These edge images are reported as being the best when employing Rothwell's edge detecting method [60]. Because the "true"  $\theta$  and  $\rho$  values are unknown for real images, the feature points belonging to a straight line are manually identified to estimate the  $\theta$  and  $\rho$  values by the least square (LS) fitting method. These estimations are considered as the "true" values. The detection errors of the strongest straight lines in these images are demonstrated in Table 6.4, where the smallest errors are shown in bold font. Table 6.4, demonstrates that, in most cases (5 of 8) the proposed REHT achieves the best detection accuracy among all the methods. In the cases that indicate the REHT is not better than other methods (3 out of 8), the detection accuracy of the proposed method is still acceptable.



FIGURE 6.12: Images contain straight line edge objects

TABLE 6.4: Comparison of detection errors

Methods		LSHT	HSHT	Magli	RHT	REHT
Briefcase	$e_\theta$	0.15	0.25	0.15	0.083	<b>0.007</b>
	$e_\rho$	1.81	2.18	2.63	1.37	<b>0.83</b>
Stairs	$e_\theta$	<b>0.03</b>	0.93	<b>0.03</b>	0.05	0.17
	$e_\rho$	0.69	6.1	0.94	0.24	<b>0.18</b>
Banana	$e_\theta$	0.08	0.08	0.08	<b>0.02</b>	0.04
	$e_\rho$	0.09	<b>0.02</b>	1.37	1.5	0.5
Brush	$e_\theta$	0.3	0.1	0.3	0.2	<b>0.04</b>
	$e_\rho$	2.25	0.83	2.96	2.13	<b>0.75</b>

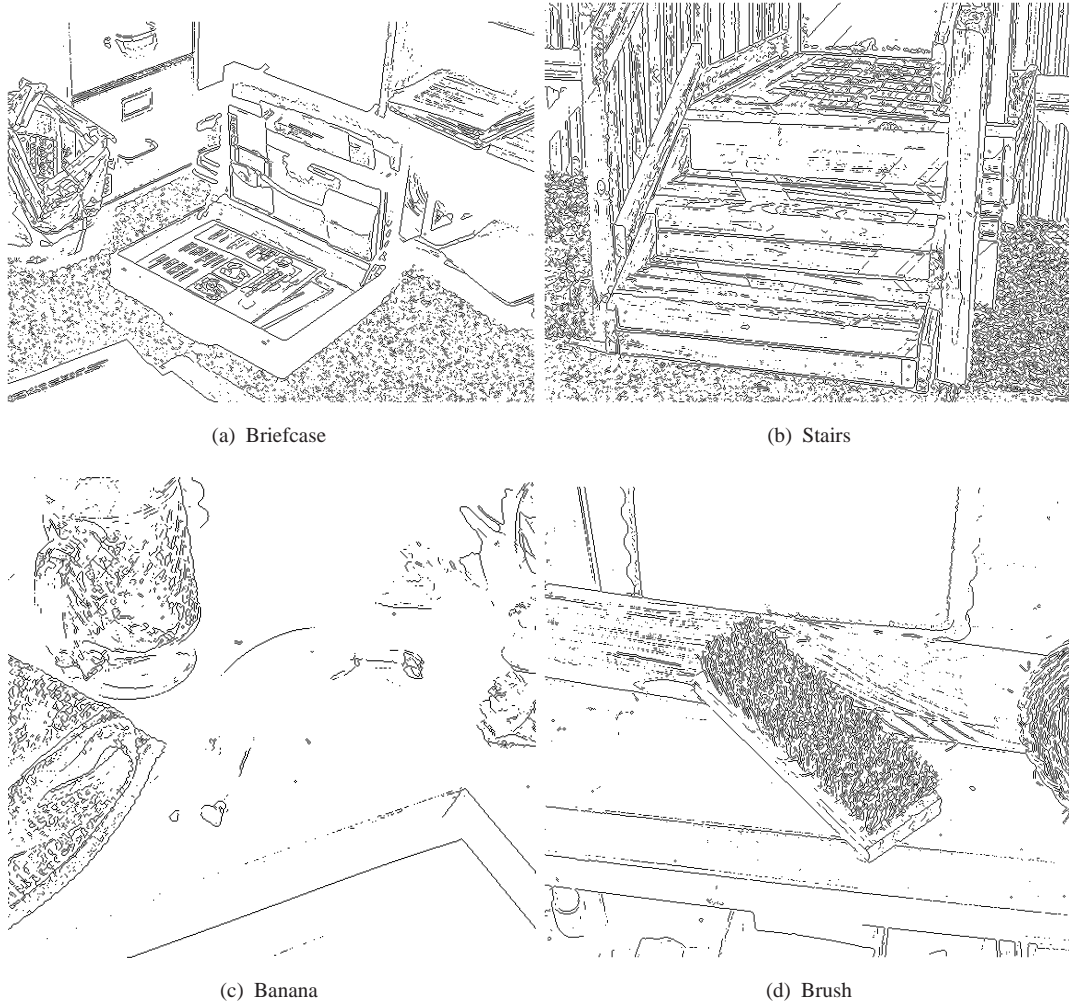


FIGURE 6.13: Edge images of Fig.6.12

# CHAPTER 7

## SUPER RESOLUTION HT

### 7.1 Super Resolution HT (SRHT)

Super resolution (SR) image reconstruction algorithms for improving resolution, using multiple low resolution (LR) images, have received much attention recently. The major merit of these resolution enhancement methods is that they save on expensive hardware costs by extracting SR from a collection of low resolution images. Pixel registration and high resolution image reconstruction are common in SR technology. Many SR techniques were reported, such as the nonuniform interpolation approach, [61], the frequency domain approach [62], projection onto convex sets [63] and iterative back-projection [64] etc.

Most SR algorithms are designed for digital optical images. Using SR techniques to improve the resolution of the HT is valuable because of the difficulties in obtaining very high resolution HT solutions. However, it is also challenging because the HT data is not just an optical image. In fact, there are differences existing in almost all the steps of SR reconstruction. The generation of multiple low resolution frames, cell (pixel) registration, and the conversion between high and low resolution frames should be re-considered.

In this research, a framework is proposed for applying super resolution techniques to improve the resolution of HT. According to the differences between normal images and HT data frames, the research covers all aspects of reconstructing a super resolution HT frame. Some important theoretical questions are addressed, such as how the images shifts affect the

HT peaks, how many shifts (the number of low resolution frames) are needed for high resolution reconstruction, the differences between shifting synthetic images and real images and, computation complexity.

It is shown that new information can be generated when applying the SHT to shifted images. The cell registration method is based on the theoretical analysis of the relationship between the HT data of the original and the shifted input images. A conversion between high and low resolution frames is proposed, based on the geometric relationship between these frames. A super resolution reconstruction method is proposed, based on iterated back-projection, to obtain a high resolution HT from low resolution HT data sequences, in order to overcome HT resolution and precision problems.

This is a novel idea. The method for the production of high resolution (HR) HT data from a sequence of low resolution (LR) HT data by applying super resolution techniques is unprecedented. The proposal in this research is the first of its kind.

### 7.1.1 Availability of Low Resolution Containing New Information

SR is based on the assumption that new information exists in LR frames. Because of the information lost due to the rounding operation in optical imaging sensors, sub-pixel biasing results in different pixel values for the same scene in different frames. The frames are observed by several cameras or by one camera in different positions. Thus, new information is generated.

For this work, only one image is employed. Therefore, the method to generate multiple HT frames from this single image is presented. Section 2.3.3 shows that if the input image is shifted, then its HT data might generate new information that cannot be obtained from the original HT data. This enables the traditional low resolution HTs to generate “new” information for super resolution reconstruction. A vertical shift is taken as an example. The following demonstrates what occurs in the HT space after the image is shifted.

For feature point  $(x, y)$ :

$$\rho = x \cos \theta + y \sin \theta. \quad (7.1)$$

After shifting vertically by  $\Delta y$  (without loss of generality assume a positive  $\Delta y$  means shifting upper):

$$\rho' = x' \cos \theta' + y' \sin \theta' \quad (7.2)$$

where

$$\begin{aligned} x' &= x \\ y' &= y - \Delta y \\ \theta' &= \theta \end{aligned} \quad (7.3)$$

that is,

$$\begin{aligned} \rho' &= x \cos \theta + (y - \Delta y) \sin \theta \\ &= x \cos \theta + y \sin \theta - \Delta y \sin \theta \\ &= \rho - \Delta y \sin \theta. \end{aligned} \quad (7.4)$$

This means, that shifting the input image, the  $\rho$  value in the column corresponding to  $\theta$  in the HT space will change by  $\Delta y \sin \theta$ . Since each column in the HT space has a different  $\theta$  value, the shifts in the HT space are column-wise. If  $\Delta y \sin \theta$  is not exactly equal to  $n\Delta\rho$  ( $n$  is an integer) then new splitting ratios for the vote of point  $(x, y)$  around cell  $(\theta, \rho)$  are generated. That is, a new vote distribution around cell  $(\theta, \rho)$  is generated after the votes of all the feature points are considered. Similar results can be obtained by shifting the given image horizontally, or both vertically and horizontally. Obviously, it is impossible for the  $\Delta y \sin \theta$  to be exactly equal to  $n\Delta\rho$  for all the columns. This implies that the HT data of a shifted input image always includes new information. Multiple HT data frames containing new information can therefore be obtained by applying low resolution HT to the shifted input image.

### 7.1.2 The Number of Frames Needed for SR Reconstruction

In Section 2.3.3, Figs. 2.8 and 2.9 depicted a very interesting feature of the HT peak height when the images are shifted horizontally and vertically. A pseudo-period pattern appears in the peak height curves. The peak heights repeat the similar sequence in each period, therefore, the HT frames in one period are logically considered to represent approximately the “complete” information set to be used in the high resolution HT data reconstruction.

The reason for this period feature is discussed. The height of the peak directly relates to the

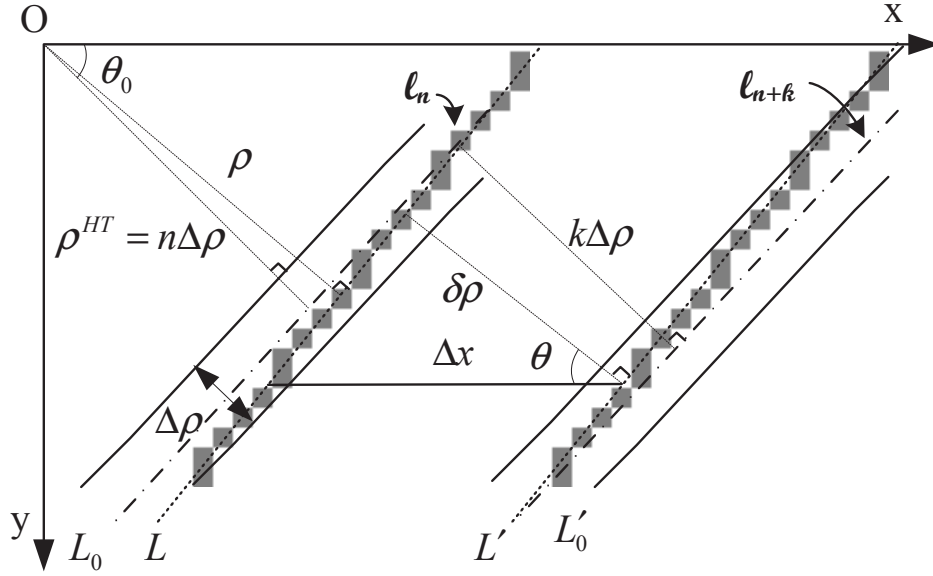


FIGURE 7.1: Horizontally move a straight line

votes distribution of the feature points lying on the straight line ( $L$ ). As depicted in Fig. 7.1, the belt (denoted by  $L_n$  and middle line  $L_0$ ) corresponding to the peak contains most of these feature points. The bias between the  $\rho$  value of the straight line and the  $\rho^{HT}$  representing the peak cell, that is, the relative position of the straight line in the belt, determines the vote contribution of these feature points.

After shifting the image horizontally by  $\Delta x$ , the position of these feature points will realise the same change. Therefore, the  $\theta$  of the straight line does not change, but the  $\rho$  value displays the following increment (or decrement, depending on the position of the straight line in the image)

$$\delta\rho = \Delta x \cos \theta. \quad (7.5)$$

If

$$\delta\rho \neq \tau\Delta\rho \quad (7.6)$$

where  $\tau$  is an integer, then the bias between  $\rho$  and  $\rho^{HT}$  will change with the shift. This leads to the rearrangement of the votes of these feature points. Therefore, the votes obtained in a cell change when the image is shifted.

After each shift, the change of this bias is

$$\varepsilon = \delta\rho - \tau\Delta\rho. \quad (7.7)$$

Therefore, the period is

$$K = \left\lceil \frac{\Delta\rho}{|\varepsilon|} \right\rceil, \quad (7.8)$$

which is also the number of frames needed in the reconstruction.

Similarly, if the image is shifted vertically by  $\Delta y$ :

$$\delta\rho = \Delta y \sin \theta. \quad (7.9)$$

It should be noted that during the shifting process the  $\Delta x$  is selected to be an integral number of pixels. This will retain the shape of the straight line in the image space, that is, no extra rounding errors occur.

### 7.1.3 Cell Registration

Cell registration, that is, aligning low resolution frames to the reference frame, is an important step in super resolution techniques. From Section 2.3.3 and Section 7.1, the application of the HT to a shifted input image can generate “new” information. Therefore, the original input image can be shifted to obtain a sequence of input images, followed by applying the HT to generate multiple HT frames from these images. Each cell in these HT frames will be registered to the reference frame (the HT data of the original image). The reference frame and registered frames are the LR HT frames used to reconstruct the HR HT frame.

In the digital optical images of the same scene, most pixels form groups and retain strong neighbour relationships ( a stable relative position in a group) among frames, and hence, the difference between frames are block based. Many macro blocks find their corresponding blocks in other frames, and therefore, motion estimation based methods, such as block matching, are effective for pixel registration.

However, in the HT space the difference between frames are column-wise, as shown in Eq. (7.4), which means conjoint pixels (cells in HT) in neighbouring columns will no longer be

conjoint in the HT frame of a shifted image, that is, neighbouring relations are lost. The bias depends on both image shift and the position of the cell in the HT space and therefore, techniques such as block matching cannot be employed in this situation.

The method to register cells of multiple HT data frames to the reference frame, that is, calculate the bias of each cell corresponding to the reference frame, is discussed. As shown in Eq. (7.4), the HT frame is biased column-wise after vertically shifting the given image. For the column corresponding to  $\theta$ , the bias is  $-\Delta y \sin \theta$ . Therefore, for a cell  $(\theta', \rho')$  in the vertically shifted HT frame, its corresponding cell in the reference frame is  $(\theta', \rho' + \Delta y \sin \theta')$ .

Similarly, as shown in Eq. (7.4), after horizontally shifting the given image by  $\Delta x$  (without loss of generality assume a positive  $\Delta x$  means shifting left):

$$\rho' = x' \cos \theta' + y' \sin \theta' \quad (7.10)$$

where

$$\begin{aligned} x' &= x - \Delta x \\ y' &= y \\ \theta' &= \theta \end{aligned} \quad (7.11)$$

that is,

$$\begin{aligned} \rho' &= (x - \Delta x) \cos \theta + y \sin \theta \\ &= x \cos \theta + y \sin \theta - \Delta x \cos \theta \\ &= \rho - \Delta x \cos \theta. \end{aligned} \quad (7.12)$$

Consequently, for a cell  $(\theta', \rho')$  in the HT data of horizontally shifted HT frame, its corresponding cell in the reference frame is  $(\theta', \rho' + \Delta x \cos \theta')$ .

If  $\Delta y \sin \theta$  and  $\Delta x \cos \theta$  are not exactly equal to  $n\Delta\rho$ , it follows that the shifts imply new information.

The peak position in the LR frame was generated by low resolution HT and hence, is not accurate. To increase the accuracy, the average of the low resolution peak coordinate of the shifted images are considered the peak position in the HR frame after registration in the reference frames.

### 7.1.4 Conversions between HR and LR HT Frames

When constructing super resolution HT data frames, the conversions between high and low resolution frames also need to be considered. For digital optical images, isotropic operators are used to preserve the intensity of pixels, such as up-sampling and down-sampling factors and “blur” and “sharpen” filters.

In HT, the intensity is the votes obtained by a cell, when the  $\rho$ –resolution is increased the intensity decreases. In fact the integral of each column is presumed to be a constant, that is,

$$\sum_{j=1}^N H(i, j) = C \quad (7.13)$$

where  $N$  is the height of the HT space and  $C$  is the number of total feature points in the image space. Each column is interpolated and up-sampled to obtain a higher  $\rho$ –resolution than scaled, in order to preserve the integral. To increase the  $\theta$ –resolution, columns are inserted between two low resolution columns with the intensity generated by interpolation.

To decrease the resolution the reverse operations are used, that is, interpolating and down-sampling the HR frame, but preserving the integral of each column.

### 7.1.5 HR Reconstruction Based on Iterated Back-Projection

After registration, a back-projection algorithm [64] is employed to reconstruct high-resolution HT data by using the following steps:

1. Shift the original image in  $x$  or  $y$  directions, then employ SHT on the images to obtain the observed low LR HT frames  $\{g_k, k = 2, \dots, K\}$ .
2. Register the LR HT frames according to Eq. (7.12) or Eq. (7.4).
3. The HR HT frame converted from the LR HT data of the original image is considered an initial guess  $f^{(0)}$  of the high resolution HT frame.
4. By interpolation and down-sampling, a low resolution HT frame  $g_1^{(n)}$  is generated from the current high resolution HT frame  $f^{(n)}$ .
5. Apply the shifting process shown in Eq. (7.4) and Eq. (7.12) to  $g_1^{(n)}$  to generate a set of low resolution HT frames  $\{g_k^{(n)}, k = 2, \dots, K\}$  corresponding to the shifts made on the given image.

6. If  $f^{(n)}$  is correct then  $\{g_k^{(n)}, k = 1, \dots, K\}$  should be identical to the observed LR HT frames  $\{g_k, k = 1, \dots, K\}$ . The error matrix  $\{(g_k - g_k^{(n)}), k = 1, \dots, K\}$  is used to improve  $f^{(n)}$  by using the “back-project” operation, that is extend the low resolution HT error matrix to the size of  $f^{(n)}$  by interpolation followed by the application of image sharpening to the extended error matrix. Weighted error matrix are then added to  $f^{(n)}$  to obtain  $f^{(n+1)}$ .
7. Repeat from Step 4 until reaching a predefined error or a given number of iterations.

The error function is

$$e^{(n)} = \frac{|f^{(n)} - f^{(n-1)}|}{|f^{(n)}|} \quad (7.14)$$

The formulation for the iterative back-projection is

$$f^{(n+1)} = f^{(n)} + \lambda E_{xt} \left( \sum_{k=1}^K (g_k - g_k^{(n)}) \right), \quad (7.15)$$

where

$f^{(n)}$ : the high-resolution solution of  $n$ -th iteration.

$\lambda$ : the step size.

$g_k$ : the  $k$ -th observed low-resolution HT data.

$g_k^{(n)}$ : the low-resolution HT frames obtained from  $f^{(n)}$  by simulating the optical imaging and HT shifting processes.

$K$ : the number of observed low-resolution frames.

$E_{xt}\{\}$ : the process of extending the size of  $\sum_{k=1}^K (g_k - g_k^{(n)})$  to the size of  $f^{(n)}$  by interpolation and then up-sampling but preserve the integral of each column.

Using this method cannot ensure the solution only contains non-negative cells, However, that the number of votes received by any cell in the HT space should be non-negative. Therefore Eq. (7.15) is modified as

$$f^{(n+1)} = P_+(f^{(n)} + \lambda E_{xt}(\sum_{k=1}^K (g_k - g_k^{(n)}))), \quad (7.16)$$

where

$$P_+[f(x)] = \begin{cases} 0, & \text{if } f(x) < 0 \\ f(x), & \text{if } f(x) \geq 0 \end{cases}. \quad (7.17)$$

This non-negative constraint ensures the solution of each iteration only contains non-negative cells.

## 7.2 Discussion

### 7.2.1 A Way to Reduce Computation Load

In the straight line detection algorithms using Hough butterflies, only the central part of the butterfly is used. Therefore, when the proposed method is used in these algorithms, only the central part needs to be rebuilt. The HT for shifted images can be limited within the requested scope in the parameter space.

To determine the requested scope in the parameter space, one needs to determine the centre of the scope, that is, the position of the new peak. In fact, the position of the peak of the shifted straight line is predictable, according to Eq.(7.5).

This predefined scope and predictable peak position greatly reduce the computation load of performing HT in shifted images.

### 7.2.2 Horizontal and Vertical Lines

When the straight line is horizontal or vertical and  $\Delta\rho$  is an integral number of pixels, the inequality in Eq. (7.6) does not hold. The  $\varepsilon$  in Eq. (7.7) will be 0. Therefore, in the frames needed for SR reconstruction, (that is, the  $K$  in Eq. (7.8)) is infinity, which means the proposed method cannot rebuild the super resolution HT data. In fact, under this situation, no new information is included in the shifted images.

## 7.3 Experiments and Results

To validate the iterative back-projection reconstruction algorithm for improving HT resolution, experiments using synthetic images and real images are carried out. In the experiments, both HT data and straight line detection errors are considered.

### 7.3.1 HT Data Generated by the Proposed Method

The first experiment aims to demonstrate the HT data obtained by the proposed method. A synthetic straight line is generated in this experiment.

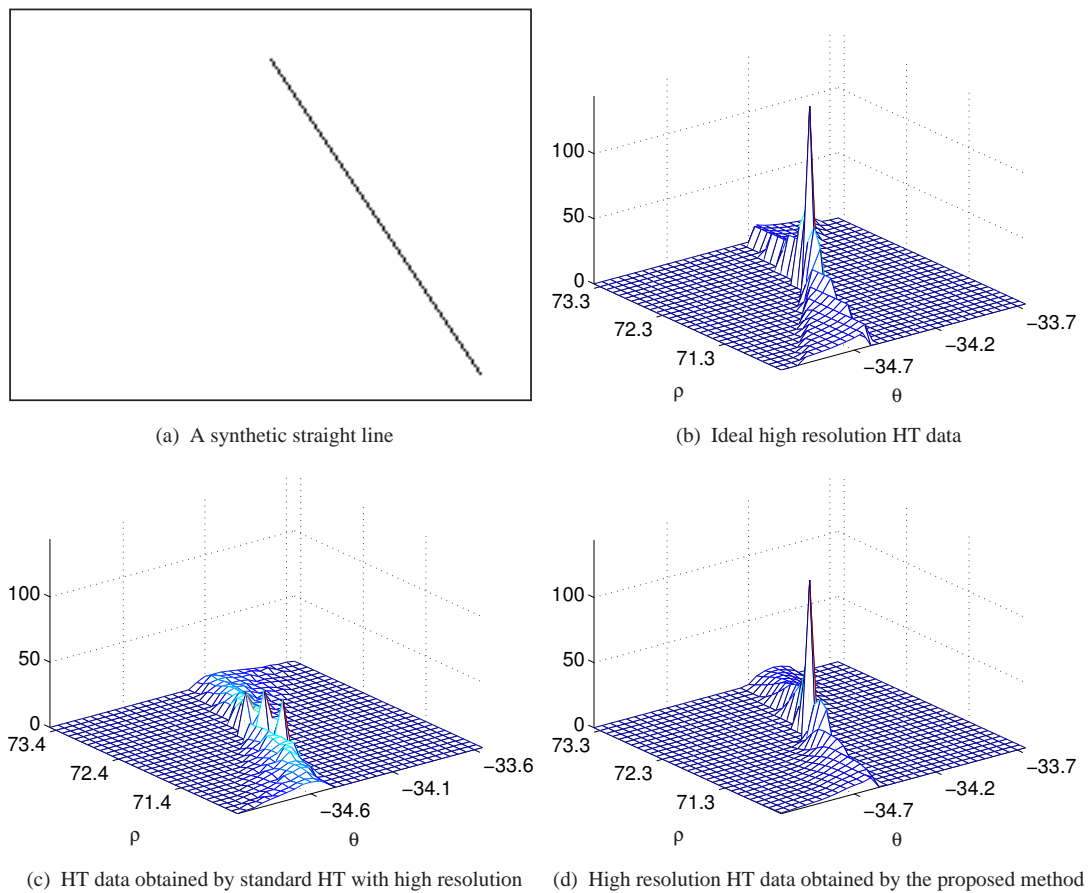


FIGURE 7.2: Performance comparison for a synthetic straight line

A randomly generated straight line is shown in Fig. 7.2(a). The image is horizontally shifted by  $\Delta x = 1$  pixel each time. The HT resolutions are  $\Delta\rho = 1$  and  $\Delta\theta = 1^\circ$  respectively. The

expected resolutions are  $\Delta\rho = 0.1$  and  $\Delta\theta = 0.1^\circ$  respectively. Fig. 7.2 demonstrates the performance comparison of the Standard HT and the proposed method. As the template for the comparison, Fig. 7.2(b) shows the “ideal” HT data generated using the known end points [65]. Fig. 7.2(c) demonstrates the HT data obtained by Standard HT with the expected high resolutions, and Fig. 7.2(d) shows the HT data from the proposed method with the same resolutions. Fig. 7.2(b) and Fig.7.2(d) indicate that the proposed method obtained the HT data very similar to the ideal one. However, the one from Standard HT (Fig. 7.2(c)) experience many problems, as discussed in Section 2.2.2.

### 7.3.2 Straight Line Detection Errors

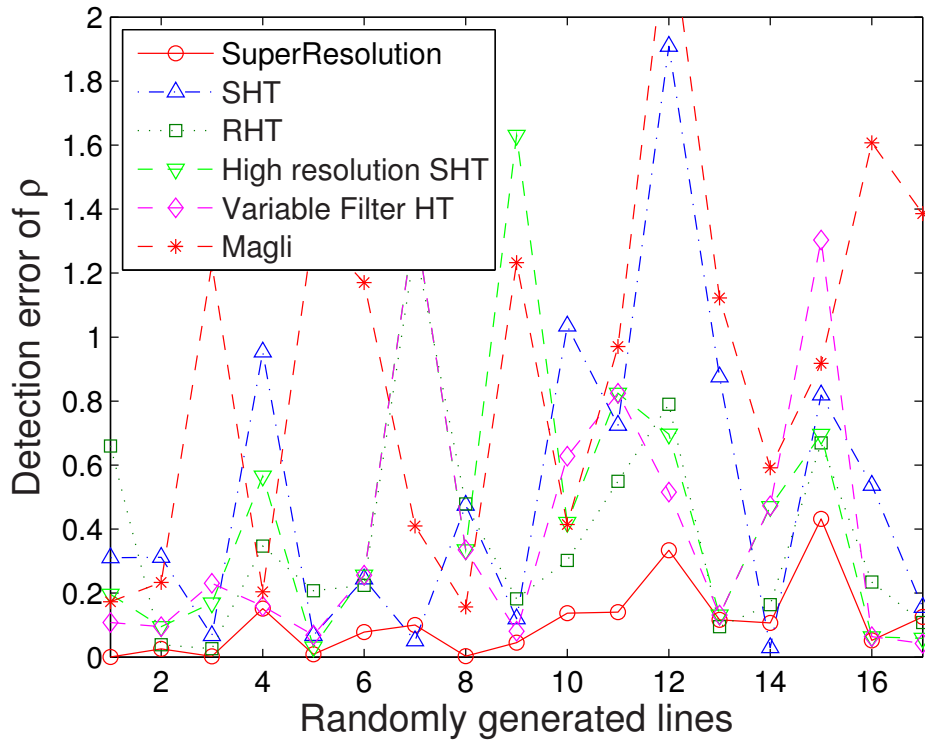
In this experiment, a series of synthetic straight lines are randomly generated (both  $\theta$  and  $\rho$  are known), and the detection errors are compared between low resolution SHT and high resolution SHT. Some other methods (variable filter HT, VFHT [66], Magli [11], Randomised HT and RHT [22]) are considered for comparison.

Fig. 7.3 depicts the detection errors of  $\theta$  and  $\rho$ . In most cases, The proposed method outperforms other methods.

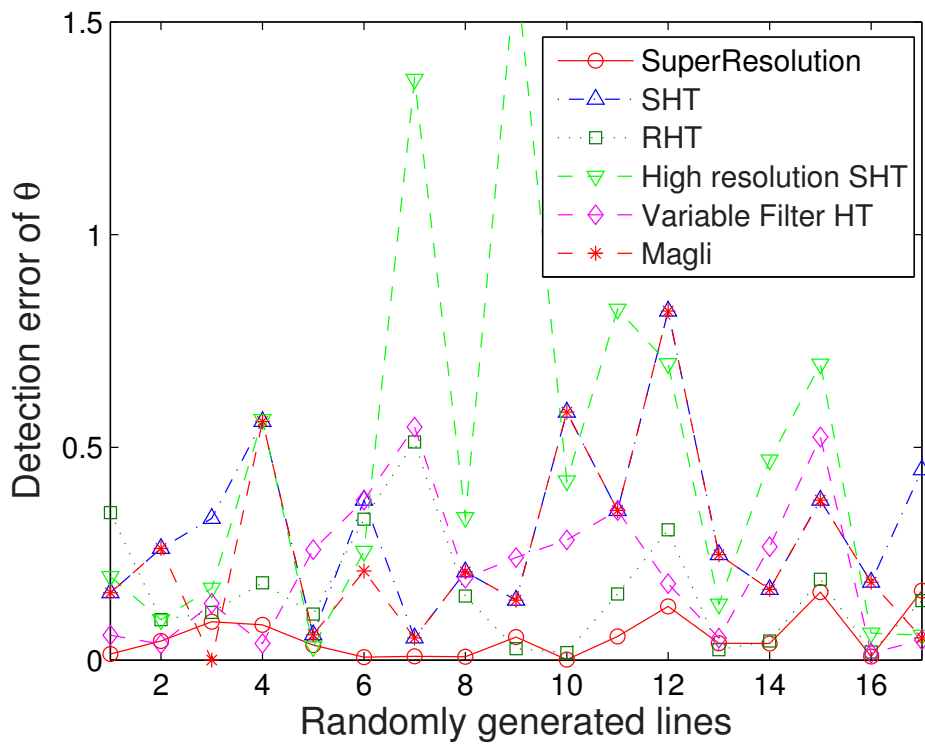
### 7.3.3 Comparison for a Real Image

As a real image, an arrow mark on the road is used. Its edges are numbered, as shown in Fig. 7.4. To estimate the detection errors, the endpoints are manually measured to calculate the “true” values of  $\theta$  and  $\rho$ . To remove the background disturbances, the windowing method proposed in [50] is employed before detecting the straight lines.

Table 7.1 demonstrates the detection errors of the different methods. For each edge, the minimum detection errors are highlighted in bold font. It is shown that the proposed method detected the straight lines with the minimum of errors in most cases.



(a) Detection error of  $\rho$



(b) Detection error of  $\theta$

FIGURE 7.3: Detection error comparison for randomly generated straight lines

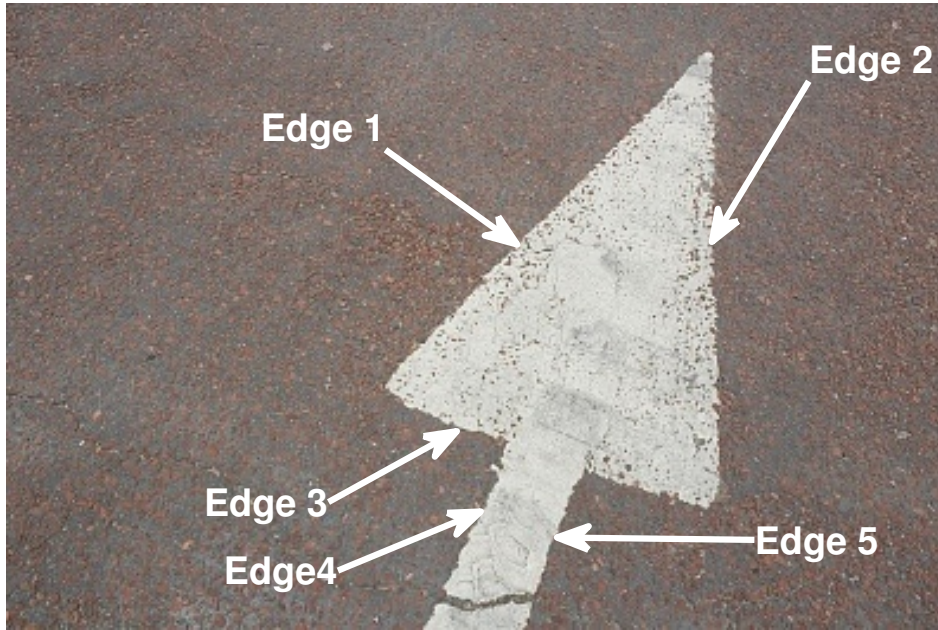


FIGURE 7.4: The edges of the arrow mark to be detected

TABLE 7.1: Comparison of detection error

Methods		LSHT	HSHT	VFHT	Magli	RHT	SRHT
Edge 1	$e_\theta$	0.13	0.82	0.92	<b>0.083</b>	0.15	0.26
	$e_\rho$	0.43	0.23	0.23	1.31	0.077	<b>0.057</b>
Edge 2	$e_\theta$	0.29	0.99	0.11	0.012	0.076	<b>0.006</b>
	$e_\rho$	0.31	1.22	0.4	1.02	0.34	<b>0.25</b>
Edge 3	$e_\theta$	0.13	0.57	0.47	0.034	0.22	<b>0.0045</b>
	$e_\rho$	0.68	2.19	1.89	0.43	0.94	<b>0.1</b>
Edge 4	$e_\theta$	0.23	0.56	0.46	0.04	0.53	<b>0.038</b>
	$e_\rho$	0.54	1.66	0.96	1.59	1.35	<b>0.0076</b>
Edge 5	$e_\theta$	0.82	0.35	0.15	0.65	0.27	<b>0.0084</b>
	$e_\rho$	2.29	1.09	0.48	2.62	0.8	<b>0.39</b>

## CHAPTER 8

# LINE POSITIONING BASED ON HT ERROR COMPENSATION

### 8.1 The $\rho$ Value Detection Error of HT

As shown in Fig. 8.1, the segment  $S_0$  belongs to the straight line  $L_0(\rho_0, \theta_0)$  in the image space. HT attempts to involve the feature points of  $S_0$  in a belt (surrounded by  $l_n$  and  $l_{n+1}$  as shown Fig. 8.1). This corresponds to the cell  $(n\Delta\rho, \theta_0)$  in the HT space. All straight line segments lying in this belt are considered to have the same  $\rho$  value.

The logic of  $\rho$  value discretisation in HT is as below. If

$$n\Delta\rho - 0.5\Delta\rho \leq \rho_0 < n\Delta\rho + 0.5\Delta\rho, \quad (8.1)$$

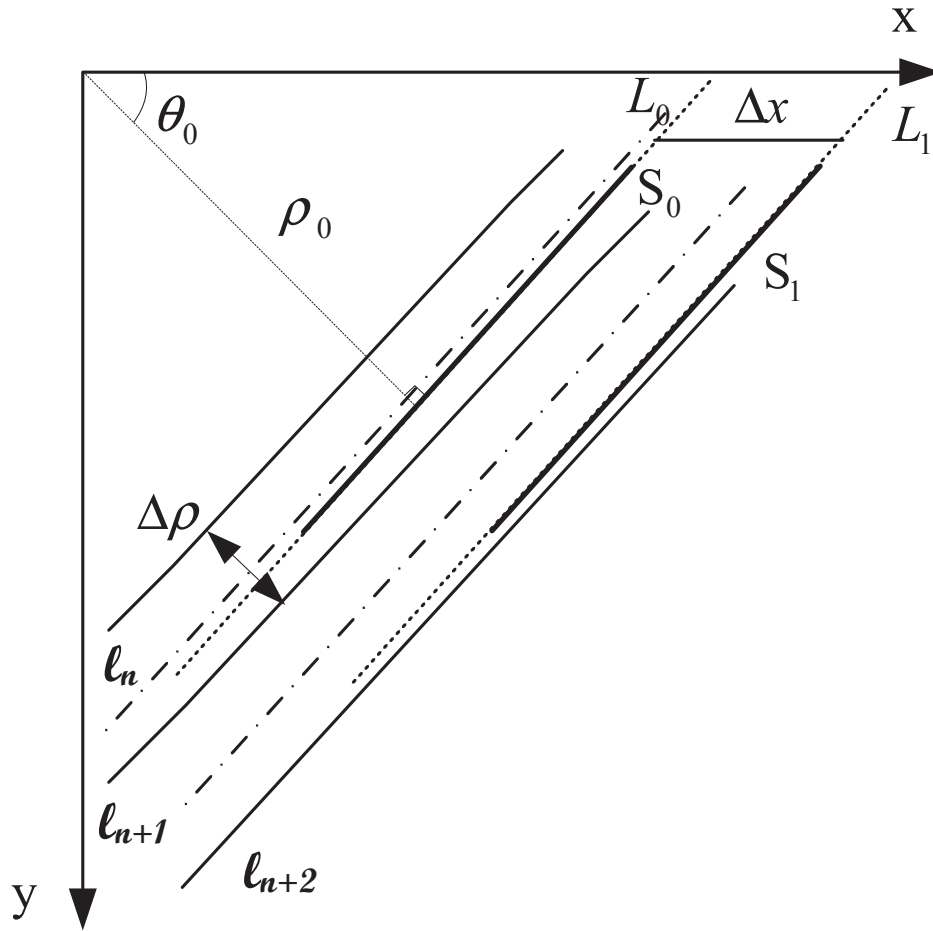
then the detected value is

$$\rho_0^{\text{HT}} = n\Delta\rho, \quad (8.2)$$

that is, the  $\rho$  value of the centre line of the belt.

Obviously, for a straight line lying in the belt, the  $\rho$  value is not equal to  $n\Delta\rho$ . For example, regarding  $S_0$  in Fig. 8.1, a detection error is generated: that is,

$$e_{\rho_0} = \rho_0 - n\Delta\rho. \quad (8.3)$$

FIGURE 8.1: The generation of  $\rho$  value detection error in HT

Because this error is omitted during the voting process, it is unknown if the  $\rho$  value of  $S_0$  can be detected by seeking the peak position in the HT space. Only the detected  $\rho$  value, that is,  $\rho_0^{\text{HT}}$  can be obtained.

## 8.2 Shifting the Image Can Generate New Detection Errors

As shown in Fig. 8.1, segment  $S_0$  is shifted horizontally by  $\Delta x$ , that is moved to  $S_1$ . Assuming the shifted segment, that is,  $S_1$ , lies in the belt  $n + k$  ( $k$  is an integer, for example  $k = 1$  in the case of Fig. 8.1), it is evident

$$\rho_1 = \rho_0 + \Delta x \cos \theta_0, \quad (8.4)$$

and

$$e_{\rho_1} = \rho_1 - (n+k)\Delta\rho, \quad (8.5)$$

where

$$k = \left\lfloor \frac{\Delta x \cos \theta_0}{\Delta\rho} \right\rfloor, \quad (8.6)$$

“ $\lfloor \quad \rfloor$ ” is the floor function.

Substitute Eq. (8.4) into Eq. (8.5),

$$\begin{aligned} e_{\rho_1} &= \rho_0 + \Delta x \cos \theta_0 - (n+k)\Delta\rho \\ &= \rho_0 - n\Delta\rho + \Delta x \cos \theta_0 - k\Delta\rho \end{aligned} \quad (8.7)$$

Substitute Eq. (8.3) into Eq. (8.7), one gets

$$e_{\rho_1} = e_{\rho_0} + \Delta x \cos \theta_0 - k\Delta\rho. \quad (8.8)$$

Obviously, if

$$\Delta x \cos \theta_0 \neq k\Delta\rho, \quad (8.9)$$

then

$$e_{\rho_1} \neq e_{\rho_0} \quad (8.10)$$

that is, a new detection error is generated.

It should be noted that the shifted segment lies in the belt  $n+k$  which means

$$|\Delta x \cos \theta_0 - k\Delta\rho| < \Delta\rho. \quad (8.11)$$

### 8.3 Measuring the Detection Error via the Sequence of Detected $\rho$ Values of the Shifted Images

The analysis in Section 8.2 demonstrates that the detection error of the shifted line is related to the detection error of the original line. If the original line is shifted in the same direction several times, for example, horizontal shifts of 1, 2, 3  $\dots$ , pixels, that is,  $\Delta x = 1, 2, 3, \dots$ , a sequence of detection errors will be generated. Denote the sequence by  $e_{\rho_0}, e_{\rho_1}, e_{\rho_2}, e_{\rho_3}, \dots$ .

Similar to Eq. (8.8):

$$\begin{aligned}
 e_{\rho_1} &= e_{\rho_0} + \cos \theta_0 - k\Delta\rho \\
 e_{\rho_2} &= e_{\rho_1} + \cos \theta_0 - k\Delta\rho \\
 &= e_{\rho_0} + 2(\cos \theta_0 - k\Delta\rho) \\
 e_{\rho_3} &= e_{\rho_2} + \cos \theta_0 - k\Delta\rho \\
 &= e_{\rho_0} + 3(\cos \theta_0 - k\Delta\rho) \\
 &\dots
 \end{aligned} \tag{8.12}$$

Obviously, if

$$\Delta x \cos \theta_0 - k\Delta\rho > 0, \tag{8.13}$$

then the sequence is an increasing arithmetical series, which means there exists an  $i$  making

$$e_{\rho_i} < 0.5\Delta\rho \tag{8.14}$$

and

$$e_{\rho_{i+1}} \geq 0.5\Delta\rho, \tag{8.15}$$

that is,

$$e_{\rho_0} + i(\cos \theta_0 - k\Delta\rho) < 0.5\Delta\rho \tag{8.16}$$

and

$$e_{\rho_0} + (i+1)(\cos \theta_0 - k\Delta\rho) \geq 0.5\Delta\rho. \tag{8.17}$$

From Eq. (8.16) and Eq. (8.17), the following is obtained,

$$0.5\Delta\rho - (i+1)(\cos \theta_0 - k\Delta\rho) \leq e_{\rho_0} < 0.5\Delta\rho - i(\cos \theta_0 - k\Delta\rho). \tag{8.18}$$

It is clear that the middle value of this interval,

$$\hat{e}_{\rho_0} = 0.5\Delta\rho - (i+0.5)(\cos \theta_0 - k\Delta\rho), \tag{8.19}$$

can be used as the estimation of  $e_{\rho_0}$  with the estimation precision  $(\cos \theta_0 - k\Delta\rho)$ .

Similar results are obtained if

$$\Delta x \cos \theta_0 - k\Delta\rho < 0, \tag{8.20}$$

but the sequence is a decreasing arithmetical series.

Similarly, if the image is shifted vertically the following is obtained,

$$\hat{e}_{\rho_0} = 0.5\Delta\rho - (i + 0.5)(\sin \theta_0 - k\Delta\rho), \quad (8.21)$$

Eq. (8.14) and Eq. (8.15) demonstrate that  $e_{\rho_{i+1}}$  is the first item in the error series that crosses the bound of a belt. Therefore  $i$  can be denoted as a *critical crossing point*.

## 8.4 High Precision $\rho$ Value Detection based on Error Compensation

From the analysis in the above sections, it is seen that the value detection error of a line can be measured if the critical crossing point is known.

In the case of horizontal shifting of the original segment by  $\Delta x$ , the shifted segment lies in belt  $n + k$ . Therefore, the detected  $\rho_1$  value is

$$\rho_1^{\text{HT}} = (n + k)\Delta\rho, \quad (8.22)$$

and

$$e_{\rho_1} < 0.5\Delta\rho, \quad (8.23)$$

Similarly,

$$\begin{aligned} \rho_2^{\text{HT}} &= (n + 2k)\Delta\rho. \\ \rho_3^{\text{HT}} &= (n + 3k)\Delta\rho. \\ &\dots \\ \rho_i^{\text{HT}} &= (n + ik)\Delta\rho, \end{aligned} \quad (8.24)$$

and

$$e_{\rho_2}, e_{\rho_3}, \dots, e_{\rho_i} < 0.5\Delta\rho. \quad (8.25)$$

From Eq. (8.15) the following is derived:

$$\rho_{(i+1)}^{\text{HT}} = (n + (i + 1)k + 1)\Delta\rho. \quad (8.26)$$

In seeking the HT peak position of the original and shifted images the following sequence is obtained:

$$H = \{n, n+k, \dots, n+ik, n+(i+1)k+1, n+(i+2)k+1, \dots\} \quad (8.27)$$

That is, the sub-series from item 0 to item  $i$  is an arithmetical series. Another arithmetical series is seen from item  $i+1$ . The difference series of Eq. (8.27) is

$$\begin{aligned} D_H &= \{H(j+1) - H(j), j = 1, 2, \dots\} \\ &= \underbrace{\{k, \dots, k, k+1, k, \dots\}}_i. \end{aligned} \quad (8.28)$$

Therefore, the critical crossing point  $i$  can be obtained by detecting the mutation in the difference series  $D_H$  of the peak position series shown in Eq. (8.27). Consequently, the compensated error measurement of  $\rho_0$  is

$$\begin{aligned} \hat{\rho}_0 &= \rho_0^{\text{HT}} + \hat{e}_{\rho_0} \\ &= n\Delta\rho + 0.5\Delta\rho - (i+0.5)(\sin\theta_0 - k\Delta\rho), \end{aligned} \quad (8.29)$$

where  $n$  is the position of the HT peak in the  $\rho$  direction which can be obtained by seeking the peak in the HT space.  $\Delta\rho$  is the  $\rho$ -resolution of the HT,  $\theta_0$  is obtained by seeking the HT peak,  $i$  is the critical crossing point obtained by detecting the mutation in the difference series  $D_H$  as shown in Eq. (8.28), and  $k$  is obtained by Eq. (8.6).

## 8.5 Experiments

Fig. 8.2 illustrates a segment and its detected position. It is clear that the proposed method detects the line position much closer to the true position than the SHT.

If the image in Fig. 8.2 is shifted, a series of shifted images are obtained, and each one contains a segment with a different position. Fig. 8.3 illustrates the detected position of the segment in each image. The detection accuracy of the proposed method is substantially superior than the SHT. Fig. 8.4 shows the positioning error of these segments where the error of the proposed method is considerably smaller than that of SHT.

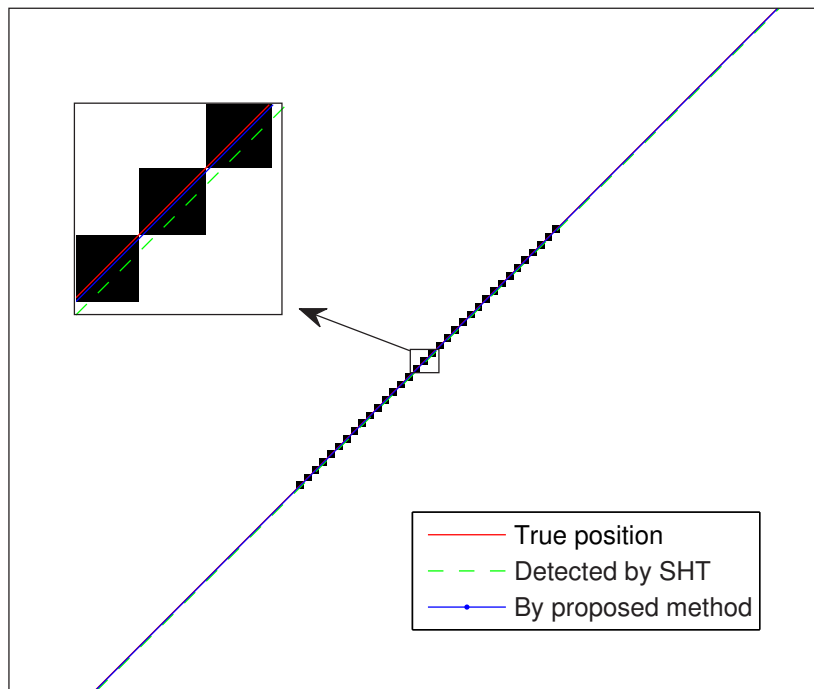


FIGURE 8.2: Comparison of detected position of given line

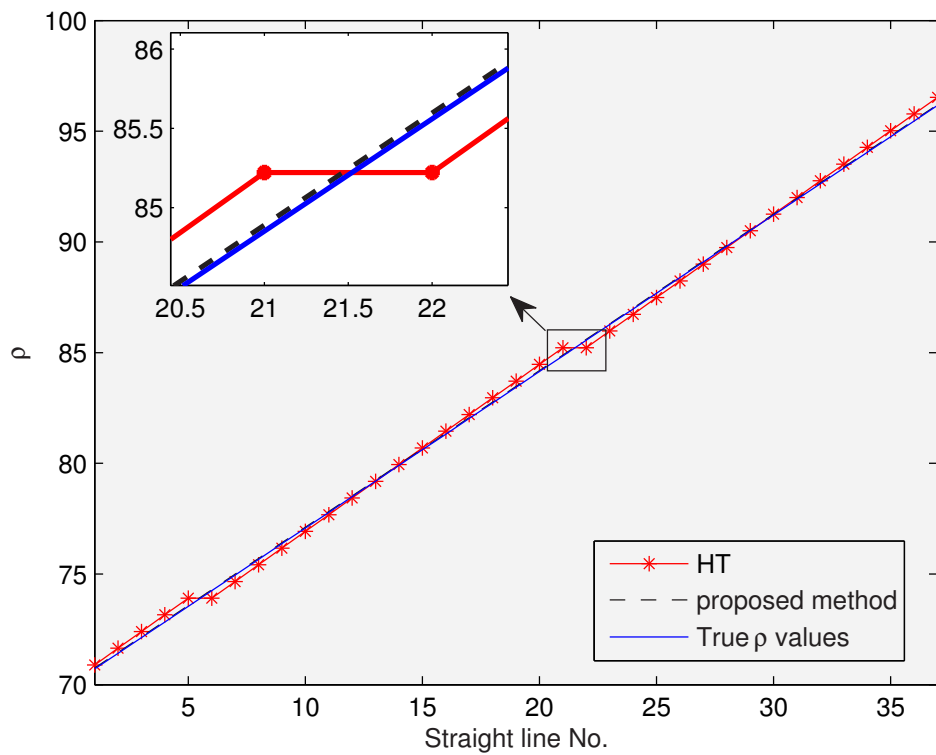


FIGURE 8.3: Comparison of detected  $\rho$  values of shifted straight lines

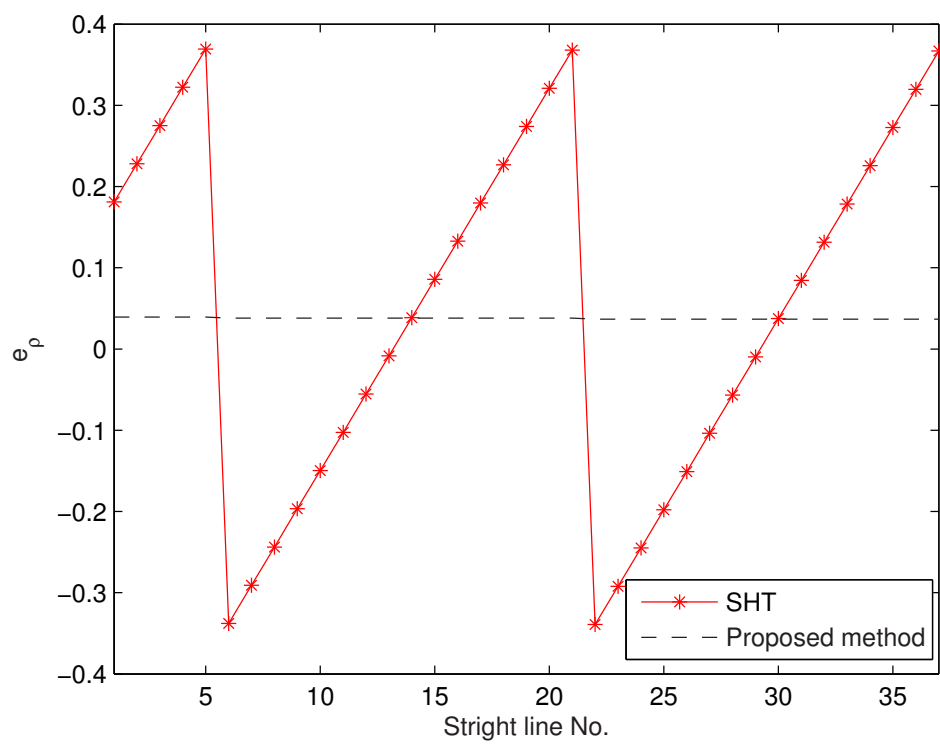


FIGURE 8.4: Comparison of detection error

## CHAPTER 9

# AN ASSESSMENT TOOL FOR HTs – “IDEAL” HT

The HT does not directly detect segments. It maps them to the parameter space and generates HT data. The peaks in HT data represent the normal parameters of the straight lines containing the segments. The HT is robust when used for straight line detection, that is, only for the detection of and, because it converts the straight line detecting problem to a peak seeking problem. However, when it is employed to detect the complete parameters of segments, such as  $(\theta, \rho)$ , width, length, end points and even collinearity and continuity, the robustness is seriously affected. To detect the complete segment parameters, a variety of HT-based methods are presented [8, 47, 50, 51, 53, 67]. Among them, the butterfly-based methods have received much attention. [47, 51, 53] Butterfly-based segment detection is based on the fact that HT is closely related to Radon Transform [68]. Therefore, detailed information about image structure, including comprehensive information about line segments, exists in the Hough space. However, these details are represented not only by the peak but also by other HT cells around the peak, that is, the butterfly. Thus, the quality of the HT butterfly directly affects the performance of segment detection. Unfortunately, the approach for assessing HT butterfly quality is an ongoing problem. Furthermore, besides the Standard HT (SHT), many HT varieties are proposed such as, Probabilistic HT (PHT), [26], Randomised HT (RHT) [22] and Fast HT(FHT) [18]. The butterflies generated by these HT varieties are different from one another, which leads to the dependency of effective evaluations based on the butterfly. This however, also yields further difficulties.

SHT cannot be used either as a segment measuring tool or as a standard to evaluate other HT methods. The comparison of the HTs’ performance via the number/accuracy of detected objects is not satisfactory because of the lack of comparison between the intermediate data used (usually the HT data). Therefore, the procedure for assessing the performance of various HT methods is an ongoing problem. This section addresses the calculation of the “ideal” HT data as the standard to assess the HT data used in the various HT methods, in order to obtain a better comparison. Since the image space  $(x, y)$  and the HT space  $(\rho, \theta)$  are discrete, quantisation and rounding errors affect the accuracy and performance of the HT.

This chapter addresses the “ideal” HT data calculation, which is independent of the HT methods, digital discretisation errors in the image space, and parameter errors due to the voting and verifying processes. The generated HT data is dependent only on the basic physical facts, that is, the endpoints of the segment. The “ideal” HT data is employed to evaluate the data generated by the HT varieties. Given a specific segment detection method, the “ideal” HT data may also be used to evaluate the performance improvement potential by assessing the HT data used.

## 9.1 Expectations of the “Ideal” HT Data

The “ideal” HT data should have the following features:

- HT data free from image space errors;
- HT data free from parameter space errors;
- The peak represents the length of the segment;
- HT data free from the effects of resolution settings;
- HT data measures the complete parameters of segments.

Considering these expectations and the fact that the “ideal” HT data is available, when the parameters of the segment are known, the calculation should depend only on the physical fact, that is, the endpoints  $(x_1, y_1)$  and  $(x_2, y_2)$ . Therefore, the peak can be determined as:

$$\theta_p = \arctan \frac{y_2 - y_1}{x_2 - x_1}, \quad (9.1)$$

$$\rho_p = x_1 \cos \theta_p + y_1 \sin \theta_p, \quad (9.2)$$

and the height of the peak should be equal to the length of the segment, that is,

$$H_p = \sqrt{(y_2 - y_1)^2 + (x_2 - x_1)^2}. \quad (9.3)$$

## 9.2 Calculation of the “Ideal” HT Data

To avoid rounding and quantification errors, the density of each cell is considered as the length of the intersection of its corresponding bar and segment. The principle of calculating ideal HT data is shown in Fig. 9.1, where  $\theta_0 = \theta_p$ .

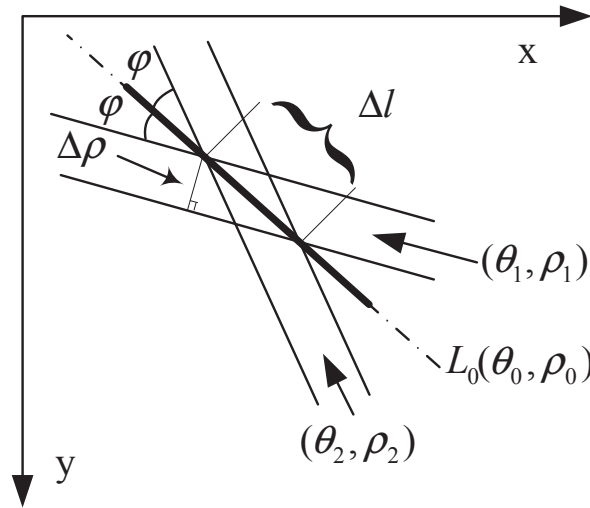


FIGURE 9.1: The principle of ideal HT data

A cell,  $(\theta_1, \rho_1)$  corresponding to the bar  $(\theta_1, \rho_1)$  in the image space, is used as an example. The width of the bar is the  $\rho$  resolution ( $\Delta\rho$ ), and the angle between the bar and the segment is  $\phi$ . Therefore, the length of their intersection when they fully intersect is:

$$\Delta l = \frac{\Delta\rho}{\sin \phi}, \quad (9.4)$$

where

$$\phi = |\theta_0 - \theta_1|. \quad (9.5)$$

All bars that are parallel with bar  $(\theta_1, \rho_1)$  and fully intersect with the segment obtain the same length intersection, that is,  $\Delta l$ . The bars that partially intersect with the segment at its ends, denoted as  $(\theta_1, \rho_{e1})$  and  $(\theta_1, \rho_{e2})$  obtain shorter intersections:

$$\Delta l_{e1} = \frac{\rho_{\theta_1}^1 - \rho_{e1}}{\sin \phi} \quad (9.6)$$

$$\Delta l_{e2} = \frac{\rho_{e2} - \rho_{\theta_1}^2}{\sin \phi} \quad (9.7)$$

where

$$\rho_{\theta_1}^1 = x_1 \cos \theta_1 + y_1 \sin \theta_1 \quad (9.8)$$

$$\rho_{\theta_1}^2 = x_2 \cos \theta_1 + y_2 \sin \theta_1 \quad (9.9)$$

are the theoretical distances from the origin to the straight lines containing the endpoints and having the angle equal to  $\theta_1$ .

The following steps summarise the calculation of the “ideal” HT data.

- Input the segment endpoints  $(x_1, y_1)$  and  $(x_2, y_2)$ , and the ranges in  $\theta$  and  $\rho$  directions of the parameter space where the HT data is to be calculated;
- Determine the peak in “ideal” HT data:
  - According to Eqs. (9.1) and (9.2) calculate  $\theta_p$  and  $\rho_p$ , that is, the peak position;
  - Calculate the length of the segment using Eq. (9.3), that is, the height of the peak.
- Refine the given range according to the peak position;
 

In SHT, the parameter space is scattered with a set of cells ranging over  $\{-90^\circ, -90^\circ + \Delta\theta, \dots, +90^\circ; -\rho_{max}, -\rho_{max} + \Delta\rho, \dots, +\rho_{max}\}$ , where  $\rho_{max}$  is the maximum distance from the origin to a feature point in the image space. It is not reasonable to assume the existence of a cell in the parameter space that exactly represent the ideal peak. Therefore, that the nearest cell to the ideal peak is moved, in order to represent the ideal peak exactly and all the other cells are moved accordingly.
- Using  $\theta_1$  in Fig. 9.1 as an example, for each column around the peak, that is, for each  $\theta$  value in the refined range,

- Calculate the first and the last cells in the parameter space whose bar partially intersects with the segment, according to Eqs. (9.8) and (9.9);
- Calculate the density of the first and the last cells according to Eqs. (9.6) and (9.7);
- Calculate the density of the middle cells whose bar in the image space fully intersects with the segment, according to Eq. (9.4).

### 9.3 Evaluate the HT Data Generated by Specific Algorithm

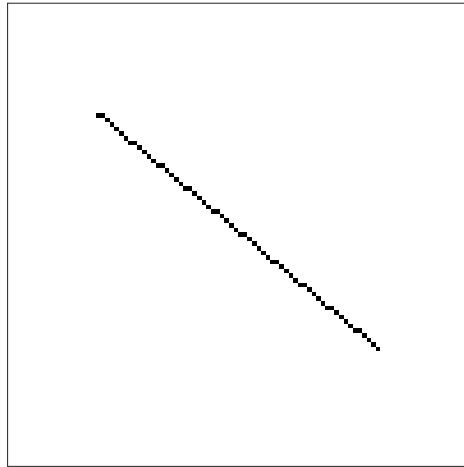


FIGURE 9.2: The segment used to evaluate SHT

In this section, an image containing a segment of 80 pixel lengths Fig. 9.2 is used, and the coordinates of the endpoints are known. As an example the performance of SHT is evaluated using the “ideal” HT data generated by the proposed method. The butterflies generated by SHT and the proposed method are shown in Figs. 9.3(a) and 9.3(b) respectively. It is not difficult to detect out the differences between these two butterflies. Firstly, the peak height of the SHT (about 60) is much smaller than in the “ideal” HT data (about 80). Secondly, the HT data in each column (the HT data in  $\rho$  direction when  $\theta$  value is specified) is undulating, but the “ideal” HT data is very smooth. More quantitative comparisons are demonstrated below.

### 9.3.1 The Peak Height vs. the Segment Length

It would be ideal if the peak height in the HT data could represent the length of the segment. However, in practice, as with other performances, the peak height usually relates to the HT resolution. This will affect the detection errors, as discussed by Tu et al [69].

To demonstrate the peak height vs. the segment length, proceed as follows:

firstly fix the  $\theta$  resolution ( $\Delta\theta = 1^\circ$ ) but change the  $\rho$ -resolution from 2 to 0.1 by 0.1 pixel each time ( $\Delta\rho = 2, 1.9, \dots, 0.1$  pixels). The peak heights detected by both SHT and the proposed method are depicted in Fig. 9.4(a). A strong decreasing trend is shown in the curve of the SHT. This is because under high  $\rho$ -resolution (very small  $\Delta\rho$ ) the width of the bar corresponding to each cell is very small. Consequently, many votes are missed due to the feature point position biases and the rounding errors during the voting process. The peak heights in the “ideal” HT data keep the same value because they are exactly equal to the length of the segment, which is not affected by the HT resolutions.

Secondly, fix the  $\rho$  resolution ( $\Delta\rho = 1$ ) but change the  $\theta$  resolution from 2 to 0.1 by 0.1 each time ( $\Delta\theta = 2^\circ, 1.9^\circ, \dots, 0.1^\circ$ ). The peak height generated by the SHT shows a trend of approximating a maximum value (that is, the number of pixels composing the segment). However, the peak heights is never equal to the length of the segment unless the segment is vertical or horizontal.

### 9.3.2 The Quality of the Generated Butterfly

For the butterfly-based methods, the performance is strongly dependent on the quality of the HT butterfly. This experiment focuses on the quality of the butterflies generated by SHT. The correlation coefficient (defined as Eq. (9.10)) between the ideal HT data and the data of SHT is used to measure the quality.

The correlation coefficient between  $A$  and  $B$ , where  $A$  and  $B$  are matrices or vectors of the same size, is defined as follows:

$$r(A, B) = \frac{\sum_m \sum_n (A_{mn} - \bar{A}) \times (B_{mn} - \bar{B})}{\sqrt{(\sum_m \sum_n (A_{mn} - \bar{A})^2) \times (\sum_m \sum_n (B_{mn} - \bar{B})^2)}}, \quad (9.10)$$

where  $\bar{A}$  and  $\bar{B}$  are the average value of matrix  $A$  and  $B$  respectively.

Fig. 9.5 depicts the correlation coefficients when the resolutions change. Clearly, increasing the  $\rho$  resolution (decrease  $\Delta\rho$ ) might lead to a poor quality of HT data. However, increasing the  $\theta$  resolution (decrease  $\Delta\theta$ ) shows a trend of increasing the quality.

### 9.3.3 Effect of Segment Parameters

This section addresses the effect of segment parameters (that is,  $\theta$ ,  $\rho$  and length) on the performance demonstrated in Sections 9.3.1 and 9.3.2.

#### 9.3.3.1 Effect of the Segment Angle ( $\theta$ )

To show the effect of  $\theta$ , the segment depicted in Fig. 9.2 is rotated around the origin. The  $\theta$  value is changed, but the  $\rho$  value and the length are held. The experiments designed in Sections 9.3.1 and 9.3.2 were repeated to obtain the results depicted in Fig. 9.6.

From the results in Fig. 9.6, it can be seen that the  $\theta$  value does not have a considerable effect on the peak height of the butterfly and its quality.

#### 9.3.3.2 Effect of the Distance from the Origin to the Segment ( $\rho$ )

To check the effect of  $\rho$ , the segment depicted in Fig. 9.2 is moved horizontally so the  $\rho$  value was changed but the  $\theta$  value and the length were held. The results are shown in Fig. 9.7.

From the results in Fig. 9.7, it can be seen also noticed that the value of  $\rho$  does not have a considerable effect on the peak height of the butterfly and its quality.

#### 9.3.3.3 Effect of Segment Length

To demonstrate this, hold both  $\theta$  and  $\rho$  but change the segment length, that is, hold one endpoint but move the other along the segment. The result is shown in Fig. 9.8. Figs. 9.8(b) and 9.8(a) do not show a considerable effect. However, Figs. 9.8(c) and 9.8(d) demonstrate

that the peak height for the shorter segment is closer to the ideal value. This is because it is easier for the bar corresponding to the peak cell to contain a larger percentage of pixels composing the segment. On the contrary, a longer segment has more chance of having a part lying outside the narrow bar corresponding to the peak cell.

Naturally, the shorter segments have more chance of being affected by noise and other objects.

### 9.3.4 Evaluation of the SHT

From Sections 9.3.1 and 9.3.2 the following conclusions regarding the SHT are depicted:

- The HT data generated by the SHT is greatly affected by the resolution.
- The HT data generated by the SHT under the best resolution is still far from the “ideal” HT data.
- Higher  $\rho$  resolution (i.e smaller  $\Delta\rho$ ) tends to affect the HT data quality negatively. However, higher  $\theta$  resolution (smaller  $\Delta\theta$ ) tends to give positive effects.

## 9.4 Weakness of the Proposed “Ideal” HT

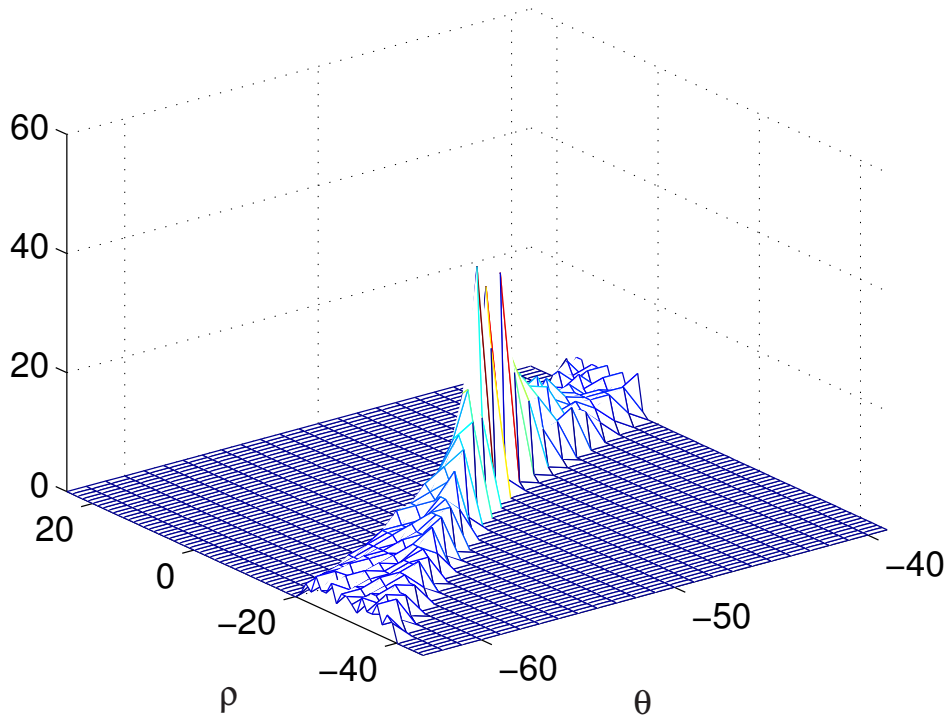
The proposed “ideal” HT was designed to evaluate complete HT butterflies, that is, all feature points are considered when generating the HT data. However, such complete butterflies are not available for generating HT data for HT varieties that consider a subset of feature points only, such as the Randomised HT, [22] where feature point pairs are randomly selected. In this case, the generated butterfly is incomplete.

## 9.5 Conclusion

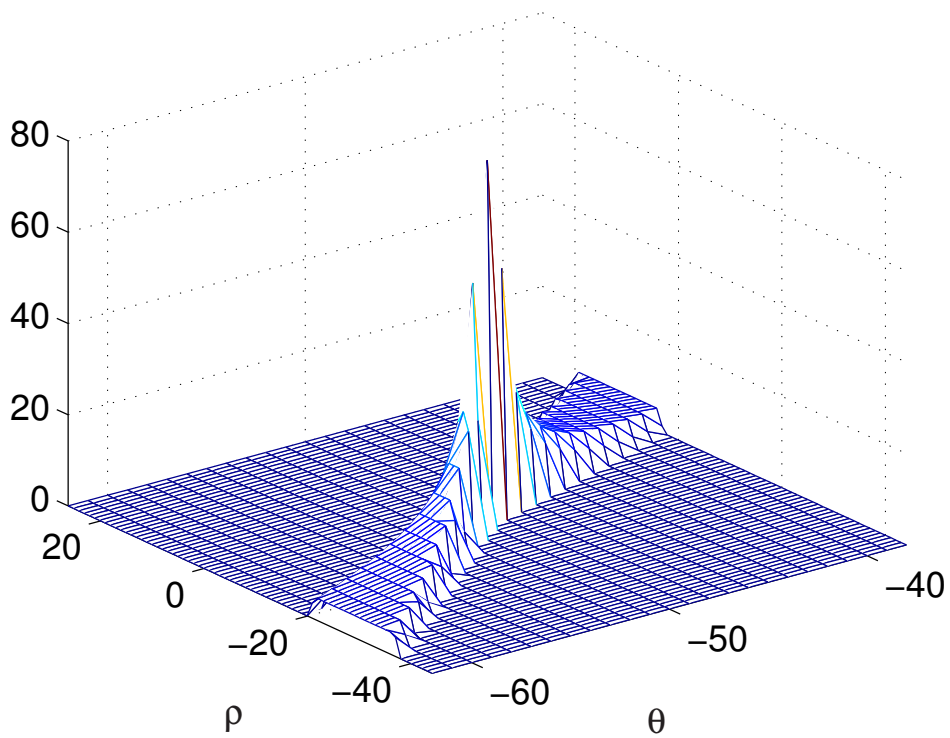
This chapter proposed a method for calculating the “ideal” HT data of segments. This HT data is not affected by the errors from the image space position biases or the parameter space rounding errors. It only depends on the basic physical factors (the endpoints of the segment).

The “ideal” HT data can be used to evaluate the performance of various HTs. The SHT is evaluated as an example.

If an appropriate range in the parameter space is given, the generated butterfly has the potential to be used to detect segments because it can be considered a model of a segment. Furthermore, the proposed method is hopefully used to optimise the resolutions of specific HT varieties to obtain the “best” performance. This will be the focus of future work.

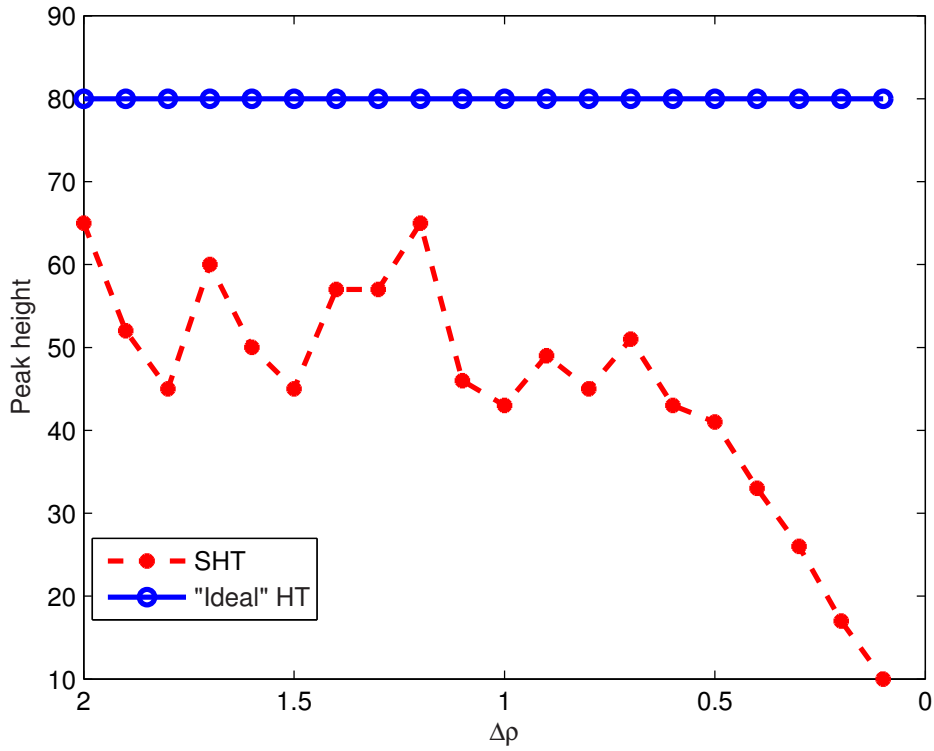


(a) Butterfly generated by SHT

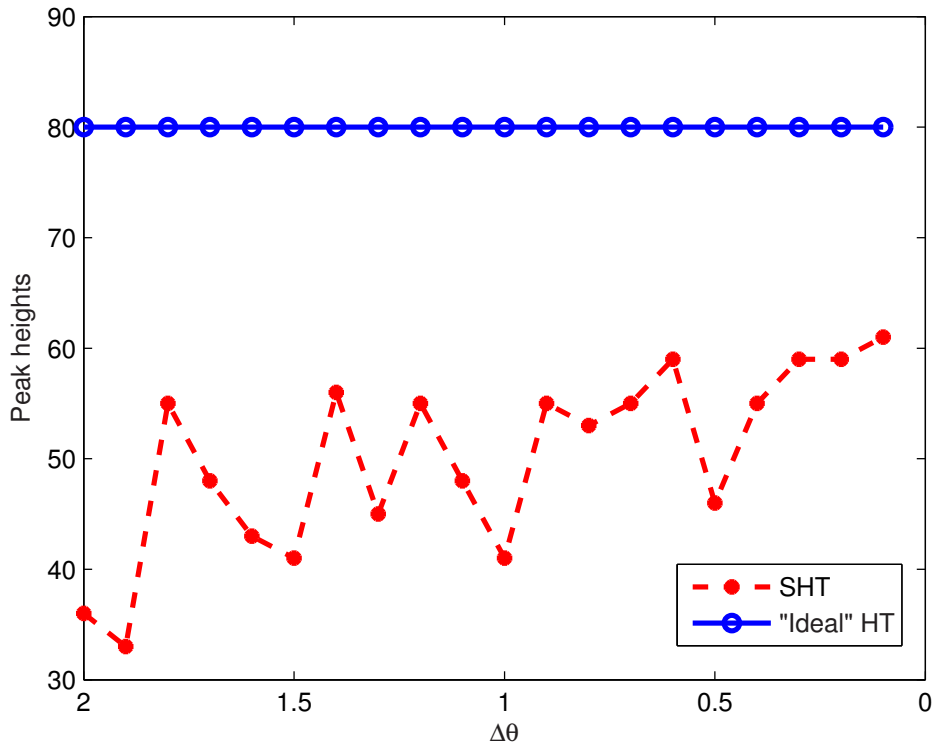


(b) Butterfly generated by the proposed method

FIGURE 9.3: Comparison of butterflies under the same resolutions ( $\Delta\theta = 1^\circ, \Delta\rho = 1\text{pixel}$ )

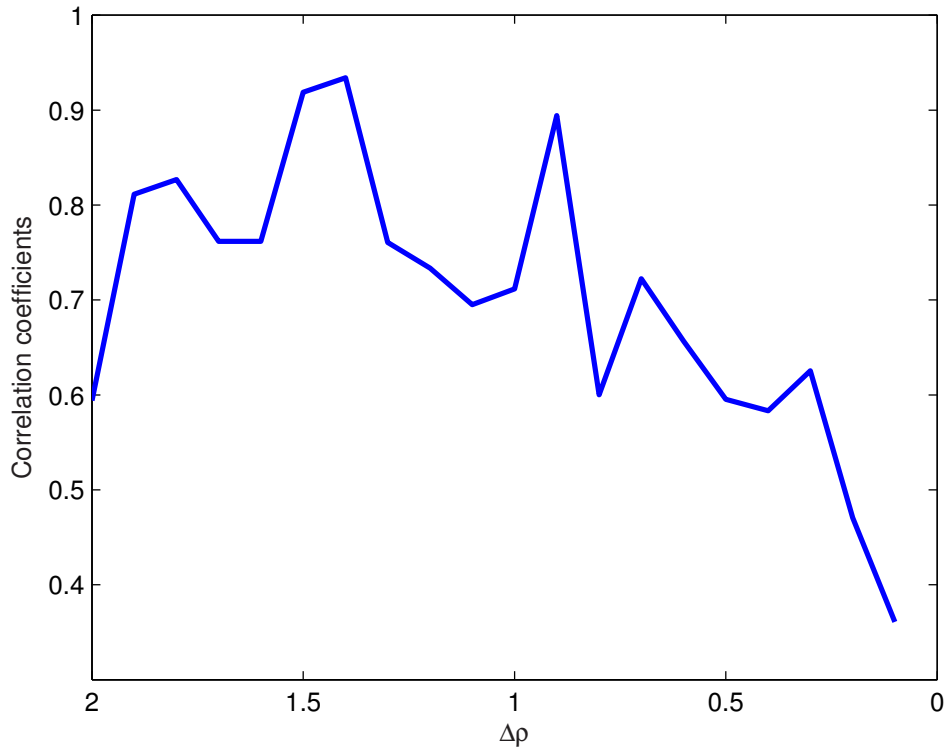


(a) The peak height vs  $\Delta\rho$

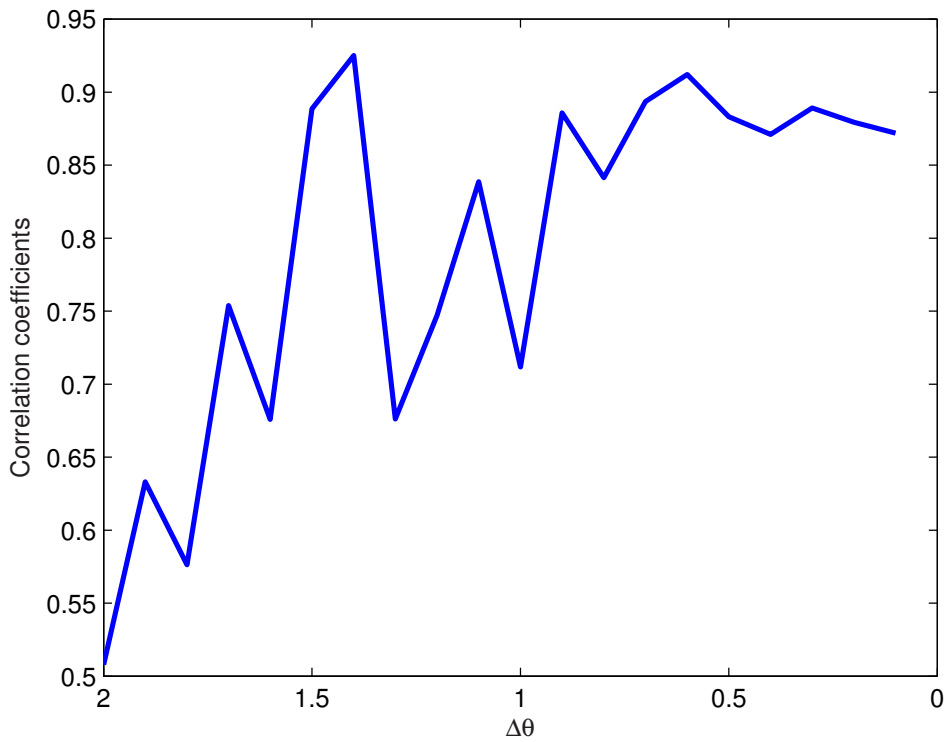


(b) The peak height vs  $\Delta\theta$

FIGURE 9.4: Peak height as the measurement of segment length

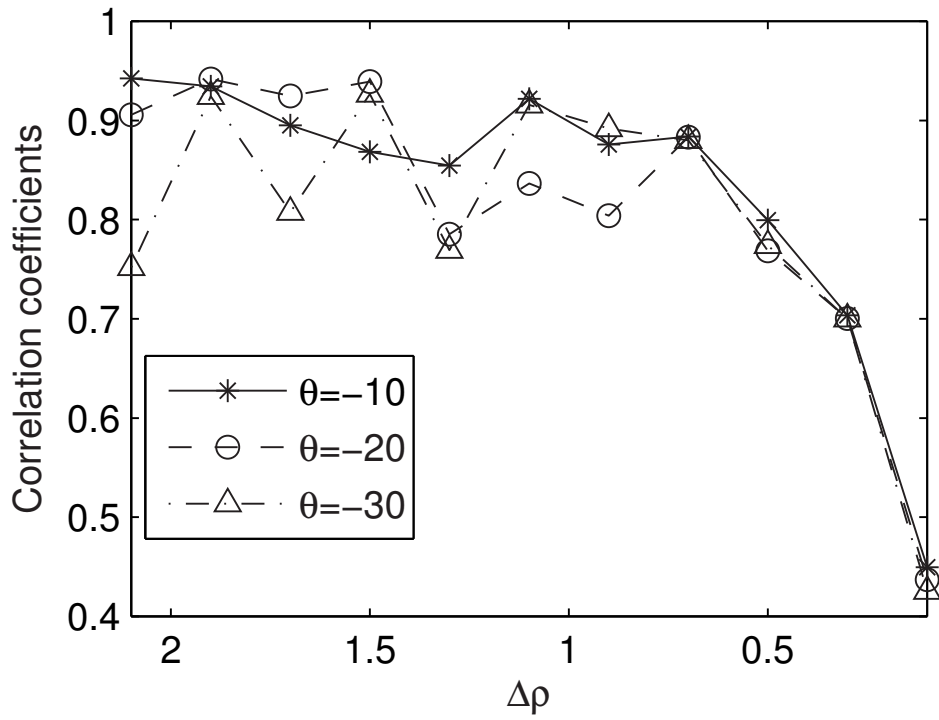


(a) The correlation vs  $\Delta\rho$

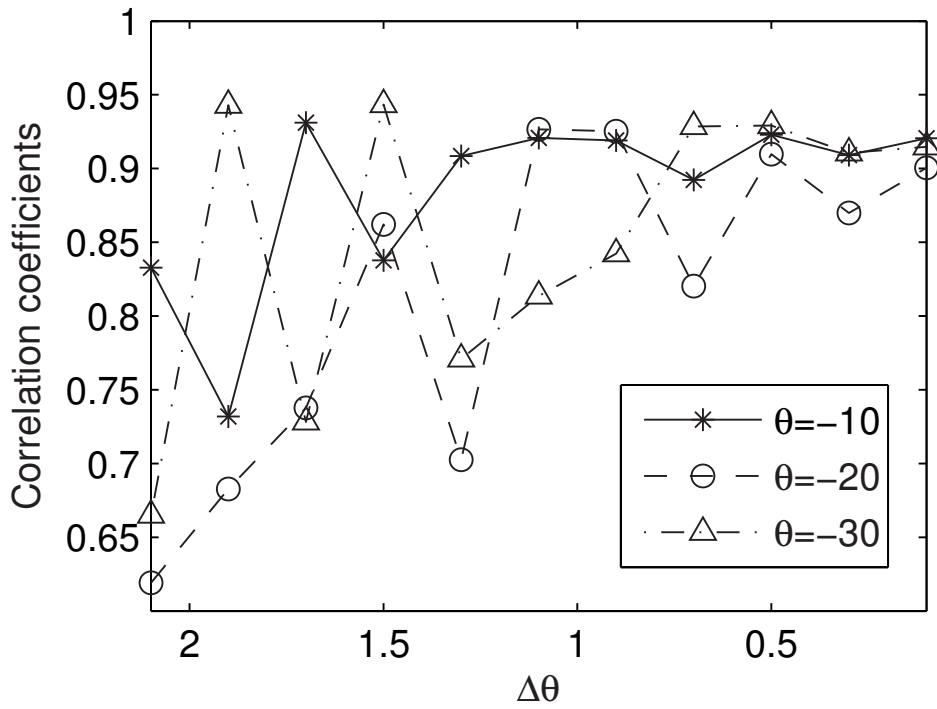


(b) The correlation vs  $\Delta\theta$

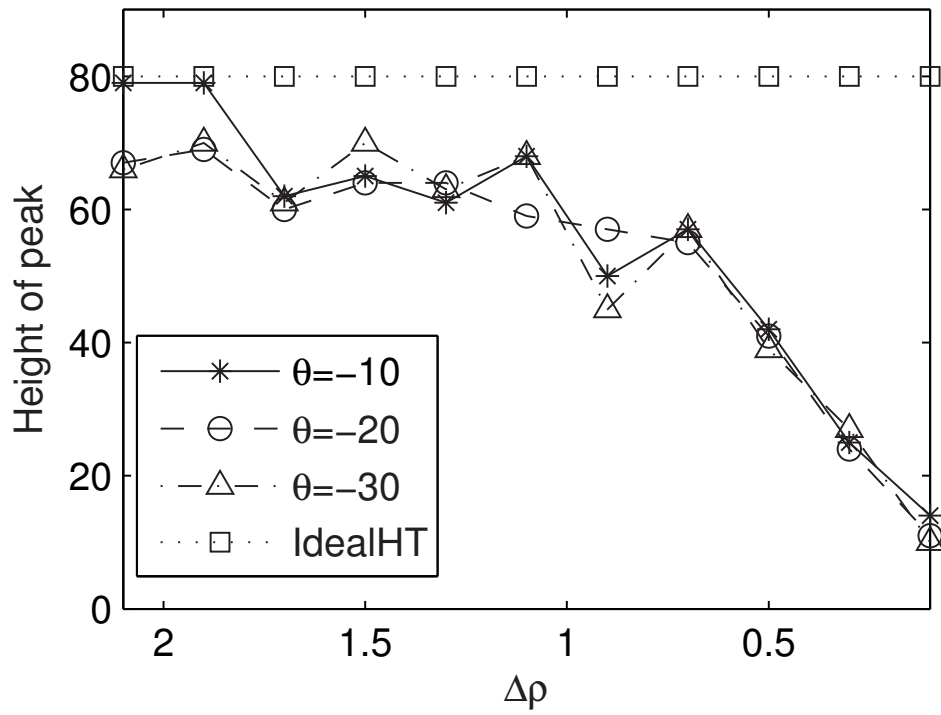
FIGURE 9.5: The quality of butterflies



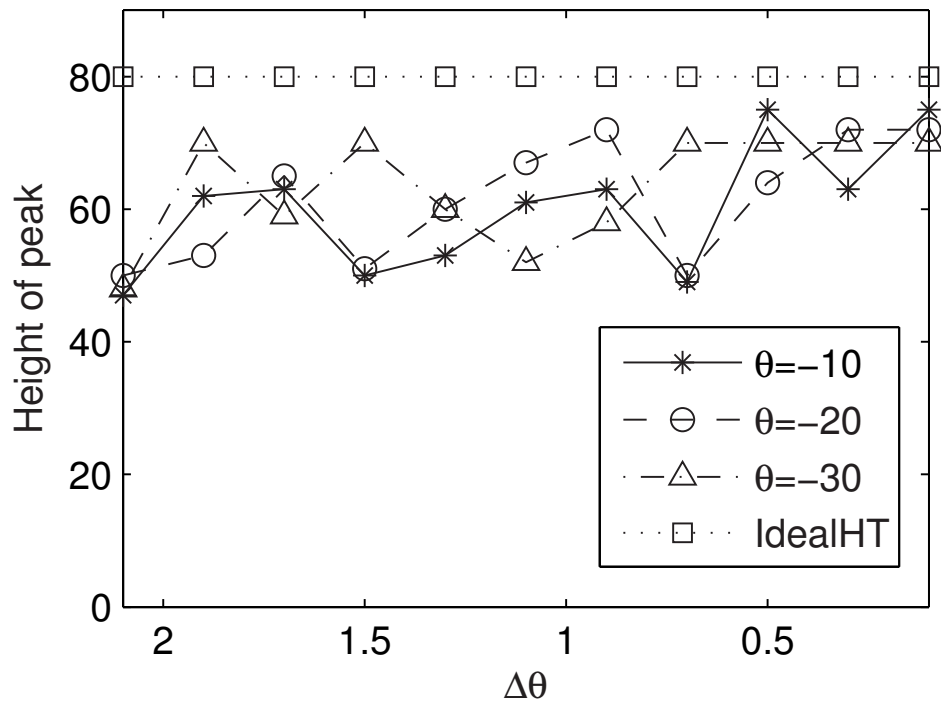
(a) The correlation vs  $\Delta\rho$  for segments with different  $\theta$  values



(b) The correlation vs  $\Delta\theta$  for segments with different  $\theta$  values

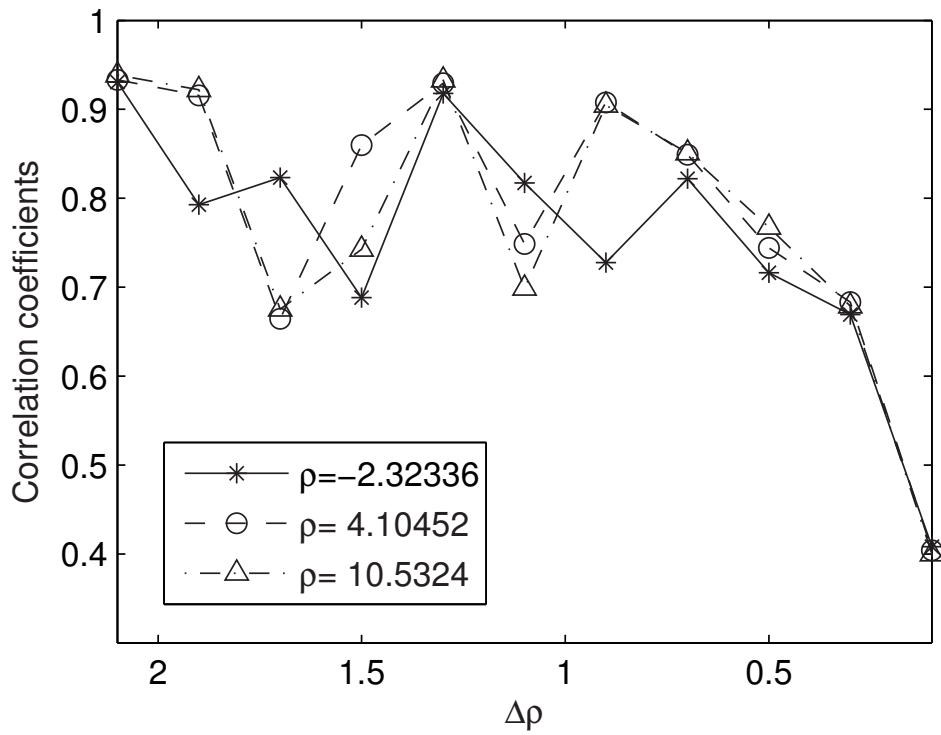


(c) The peak height vs  $\Delta\rho$  for segments with different  $\theta$  values

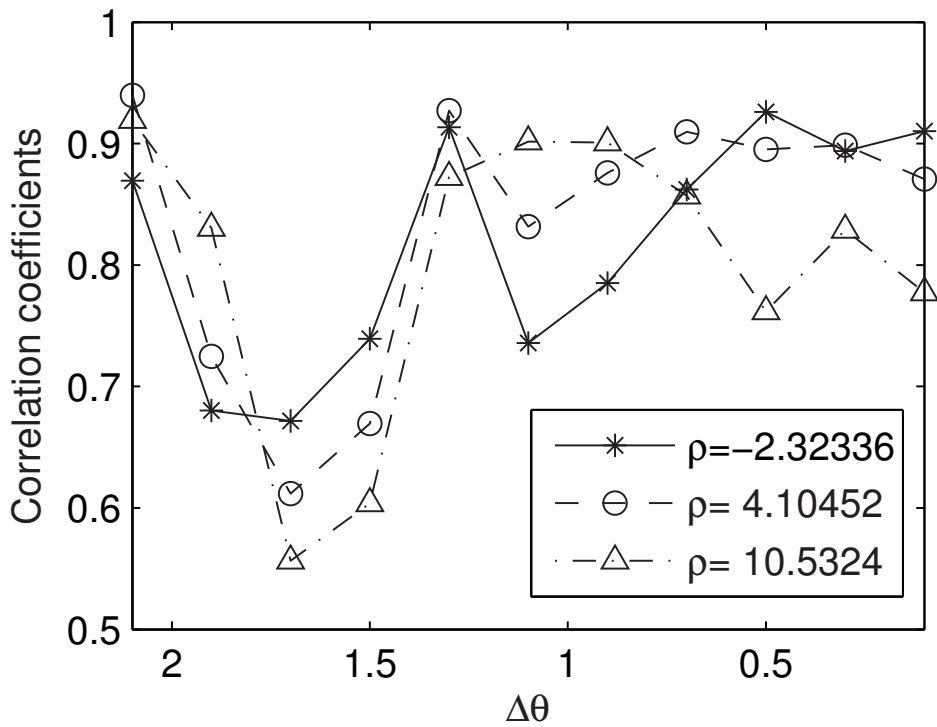


(d) The peak height vs  $\Delta\theta$  for segments with different  $\theta$  values

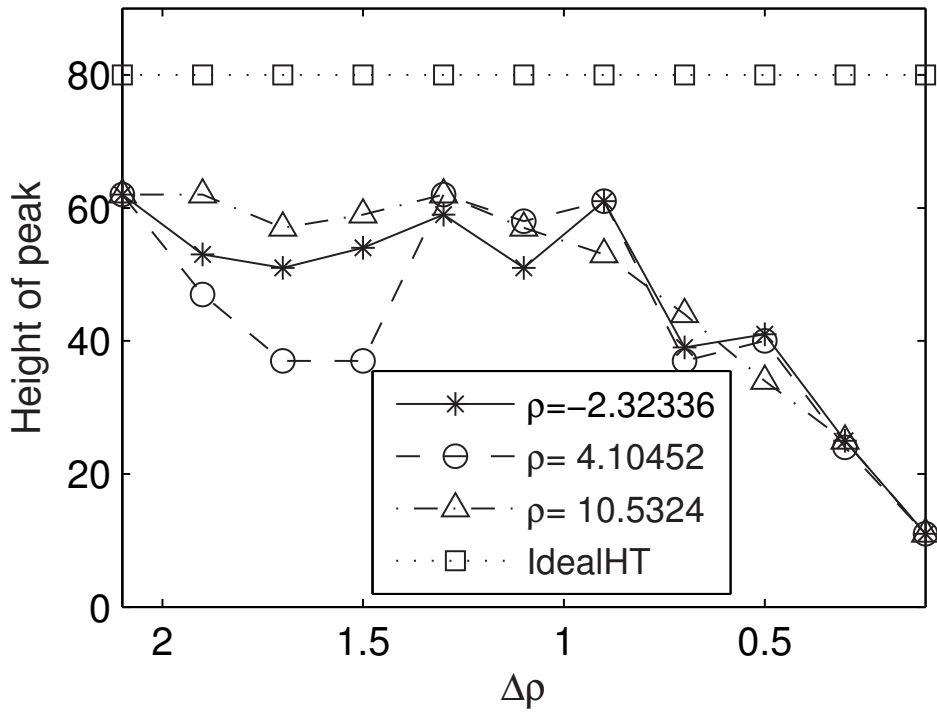
FIGURE 9.6: The effect of segment  $\theta$  value



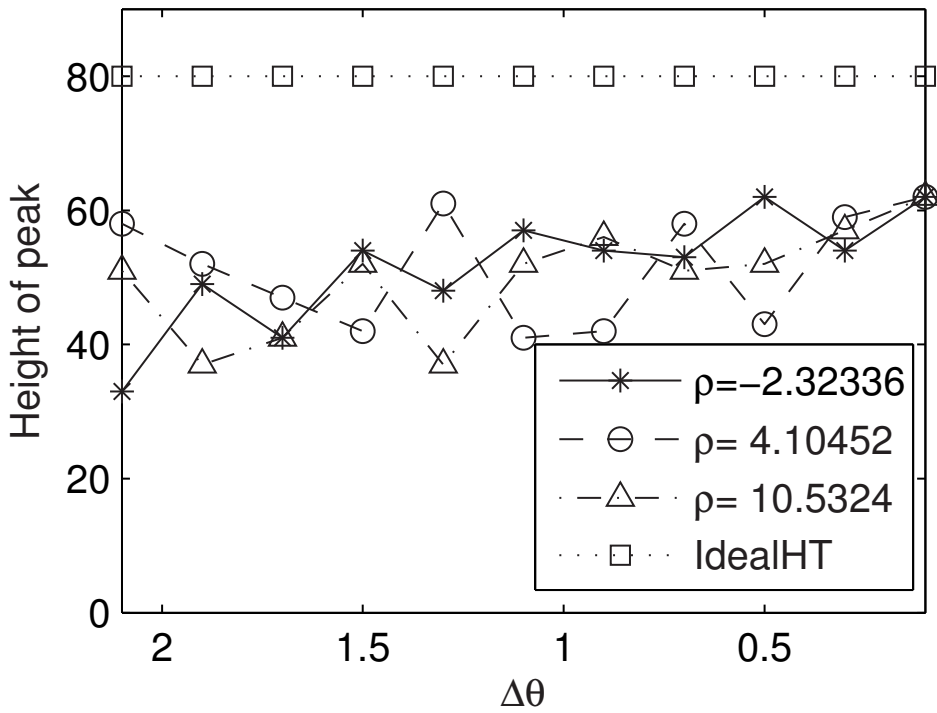
(a) The correlation vs  $\Delta\rho$  for segments with different  $\rho$  values



(b) The correlation vs  $\Delta\theta$  for segments with different  $\rho$  values

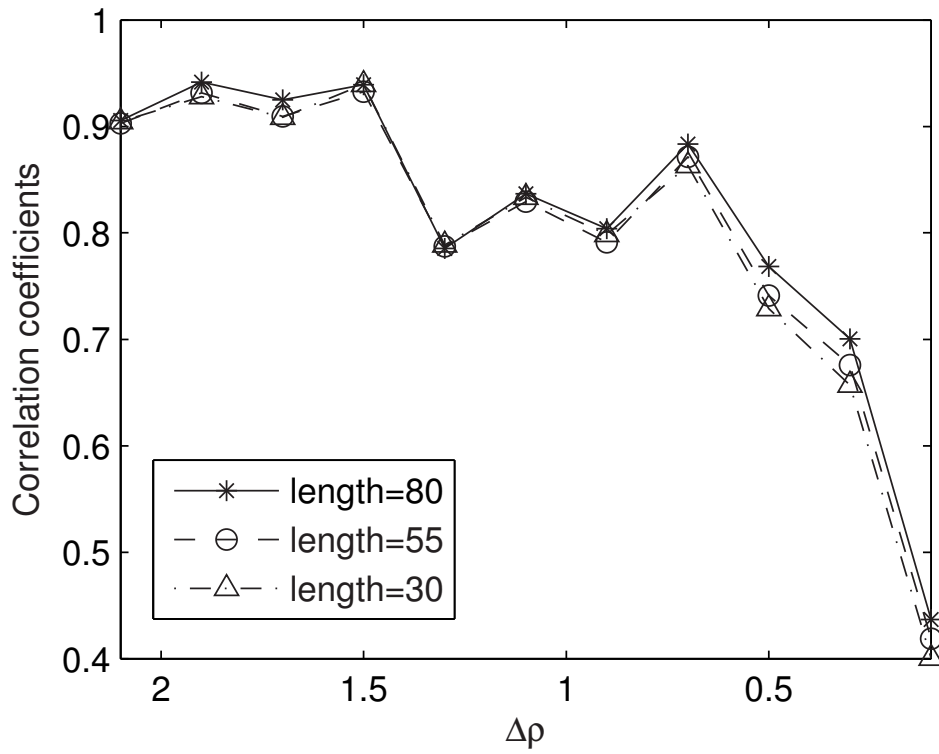


(c) The peak height vs  $\Delta\rho$  for segments with different  $\rho$  values

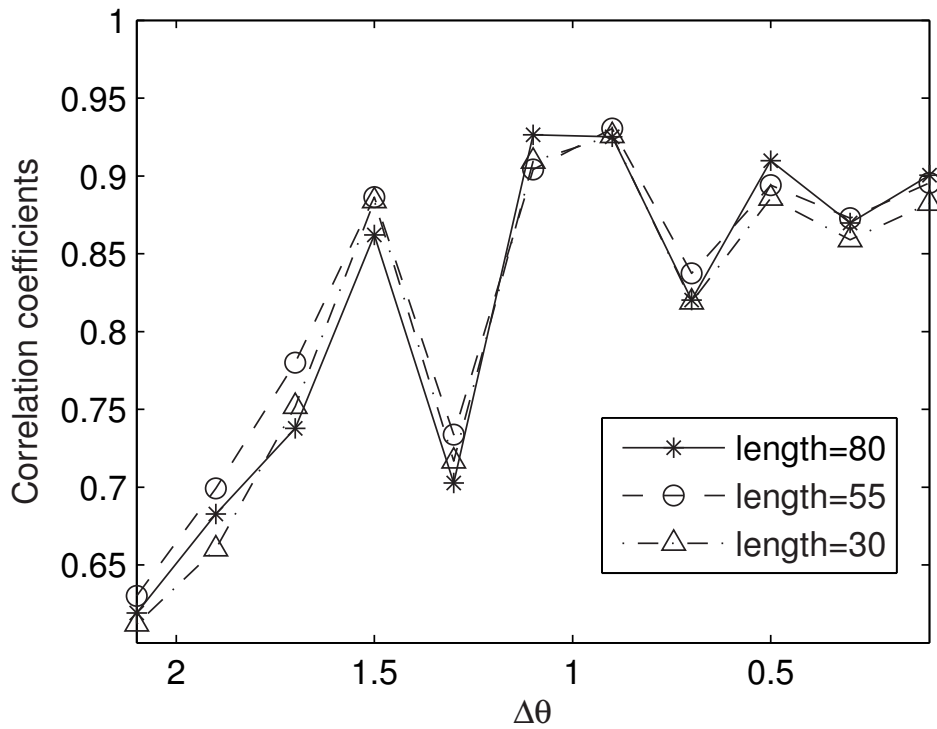


(d) The peak height vs  $\Delta\theta$  for segments with different  $\rho$  values

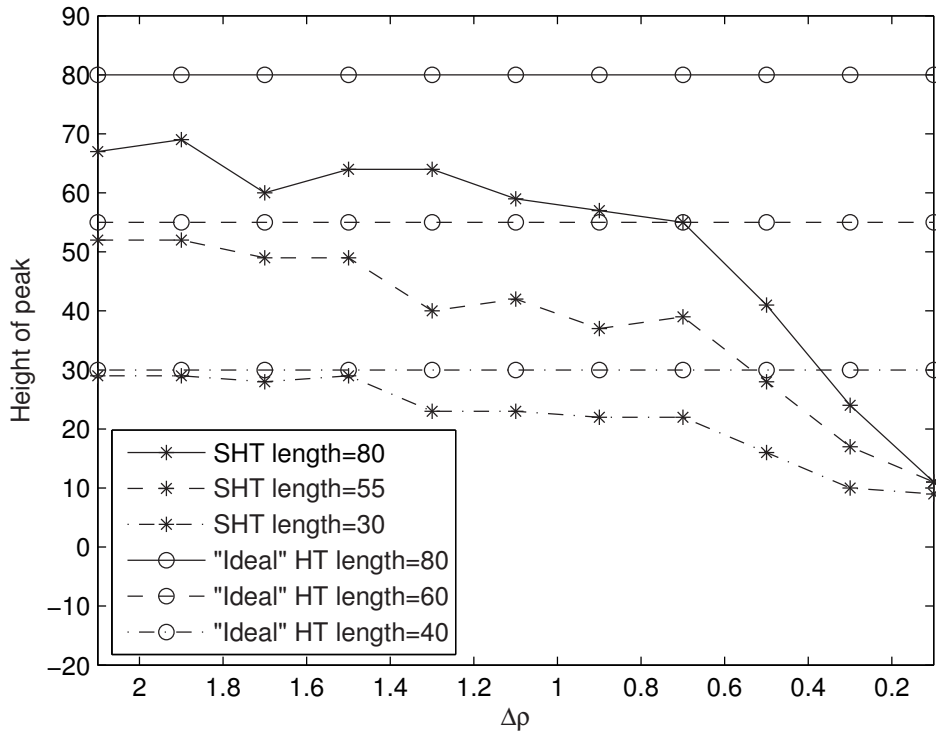
FIGURE 9.7: The effect of segment  $\rho$  value



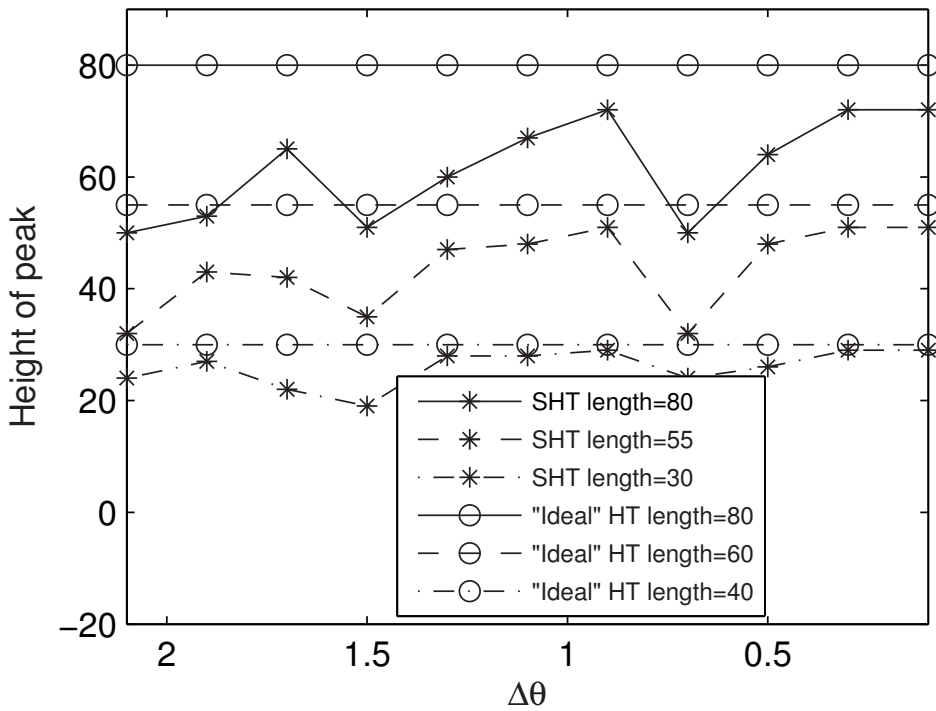
(a) The correlation vs  $\Delta\rho$  for segments with different length



(b) The correlation vs  $\Delta\theta$  for segments with different length



(c) The peak height vs  $\Delta\rho$  for segments with different length



(d) The peak height vs  $\Delta\theta$  for segments with different length

FIGURE 9.8: The effect of segment length value

## **Part III**

# **CONCLUSION AND FUTURE WORK**

## CHAPTER 10

### CONCLUSION

This thesis addressed the efforts for improving the performance of HT. Due to the fact that HT is based on simple and clearly defined geometric principles, it is possible to improve its performance by making use of this property. Various methods were proposed, from different aspects.

Firstly, the question of what is a “good” resolution setting for HT was discussed. Relevant definitions were produced, which are valuable to evaluate existing HTs. The relationship between the detection errors and resolution settings of the SHT when it is employed in straight line detection was addressed. The “best” resolution of SHT was defined. To demonstrate the existence of the “best” resolution, the error-resolution curves were studied and the inflexions existing on the curves were uncovered. It is shown that the inflexions are related to the parameters of the straight lines to be detected. An interesting area on the resolution plane that contains “good” resolution settings was uncovered. This can be considered a guide for choosing the resolutions for SHT.

The self-similarity in HT butterflies was discovered, and based on this property, a simple method was proposed to obtain a very high resolution HT without the limitations associated with peak splitting and vote spreading. The distinct butterfly is preserved when the resolution increases.

A mathematical method for constructing high resolution HT butterflies from low resolution HT data was proposed by analysing the relationship between the HT data of different resolutions. Compared to the existing HT related methods, the proposed method has at least three advantages: (i) a high resolution HT is obtained mathematically from a low resolution HT

data, which significantly decreases computational cost; (ii) only the essential parts (butterfly areas) around the peaks are rebuilt, hence, the storage requirement is greatly reduced; (iii) arbitrary resolution settings of the HT are achievable, that is, the proposed method can find any high resolution HT while circumventing the limitations associated with a range of HTs. The  $\Delta\rho$  and  $\Delta\theta$  can be sufficiently small without seriously affecting the performance of the HT. This means the proposed method can find solutions approximating the Continuous HT (CHT).

A super resolution reconstruction approach, based on an iterative back-projection algorithm, was proposed to enhance HT resolutions. Based on the differences between optical images and HT data, a method of generating multiple low resolution HT frames was proposed. The standard low resolution HT was applied on vertically and horizontally shifted images to obtain multiple low resolution HT frames. A theoretical analysis showed that these low resolution frames contain new information, which ensures the possibility of reconstructing high resolution HT data via the super resolution (SR) method. The pseudo-periodic property when shifting the image was discovered. The period was calculated to determine the number of low resolution frames needed to reconstruct the super resolution HT data. The cell registration method was also derived, according to the column-wise biasing nature of the HT data of the shifted images. According to the difference between normal images and HT frames, specific conversions between high and low resolution HT frames were discussed. The experiments demonstrated the effectiveness of the proposed approach.

The research formulated a high precision line positioning method based on HT detection error compensation. The HT discretisation error was analysed. By vertically or horizontally shifting the given image by a known distance, a detection error series composed of the detection errors of each shifted image was obtained. Theoretical analysis showed that a critical crossing point exists in this series, and this was used to compensate for the HT detection errors. Experiments showed the proposed method has high positioning precision.

# CHAPTER 11

## FUTURE WORK

The research presented in this thesis shows the importance and the possibility of making use of the geometric principles of HT when improving the HT performance. In future, efforts will be aimed at uncovering more useful properties of HT data, which can be applied to the requirements of higher performance HT and its specific applications. The research demonstrates that simple geometric transform in the image space could lead to significant changes in the parameter space. This discovery reveals significant potential for improving HT performance and solving HT problems by introducing the geometric transforms to the image space before the HTs are employed. In-depth studies on further geometric transforms in the image space and their effects on the parameter space comprise future work.

The value of the HT butterfly in straight line detection is demonstrated in literatures. Procedures for highlighting the butterflies in HT data is another important aspect of the work to be done. Transforms applied on HT data for this purpose will receive more emphasis.

The methods proposed in this thesis are based on determined 2D signals (images), where a pixel exclusively belongs to objects or the background without considering the random nature of the signal. With this nature, a pixel belongs to objects or the background with probabilities. So the votes that a feature point contributed to a HT cell could be a probability instead of the constant “1”, which should be considered in the future work.

Another important point was not concerned in HTs is the orientation of object edges. A feature point should bear this orientation when votes HT cells, which means the cells representing the orientation could get more weights than others. This point to be considered.

Industry application of the proposed method is another important content for future work.

# REFERENCES

- [1] Hough PVC. A method and means for recognizing complex patterns. US Patent No. 3,196,212. 1962: P.069-654.
- [2] Hart PE. How the Hough transform was invented [DSP History]. Signal Processing Magazine. IEEE. 2009 Nov 26; 6:p.18-22.
- [3] Rosenfeld A. Picture Processing by Computer. New York: Academic. 1969; p.335-336.
- [4] Duda RO, Hart PE. Use of Hough transform to detect lines and curves in pictures. Communications of the ACM. 1972;15(1):p. 11-15.
- [5] Shapiro SD, Lannino A. Geometric constructions for predicting Hough transform performance. Pattern Analysis and Machine Intelligence. IEEE Transactions. 1979; 3:p. 310-317.
- [6] Van Veen TM, Groen FCA. Discretization errors in the Hough transform. Pattern Recognition. 1981; 14(1-6):p.137-145. ISSN 0031-3203.
- [7] M. Atiquzzaman, M. W. Akhtar. Complete line segment description using the Hough transform. Image Vision Comp, 1994; 12(5): p.267-273.
- [8] Atiquzzaman M, Akhtar MW. A robust Hough transform technique for complete line segment description. Real-Time Imaging. 1995;1(6):p. 419-426.
- [9] Niblack W, Petkovic D. On improving the accuracy of the Hough transform: theory, simulations, and experiments. Computer Vision and Pattern Recognition, 1988. Proceedings CVPR'88. Computer Society Conference ; 1988; p. 574-579.
- [10] Morimoto M, Akamatsu S, Suenaga Y. A High-resolution Hough Transform using Variable Filter. Proceedings of the 11th ICPR; 1992; Hague: p. 280-284. 122.

- [11] Magli E, Olmo G. On high resolution positioning of straight patterns via multiscale matched filtering of the Hough transform. *Pattern Recognition Letters*. 2001;22:p. 705-713. ISSN 0167-8655.
- [12] Ji Q, Haralick RM. Error propagation for the Hough transform. *Pattern Recognition Letters*. 2001;22(6-7):p. 813-823. ISSN 0167-8655.
- [13] Shapiro V. Accuracy of the straight line Hough Transform: The non-voting approach. *Computer Vision and Image Understanding*. 2006;103(1):p. 1- 21. ISSN 1077-3142.
- [14] Guo S, Pridmore T, Kong Y, Zhang X. An improved Hough transform voting scheme utilizing surround suppression. *Pattern Recognition Letters*. 2009;30(13):p. 1241-1252. ISSN 0167-8655.
- [15] Fernandes LA, Oliveira MM. Real-time line detection through an improved Hough transform voting scheme. *Pattern Recognition*. 2008;41(1):p. 299-314. ISSN 0031-3203.
- [16] Song J, Lyu. Michael R . A Hough transform based line recognition method utilizing both parameter space and image space. *Pattern Recognition*. 2005;38 Issue 4:p. 539-552. ISSN 0031-3203.
- [17] Cha J, Cofer RH, Kozaitis SP. Extended Hough transform for linear feature detection. *Pattern Recognition*. 2006;39(6):p. 1034-1043. ISSN 0031-3203.
- [18] Li H, Lavin MA, Le Master RJ. Fast Hough Transform: A hierarchical approach. *Computer Vision, Graphics, and Image Processing*. 1986;36(2):p. 139-161.
- [19] Illingworth J, Kittler J. The Adaptive Hough Transform. *Pattern Analysis and Machine Intelligence*. *IEEE Transactions*. 1987;Volume PAMI-9(5):p. 690-698.
- [20] Atiquzzaman M. Multiresolution Hough Transform An Efficient Method of Detecting Patterns in Images. *IEEE Transactions on Pattern Analysis and Machine Intelligence*. 1992;14(11):p. 1090-1095.
- [21] Ben-Tzvi D, Sandler MB. A combinatorial Hough transform. *Pattern Recognition Letters*. 1990;11(3):p.167-174. ISSN 0167-8655.
- [22] Xu L, Oja E, Kultanen P. A new curve detection method: Randomized Hough transform(RHT). *Pattern Recognition Letters*. 1990;11(5):p. 331-338. ISSN 0167-8655.

- [23] Xu L, Oja E. Further developments on RHT: Basic mechanisms, algorithms, and computational complexities. Conference A: Computer Vision and Applications, Proceedings., 11th IAPR International Conference. 1992; The Hague, Netherlands: p. 125-128.
- [24] Xu L, Oja E. Randomized Hough Transform (RHT): Basic Mechanisms, Algorithms, and Computational Complexities. CVGIP: Image Understanding. 1993;57(2):p. 131-154.
- [25] Kalviainen H, Hirvonen P, Xu L, Oja E. Probabilistic and non-probabilistic Hough transforms: overview and comparisons. Image and Vision Computing. 1995;13(4):p. 239-252. ISSN 0262-8856.
- [26] Kiryati N, Eldar Y, Bruckstein AM. A probabilistic Hough transform. Pattern Recognition. 1991;24(4):p. 303-316. ISSN 0031-3203.
- [27] Gatos B, Perantonis SJ, Papamarkos N. Accelerated Hough transform using rectangular image decomposition. Electronics Letters. 1996; 32(8):p. 730-732.
- [28] Zhang Y, Webber R. A windowing approach to detecting line segments using Hough transform. Pattern Recognition. 1996;29(2):p. 255-265. ISSN 0031-3203.
- [29] Ho CG, Young RCD, Bradfield CD, Chatwin CR. A fast Hough transform for the parametrisation of straight lines using Fourier methods. Real-Time Imaging. 2000;2:p. 113-127.
- [30] Chung KL, Chen TC, Yan WM. New memory- and computation-efficient Hough transform for detecting lines. Pattern Recognition. 2004;37:p. 953-963.
- [31] Xiao F, Chiang IJ, Wong J, Tsai Y, Huang K, Liao C. Automatic measurement of mid-line shift on deformed brains using multiresolution binary level set method and Hough transform. Computers in Biology and Medicine. 2011; 41(9):p. 756-762. ISSN 0010-4825.
- [32] Beltrametti MC, Robbiano L. An algebraic approach to Hough transforms. Journal of Algebra. 2012;371:p. 669-681. ISSN 0021-8693.
- [33] Carlson BD, Evans ED, Wilson SL. Search radar detection and track with the Hough transform. I. system concept. IEEE Transactions on aerospace and electronic systems. 1994;30(1):p. 102-108.

- [34] Moqiseh A, Nayebi MM. 3-D Hough transform for surveillance radar target detection. Proceedings of the Radar Conference 2008. RADAR '08. IEEE. 2008; p. 1-5.
- [35] Murillo-Bracamontes EA, Martinez-Rosas ME, Miranda-Velasco MM, Martinez-Reyes HL, Martinez-Sandoval JR, Cervantes-de-Avila H. Implementation of Hough transform for fruit image segmentation. *Procedia Engineering*. 2012;35:p. 230-239. ISSN 1877-7058.
- [36] Gao C, Deng X, Shi C. Detection of Dim Maneuvering Target based on Randomized Hough Transform. *Procedia Engineering*. 2012;29:p. 808-813. ISSN 1877-7058.
- [37] Pacey A, Macpherson CG, McCaffrey KJW. Linear volcanic segments in the central Sunda Arc, Indonesia, identified using Hough Transform analysis: Implications for arc lithosphere control upon volcano distribution. *Earth and Planetary Science Letters*. 2013;369-370:p. 24-33. ISSN 0012-821X.
- [38] Plo P, Rupitsch SJ, Frohlich T, Lerch R. Identification of Acoustic Wave Orientation for Ultrasound-Based Flow Measurement by Exploiting the Hough Transform. *Procedia Engineering*. 2012;47:p. 216-219. ISSN 1877-7058.
- [39] Davies ER. Application of the generalised hough transform to corner detection. *IEEE Proceedings. Computers and Digital Techniques*. 1988;135(1):p. 49- 54.
- [40] Kwan KS, Choung Y, Park JA. Image corner detection using Hough transform. *Pattern Recognition and Image Analysis*. Heidelberg, Berlin: Springer; 2005. p. 279- 286.
- [41] Du S, Van Wyk BJ, Tu C, Zhang X. An improved Hough transform neighborhood map for straight line segments. *IEEE Transactions on Image Processing*. 2010;19(3):p. 573-585.
- [42] Duan H , Liu X, Liu H. A nonuniform quantization of Hough space for the detection of straight line segments. *Proceedings of the International Conference on Pervasive Computing and Applications*; 2007; Volume ICPCA, No. 07. p. 149-153.
- [43] Walsh D, Raftery AE. Accurate and efficient curve detection in images: the importance sampling Hough transform . *Pattern Recognition*. 2002;35:p. 1421-1431.
- [44] Ching YT. Detecting line segments in an image - a new implementation for Hough Transform. *Pattern Recognition Letters*. 2001;22:p. 421-429.

- [45] Fernandes LAF, Oliveira MM. Real-time line detection through an improved Hough transform voting scheme. *Pattern Recognition*. 2008;41:p. 299-314.
- [46] Kamat V, Ganesan S. A robust hough transform technique for description of multiple line segments in an image. *Proceedings of 1998 International Conference on Image Processing (ICIP'98)*; 1998; Volume 1: p. 216-220.
- [47] Furukawa Y, Shinagawa Y. Accurate and robust line segment extraction by analyzing distribution around peaks in Hough space. *Computer Vision and Image Understanding*. 2003;92(1):p. 1-25.
- [48] Ji J, Chen G, Sun L. A novel Hough transform method for line detection by enhancing accumulator array. *Pattern Recognition Letters*. 2011;32:p. 1503- 1510.
- [49] Ji Q, Haralick RM. An improved Hough transform technique based on error propagation. *Proceedings of IEEE International Conference on Systems, Man, and Cybernetics*; 1998; Volume 5: p. 4653-4658.
- [50] Du S, Tu C, Van Wyk BJ, Chen Z. Collinear segment detection using ht neighborhoods. *IEEE Transactions on Image Processing*. 2011;20(12):p. 3912-3920.
- [51] Tu C, Du S, Van Wyk BJ, Djouani K, Hamam Y. High resolution Hough transform based on butterfly self-similarity. *Electronic Letters*. 2011;47(26):p. 1360-1361.
- [52] Du S, Tu C, Van Wyk BJ, Chen Z, Ochola E. Measuring straight line segments using HT butterflies. *PLOS ONE*. 2012;7(3):p. e33790.
- [53] Du S, Tu C, Sun M. High accuracy Hough transform based on butterfly symmetry. *Electronic Letters*. 2012;48(4):p. 199-201.
- [54] Nguyen TT, Pham XD, Jeon J. An improvement of the Standard Hough Transform to detect line segments. *Proceedings of IEEE International Conference on Industrial Technology(ICIT '08)*; 2008; p. 1-6.
- [55] Svalbe ID. Natural representations for straight lines and the hough transform on discrete arrays. *IEEE Transactions On Pattern Analysis And Machine Intelligence*. 1989;11(9):p. 941-950.

- [56] Niblack W, Petkovic D. On Improving the accuracy of the Hough transform: theory, simulations, and experiments. Proceedings of Computer Society Conference on Computer Vision and Pattern Recognition (CVPR '88); 1988; p. 574-579.
- [57] Niblack W, Petkovic D. On improving the accuracy of the Hough transform. Machine Vision and Applications. 1990;3(2):p. 87-106.
- [58] Zhang M. On the discretization of parameter domain in Hough transform. Proceedings of IEEE (ICPR '96); 1996; p. 527-531.
- [59] O'Rourke J. Dynamically quantized spaces for focusing the Hough transform. Proceedings of the 7th International Joint Conference on Artificial Intelligence; 1981; p. 737-739.
- [60] Heath MD, Sarkar S, Sanochi T, Bowyer KW. A robust visual method for assessing the relative performance of edge-detection algorithms. IEEE Transactions on Pattern Analysis and Machine Intelligence. 1997;19(12):p. 1338-1359.
- [61] Clark JJ, Palmer MR, Laurence PD. A transformation method for the reconstruction of functions from nonuniformly spaced samples. IEEE Transactions on Acoustics, Speech and Signal Processing. 1985;Volume ASSP-33:p. 1151-1165.
- [62] Tsai RY, Huang TS. Multiple frame image restoration and registration. Advances in Computer Vision and Image Processing. Cape Town , Greenwich: JAI Press Inc.; 1984. p. 317-339.
- [63] Stark H, Oskoui P. High resolution image recovery from image-plane arrays, using convex projections. JOSA A. 1989;6(11):p. 1715-1726.
- [64] Irani M, Peleg S. Super resolution from image sequences. Proceedings of the 10th International Conference on pattern recognition; 1990; Volume 1(2): p. 115-120.
- [65] Tu C, Hamam Y, Van Wyk BJ, Djouani K, Du S. Ideal HT: a useful tool for Hough transforms assessment. SAIEEE, Africa Research Journal. 2013;104(3):p. 98-114.
- [66] Morimoto M, Akamatsu S, Suenaga Y. A high-resolution Hough transform using variable filter. Pattern Recognition, Conference C: Proceedings of the 11th IAPR International Conference on Image, Speech and Signal Analysis; 1992; Volume III: p. 280-284.

- 
- [67] Guil N, Villalba J, Zapata EL. A fast Hough transform for segment detection. *IEEE Transactions On Image Processing*. 1995;4(11):p. 1541-1548.
- [68] Fiddy MA. The Radon Transform and Some Of its Applications. *Journal of Modern Optics*. 1983;32(1):p. 3-4.
- [69] Tu C, Djouani K, Van Wyk BJ, Hamam Y, Du S. Good resolutions for Hough transform. *Proceedings of the 10th World Congress on Intelligent Control and Automation*; 2012; Beijing, China: p. 4917-4920.